PEOPLE'S DEMOCRATIC REPUBLIC OF ALGERIA

MINESTRY OF HIGHER EDUCATION AND SCIENTIFIC RESEARCH

MOHAMED BOUDIAF UNIVERSITY- M'SILA

FACULTY OF SCIENCES

PHYSICS DEPARTMENT

N°: PH/MAT/11/2024

DOMAIN: Material sciences.

FIELD: Physics.

OPTION: Physics of materials.

Thesis presented for the award of

The Academic Master's Degree

By: BOUAOUINA Amani

Title:

The influence of dimension on the electronic structure of materials

Supported on the: June,10 th,2023 in front of the jury composed of:

BAAZIZ Hakim	M'sila University	Chair
CHARIFI Zoulikha	M'sila University	Supervisor
GHELLAB Torkia	M'sila University	Examiner

Academic year: 2023/2024

Acknowledgements

First of all, I thank God, الحمد لله

The realization of this dissertation was possible thanks to the help of several people to whom I would like to express my gratitude ;

First of all, I would like to express my gratitude to my research supervisor, Pr. **Charifi Zoulikha** , for her patience, availability and, above all, her judicious advice, which helped to fuel my thinking.

I would also like to thank all my teachers at Mohamed Boudiaf M'sila University FACULTY OF SCIENCES PHYSICS DEPARTMENT for their constant guidance and support during my five years of training. My thanks also go to the members of the jury who agreed to evaluate this work.

A teacher is a compass that activates the magnets of curiosity, knowledge and wisdom in students'.

Dedication

I dedicate this work ;

To my dear parents, my father Salehet and my mother Nassirapour for all their sacrifices, love, tenderness, support and prayers throughout my studies.

To my husband Abderrahim for their moral support and invaluable advice throughout the preparation of this modest work.

To my dear brothers and sisterswho(Nadjat Saloua Ibtissam Ameur Hadda Nacer Laid) and tomy brothers' wives swho have shared with me all the emotional moments during the realisation of this work. They have warmly supported and encouraged me along the way.

To my husband's family, my second family who shared these moments with me and for their support throughout the process.

To all my dear friends, each and every one of them by name (Suhaila, Amani, Noor, Razika, Khulood, Assia, Weam, Fatima Zahra, Ikram .....) who have always encouraged me and to whom I wish more success.

Thank you for always standing by my side

Summary

Chapter II: Nanomaterials And its applications

Tables List

List of Figures

General Introduction

General Introduction

Condensed matter physics is a branch of physics that studies the properties of materials in their solid state. the research in this field has led to many important technological applications of nanotechnology Is the foundation upon which the study of nanophysics is built, by applying the fundamental concepts of condensed matter to complex multiphase media, including materials of technological interest. Nanophysics is critical to the development of modern science because it enables scientists to study and manipulate matter at the nanoscale "which ranges from to 1 nm to ~ 100 nm "**[1]**. Nanomaterials exhibit unique properties and behaviors. These materials exhibit well-defined optical, electrical, mechanical, and quantum-mechanical features at this size that can differ significantly from their bulk counterparts due to their reduced size, and increased surface-to-volume ratio.

Nanomaterials can be Two-dimensional materials this class of nanomaterials are characterized by their small dimensions, with one-dimensional scale of less than 100 nanometers. These materials have unique physical and chemical properties that distinguish them from traditional large-grained materials. 2D materials are used in a wide range of applications, including nanoelectronics, energy technology, medicine and healthcare. Ideal for the analysis of fundamentals and the development of advanced technologies, 2D materials offer unique properties that make them a focus for innovation and development in various fields. The use of these materials could revolutionize the manufacture of advanced electronic devices and quantum computers in the future.

One of the most well-known 2D materials is graphene, a thin layer of carbon composed of carbon atoms arranged in a two-dimensional geometric arrangement. Graphene is characterized by extremely high strength, flexibility, and superior thermal and electrical conductivity. In addition to graphene, there are a variety of other 2D materials such as Gallium sulfide (GaS), Gallium sulfide (GaSe), and Gallium telluride (GaTe), They exhibit unique properties that make them interesting materials in areas such as nanoelectronics, sensor technology, energy, and medicine.

The focus of this research is studying the physical properties of the above-mentioned two-dimensional materials gallium sulfide (GaS), gallium sulfide (GaSe) and gallium telluride (GaTe), which are semiconductor materials with hexagonal structures of great importance in modern technology used in the semiconductor industry to manufacture electronic components and optoelectronic devices and its potential in next-generation solar cells is studied **[2]**.

In this thesis, a theoretical examination is presented based on density functional theory (DFT). The structural and electronic properties are computed using the Wien2k code **[3]**.

The structure of this thesis consists of three chapters, organized as follows:

- ✓ The first chapter is devoted to density functional theory (DFT), as well as the Kohn-Sham equations and the different approximations used to determine the exchange and correlation potential determination of the exchange and correlation potential, namely the local density approximation (LDA) **[4]** and the generalized gradient approximation (GGA) **[5]** and Modified Becke-Johnson (mBJ) approximation and EV-GGA approximation **[6]**. In the second part of chapter I, we have recalled the principle of the linearized augmented plane wave (FP-LAPW), as well as a description of the algorithm of the Wien2k calculation code.
- ✓ The second chapter provides a comprehensive overview of nanomaterials and their applications, we presented a thorough explanation of the compounds.
- ✓ Third chapter present the results and discussions of the structural, electronic and elastic of two-dimensional (2D) and three-dimensional (3D) GaS, GaSe and GaTe compounds.

Finally, this work concludes with a general conclusion of all the main results obtained throughout the study.

References

[1] Wilfred L.F. Armarego. Chapter 5 – Nanomaterials. Purification of Laboratory Chemicals (Ninth Edition). 2 September 2022 586-630. https://doi.org/10.1016/B978-0-323-90968-6.50005-9.

[2] Group of expert Nanotechologists. Gallium sulfide Powder. Nano Research https://www.nanorh.com/product/gallium-sulfide-powder/

[3] P. Blaha, K. Schwarz, G. Madsen, D. Kvasnicka, J. Luitz, Wien2k, Techn. Universitat, Vienna, Austria, (2001).

[4] D. M. Ceperley, B. J. Alder, Phys. Rev. Lett. 45 (1980) 566.

[5] J. P. Perdew, S. Burke et M. Ernzerhof, Phys. Lett. 77 (1996) 3865.

[6] Reshak, Ali Hussain, et al. "X-ray photoelectron spectrum and electronic properties of a noncentrosymmetric chalcopyrite compound HgGa2S4: LDA, GGA, and EV-GGA." The Journal of Physical Chemistry B 113.17 (2009) 5803-5808.

CHAPTER I

- Calculation approach -

Density Functional Theory (DFT)

And the augmented plane wave method (FP-LAPW)

I.1.Introdaction

Condensed matter physics and materials science primarily focus on understanding and exploiting the properties of interacting electron and atomic nucleus systems, a concept known since the emergence of quantum mechanics. However, it is recognized that at least approximately all properties of materials can be studied using suitable computational tools to solve this specific problem in quantum mechanics [**1].**

It is recognized that the system consisting of electrons and nuclei is a highly interacting many-body system, making solving the Schrödinger equation exceptionally difficult. As Dirac pointed out (in 1929) progress relies on developing approximate techniques with sufficient accuracy. Describing materials requires understanding their properties, which necessitates grasping the interactions between electrons and ions composing these materials. Nonetheless, classical mechanics fails to solve this problem, necessitating resorting to quantum mechanics, which primarily relies on solving the Schrödinger equation **[2].** To determine the properties of materials, we can rely on simulation to obtain the necessary characteristics through computational codes (such as **WIEN2K)**, which are based on density Functional Theory (**DFT) [3].**

This theory is now widely used in our daily computational investigations of atoms, molecules, solids, and nanomaterials, and it is crucial to modern many-body computing techniques. Therefore, the main goal is to show that there are definitely ways to improve DFT **[4].**

It has its origins in the model developed by Thomas and Fermi in the late 1920s, but it was not until the mid-1960s that the contributions of Hohenberg and Kohn **[5]** on the one hand and Kohn et Sham **[6]** established the theoretical formalism on which the current method is based.

In simpler terms, Density Functional Theory (DFT) proves to be a robust method for addressing complex many-body problems. However, the selection of an appropriate wave function basis is critical for solving the Kohn-Sham equations effectively. Various techniques exist for solving the Schrödinger equation, each distinguished by the choice of potential and basis wave functions. These encompass approaches such as Linear Combination of Atomic Orbitals (LCAO), Orthogonal Plane Wave (OPW) methods, Augmented Plane Wave (APW) cellular methods, and linearized methods developed by

Andersen, including Linearized Augmented Plane Waves (LAPW) and Linearized Muffin-Tin Orbitals (LMTO). These methods significantly reduce computational time and facilitate the treatment of transition metals and conduction bands characterized by individual metal "s-p" properties **[7]**.

We will begin by briefly explaining the fundamental principles of **DFT**. We will then look in detail at the various levels of approximation used in its practical application. Finally, we will go over its implementation in the **Wien2K** code, focusing on the parameters that influence the accuracy of the results.

I.2.Schrödinger's Equation

The description of a molecular or crystalline system's non-relativistic quantum system is based on the equation established by Erwin Schrödinger.

The introduction primarily involves presenting the exact Schrödinger equation (the equation for many-body systems), which will then be simplified through various approximations to make it solvable. Addressing this many-particle problem in quantum mechanics involves seeking solutions to the following Schrödinger equation **[8]**:

$$H\Psi = E\Psi \qquad \textbf{(I.1)}$$

Where:

H : Hamiltonian.

Ψ : Wave function.

E : Total energy of the system.

The exact Hamiltonian of the crystal arises from the presence of electrostatic interaction forces: either repulsion or attraction depending on the charge of the particles (ions, electrons, nuclei, etc.) **[9]**.

the general relation gives it:

$$H_T = T_n + T_e + V_{n-e} + V_{e-e} + V_{n-n} \qquad \textbf{(I.2)}$$

In which the terms $T_e, T_n, V_{n-n}, V_{e-e}, V_{n-e}$ correspond respectively to the following terms:

- The kinetic energy of electrons:

$$T_e = -\frac{\hbar^2}{2}\sum_i \frac{\nabla^2_{\vec{r_i}}}{m_e} \quad \textbf{(I.3)}$$

- The kinetic energy of nuclei:

$$T_n = -\frac{\hbar^2}{2}\sum_i \frac{\nabla^2_{\vec{R_i}}}{M_n} \quad \textbf{(I.4)}$$

- The repulsive Coulomb interaction (electron-electron):

$$V_{e-e} = \frac{1}{8\pi\varepsilon_0}\sum_{i\neq j}\frac{e^2}{|\vec{r_i}-\vec{r_j}|} \quad \textbf{(I.5)}$$

- The repulsive Coulomb interaction (nucleus-nucleus):

$$V_{n-n} = \frac{1}{8\pi\varepsilon_0}\sum_{i\neq j}\frac{e^2 Z_i Z_j}{|\vec{R_i}-\vec{R_j}|} \quad \textbf{(I.6)}$$

- *The attractive Coulomb interaction (nucleus-electron):*

$$V_{n-e} = -\frac{1}{4\pi\varepsilon_0}\sum_{i,j}\frac{e^2 Z_i}{|\vec{r_i}-\vec{R_j}|} \quad \textbf{(I.7)}$$

e: is the charge of the electron

m: is the mass of the electron

M: is the mass of the nucleus

r_i, r_j : defining the positions of electrons (i) and (j) respectively.

R_i, R_j: definine the positions of the nuclei (i) and (j) respectively.

So, total Hamiltonian writes:

$$H = -\frac{\hbar^2}{2}\sum_i \frac{\nabla^2_{\vec{r_i}}}{m_e} - \frac{\hbar^2}{2}\sum_i \frac{\nabla^2_{\vec{R_i}}}{M_n} + \frac{1}{8\pi\varepsilon_0}\sum_{i\neq j}\frac{e^2}{|\vec{r_i}-\vec{r_j}|} + \frac{1}{8\pi\varepsilon_0}\sum_{i\neq j}\frac{e^2 Z_i Z_j}{|\vec{R_i}-\vec{R_j}|} - \frac{1}{4\pi\varepsilon_0}\sum_{i,j}\frac{e^2 Z_i}{|\vec{r_i}-\vec{R_j}|} \quad \textbf{(I.8)}$$

This equation contains $3(Z+1)N_\alpha$ variables, and since there are nearly 10^{22} atoms in one $1cm^3$ of a crystalline solid, it is more than obvious that a solution cannot be obtained because it is an N-body problem that can only be solved by several approximations**[10]**. So, there are different levels of approximation that must be considered when simplifying mathematical expressions. The three main levels of simplification generally used are :

↳ The Born-Oppenheimer approximation.

- The Hartree-Fock approximation.
- The formalism of the density functional theory.

I.2. Born-Oppenheimer approximation

Following Born and Oppenheimer, we begin by neglecting the motion of the nuclei compared with that of the electrons this is justified by the fact that the mass of the nuclei is greater than the mass of the electrons, so the electrons move faster than the atomic nuclei therefore, the kinetic energy of the nuclei is thus neglected **($T_n \approx 0$)** and the potential energy of nuclei becomes a constant ($V_{n-n} = C^{ste}$) that can be chosen as the new origin of energies **[11]**.

The electronic Hamiltonian became the following:

$$H_e = T_e + V_{e-e} + V_{e-n} \quad \textbf{(I.9)}$$

With:

T_e : the kinetic energy of electrons.

V_{e-e} : The repulsive Coulomb interaction (electron-electron).

V_{e-n} : The attractive Coulomb interaction (electron-nucleus).

Schrödinger's equation can be written as:

$$H_e \Psi_e = H_e \Psi_e \quad \textbf{(I.10)}$$

$$\left[-\frac{\hbar^2}{2} \sum_i \frac{\nabla_{\vec{r}_i}^2}{m_e} + \frac{1}{8\pi\varepsilon_0} \sum_{i \neq j} \frac{e^2}{|\vec{r}_i - \vec{r}_j|} - \frac{1}{4\pi\varepsilon_0} \sum_{i,j} \frac{e^2 Z_i}{|\vec{r}_i - \vec{r}_j|} \right] \Psi_e = H_e \Psi_e \quad \textbf{(I.11)}$$

Where:

E_e : Represent the energy of electrons moving in the field created by fixed nuclei.

This approximation is not sufficient to solve the Schrödinger equation, due to the complexity of electron-electron interactions. This is why it is very often coupled with the Hartree approximation **[12]**. So, we have to resort to other approximations.

I.3. Hartree approximation:

In 1928, Hartree considered that each electron moves independently in the mean-field created by the nuclei and all the other electrons **[13]**. The Hamiltonian can be written as a sum of Hamiltonians, each describing the behavior of a single electron.

$$H = \sum_i H_i \quad \textbf{(I.12)}$$

$$H_i = -\frac{\hbar^2}{2m}\Delta_i + U_i((\vec{r_i}) + V(\vec{r_i}) \quad \textbf{(I.13)}$$

With:

Such as:

$$U_i(\vec{r_i}) = -\sum_K \frac{Z_K e^2}{|\vec{r_i} - \overrightarrow{R_K^0}|} \quad \textbf{(I.14)}$$

This is the potential energy of the electron (i) in the field of all the nuclei (k).

R_K^0: is the fixed position of the cores (k).

$$V_i(\vec{r_i}) = \frac{1}{2}\sum_j \frac{Z_K e^2}{|\vec{r_i} - \vec{r_j}|} \quad \textbf{(I.15)}$$

This is the effective Hartree field.

The effective potential is the sum of these two contributions:

$$V_{eff}(\vec{r}) = V_H(\vec{r}) + V_N(\vec{r}) \quad \textbf{(I.16)}$$

$V_H(\vec{r})$: Hartree's potential

$V_N(\vec{r})$: The electron-all other nuclei interaction potential

By introducing the effective potential into Schrödinger's equation.

We find:

$$-\frac{\hbar^2}{2m}\nabla^2\Psi_i(\vec{r}) + V_{eff}(\vec{r})\Psi_i(\vec{r}) = E_i\Psi_i(\vec{r}) \quad \textbf{(I.17)}$$

The wave function of the electron system has the form of a product of the wave functions of the electrons, and the energy of this system is equal to the sum of the energies of all the electrons **[14]**.

$$\Psi(\vec{r_1}, \vec{r_2}, \dots\dots\dots, \vec{r_n}) = \Psi_1(\vec{r_1})\Psi_2(\vec{r_2}) \dots\dots\dots \Psi_n(\vec{r_n}) \quad \textbf{(I.18)}$$

$$E = E_1 + E_2 + \cdots\dots\dots + E_n \quad \textbf{(I.19)}$$

I.4. Hartree-Fock approximation

In 1930, Fock demonstrated that the Hartree method does not adhere to the principle of anti-symmetry of the wave function. Indeed, according to the Pauli exclusion principle, two electrons cannot be simultaneously in the same quantum state **[15]**. To correct this deficiency, Fock proposed applying the Pauli exclusion principle, so the electronic wave function is expressed in the form of a Slater determinant **[14]:**

$$\Psi_{SD}(\overrightarrow{r_1},\dots,\overrightarrow{r_n}) = \frac{1}{\sqrt{n!}}\begin{pmatrix}\Psi_1(x_1) & \cdots & \Psi_n(x_1)\\ \vdots & \ddots & \vdots \\ \Psi_1(x_n) & \cdots & \Psi_n(x_n)\end{pmatrix} \quad \textbf{(I.20)}$$

$\frac{1}{\sqrt{n!}}$**:** is a normalization factor.

The Hartree-Fock equations can be obtained by applying the variational principle to the problem of minimizing the total energy to the monoelectronic wave function Ψ_i **.**

The equations are given in the following forms:

$$\left[-\frac{\hbar^2}{2m_e}\vec{\nabla}^2 + \quad V_{ext}(\vec{r}) + V_H(\vec{r}) + V_X(\vec{r})\right]\Psi_i(\vec{r}) = E\Psi_i(\vec{r}) \quad \textbf{(I.21)}$$

Where:

$V_{ext}(\vec{r})$: Represent the attractive interaction between the electron and the nuclei of coordinate $\vec{R}$.

$$V_{ext}(\vec{r}) = -\sum_i \frac{Z_i e^2}{|\vec{r_i}-\overrightarrow{R'}|} \quad \textbf{(I.22)}$$

$V_H(\vec{r})$: is the Hartree potential arising from the repulsive coulomb interaction between an electron of coordinate $\vec{r_i}$ in the mean field of the other electrons of the coordinate $\vec{r_j}$.

$$V_H(\vec{r}) = -\int d\overrightarrow{r'}\rho(\overrightarrow{r'})\frac{1}{|\vec{r_i}-\overrightarrow{r'}|} \quad \textbf{(I.23)}$$

$V_X(\vec{r})$: The Fock term is defined by its action on a wave function $\Psi_i(\vec{r})$. The Hartree-Fock equations differ from the Hartree equations by the exchange term:

$$V_X(\vec{r})\Psi(r) = \sum_{i\neq j}\int dr\,\frac{\psi_j^*(r')\psi_i^*(r')}{(\vec{r}-\overrightarrow{r'})}\Psi_j(r) \quad \textbf{(I.24)}$$

This Hartree-Fock approximation leads to good results, particularly in molecular physics. In the case of a metal, this method leads to results that contradict experience **[16]**. We find

that the density of states of a metal is zero at the Fermi surface, which is in total contradiction with this observation highlighting an important physical phenomenon that is neglected in the Hartree-Fock theory: electronic correlation. However, there is a modern and certainly more powerful method, which is density functional theory (DFT).

I.5. Density Functional Theory

This method is based on the postulate proposed by Tomas **[17]** and Fermi **[18]**, The method proposed by Thomas and Fermi demonstrated how DFT works, but was not precise enough to be applied to modern electronic structure calculations. They proposed a method in which the kinetic energy is expressed as a function of electron density and takes into account electron-electron interactions through the mean-field potential. Their approach is similar to that proposed by Hartree and Fock, but their approach ignores exchange correlations. Dirac proposed a local approximation of commutation, which is still used today but does not significantly improve the method. Today, Hohenberg, Kohn, and Sham proposed and developed the modern DFT formulation, which uses particle density as a fundamental variable to describe any type of many-electron system. In other words, we can say that modern DFT is based on the Hohenberg and Kohn theorems **[19]**.

I.5.1-Hohenberg-Kohn Theorems

I.5.1-1-First Theorem

Hohenberg and Kohn's first theorem states that the external potential is a unique function of the ground-state electron density, which means that any ground-state configuration of electrons is uniquely determined by the external potential **[20]**.

$$\frac{\partial E[\rho(\vec{r})]}{\partial \rho(\vec{r})}\Big|_{\rho(\vec{r})-\rho_0(\vec{r})} = 0 \qquad \textbf{(I.25)}$$

The Hohenberg-Kohn theorem doesn't specify the form of the universal functional $E\left[\rho(\vec{r})\right]$, a key component in density functional theory. Nonetheless, it asserts the universality of this functional $E\left[\rho(\vec{r})\right]$ across systems with multiple electrons. Once the functional $E\left[\rho(\vec{r})\right]$ is determined, applying the principle to a given external potential becomes relatively straightforward **[21]**.

I.5.2-2-Second Theorem

This theory proves the existence of a universal function, denoted E(ρ), which represents energy in terms of electron density $\rho(\vec{r})$, this function is generally applicable to any

external potential V_{ext}. For a given potential V_{ext} and number of electrons N, the ground state energy of the system is the value that minimizes this functional, and the density $\rho(\vec{r})$ associated with it corresponds to the exact density $\rho_0(\vec{r})$ of the ground state. Consequently, the ground state electron density uniquely determines the external potential V_{ext} (r), up to some constant **[21]**.

$$\left.\frac{\partial E[\rho(r)]}{\partial \rho(r)}\right|_{\rho-\rho_0} = 0 \Rightarrow E(\rho_0) = MinE(\rho) \qquad \textbf{(I.26)}$$

ρ_0 : the density of the ground state.

Hence, the total energy functional of the ground state is written as follows:

$$E\left[\rho(\vec{r})\right] = F_{HK}\left[\rho(\vec{r})\right] + \int V_{ext}(\vec{r})\rho(\vec{r})d\vec{r} \qquad \textbf{(I.27)}$$

$F_{HK}\left[\rho(\vec{r})\right]$: The universal functional of Hohenberg and Kohn for any system has several electrons.

$V_{ext}(\vec{r})$:is the external potential acting on these particles.

$$F_{HK}\left[\rho(\vec{r})\right] = T_e\left[\rho(\vec{r})\right] + V_{e-e}\left[\rho(\vec{r})\right] \qquad \textbf{(I.28)}$$

With:

$\left[\rho(\vec{r})\right]$: the density functional for kinetic energy.

$V_{e-e}\left[\rho(\vec{r})\right]$: the density functional for electron-electron interaction.

The Hohenberg-Kohn theorem offers a method for determining the electron-nucleus interaction based on the electron density. However, directly calculating the kinetic energy and the electron-electron interaction potential from the electron density is not feasible due to the unknown structure of the energy functional **[20]**. This inconvenient of the unknown form of the functional $F_{HK}\left[\rho(\vec{r})\right]$ in the Hohenberg-Kohn theorem ca be resolved by using the Kohn-Sham approximation.

I.5.2- Kohn-Sham's equations

The Kohn-Sham theory **[6]** is based on the hypothesis that it is possible to reproduce the density of the fundamental state of a system of N interacting particles by an auxiliary system made up of independent particles The real system made up of interacting electrons is replaced by a set of fictitious and independent particles evolving in an effective potential All the N-

body interactions being contained in an exchange and correlation functional depending on the electron density given by:

$$\rho(\vec{r}) = \sum_{i}^{n} |\Psi_i(\vec{r})|^2 \qquad \textbf{(I.29)}$$

The ground state energy and density of a system of interacting electrons can be obtained using the variational principle. The energetic functional is then written by the following:

$$E_{V_{ext}}[\rho(\vec{r})] = T_0[\rho(\vec{r})] + V_H[\rho(\vec{r})] + V_{XC}[\rho(\vec{r})] + V_{ext}[\rho(\vec{r})] \qquad \textbf{(I.30)}$$

Hence:

T_0 : the kinetic energy of the system without interaction.

V_H : the Hartree term (the classical Coulomb interaction between electrons).

V_{XC} : the term that refers to the effects of exchange and correlation.

V_{ext} : includes the colombic interaction of electrons with nuclei and nuclei with each other.

The Hartree limit and the kinetic energy limit are crucial in describing the states of free electrons and are essential in the treatment of electron interactions. The difference between the true kinetic energy and the energy of non-interacting electrons, as well as the difference between the true interaction energy and the Hartree energy, is taken into account in the exchange energy and binding energy. The Hartree-Fock approximation stands out as one of the primary ways to treat the kinetic energy of electrons. The Kohn-Sham equations include the non-interacting kinetic energy, the long-range Hartree term, the external potential, and the cross-correlation energy. Thus, the Schrödinger equation can be expressed as follows **[21]**.

$$\left[-\frac{\hbar^2}{2m_e}\nabla_i^2 + V_H(\rho(\vec{r})) + V_{XC}(\rho(\vec{r})) + V_{ext}(\rho(\vec{r}))\right]\Psi_i(\vec{r}) = E_i\Psi_i(\vec{r}) \qquad \textbf{(I.30)}$$

The exchange and correlation potential of the Kohn-Sham density-functional is given by the derived functional:

$$V_{XC}(\vec{r}) = \frac{\partial E_{XC}}{\partial \rho(\vec{r})} \qquad \textbf{(I.31)}$$

The Kohn-Sham equation is a non-interacting Schrödinger equation of a fictitious system of non-interacting particles that generate the same density as a real system of interacting electrons. The Kohn-Sham equation is defined by a local effective external potential in which the non-interacting particles move, typically denoted as $V_{eff}(\vec{r})$, which is the summation of the three terms $V_H(\vec{r}), V_{ext}(\vec{r})$ and $V_{XC}(\vec{r})$:

$$V_{eff}(\vec{r}) = V_H(\vec{r}) + V_{ext}(\vec{r}) + V_{XC}(\vec{r}) \qquad \textbf{(I.32)}$$

Then the Kohn-Sham equation is as follows:

$$\left[-\frac{\hbar^2}{2m_e}\nabla_i^2 + V_{eff}(\vec{r})\right]\Psi_i(\vec{r}) = E_i\Psi_i(\vec{r}) \qquad \textbf{(I.33)}$$

I.6. Self-Consistent Procedure

The self-consistent cycle involves the solving of the equation **(I.33)** iteratively. The procedure starts by defining the initial electron density ρ_{in} (which is usually constructed from a superposition of atomic densities $\rho_{in} = \rho_{cristal} = \sum_{at}\rho_{at}$) **[22]**, after assuming the initial electron density, the next step is to diagonalize the secular equation:

$$(H - E_i S)C_i = 0 \qquad \textbf{(I.34)}$$

Where:

H : is the Hamiltonian matrix.

S : represents the recovery matrix.

Then we get the solution of new density ρ_{out}, if the calculations do not converge, the charge densities ρ_{in} and ρ_{out} are mixed as follows:

$$\rho^{i+1}{}_{in} = (1-\alpha)\rho^{i}_{in} + \alpha\rho^{i}{}_{out} \qquad \textbf{(I.35)}$$

i : represents the (i-th) iteration.

α : mixing parameter.

The iterative procedure is continued until convergence is achieved, which can be tested on energy and/or loads. The self-consistent procedure is illustrated in the general scheme in Figure **(I.1)**.

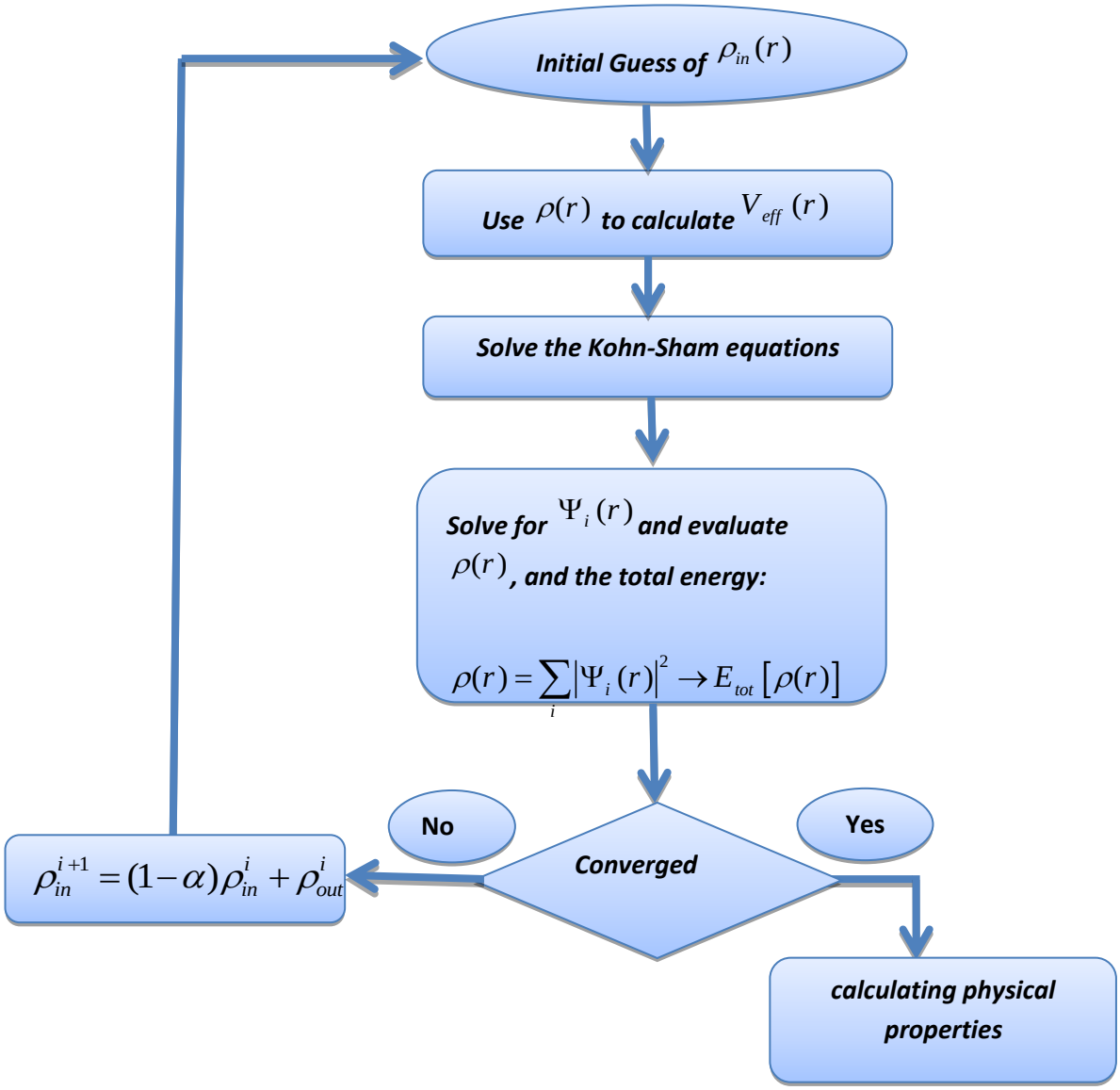

Figure (I.1): A general self-consistent scheme of Density Functional Theory.

I.7. The different types of functionalities

As we have seen, all energy terms and associated potentials can be evaluated, except for the exchange and correlation terms, which is the main difficulty in DFT. There are many approximations for the cross-correlation function. Four classes of functions are available.

I.7.1- Local Density Approximations LDA

Local Density Approximation (LDA) **[23]** considers the exchange and correlation potential to be a local quantity, defined at a point $\vec{r}$, which depends only slightly on variations in density around this point $\vec{r}$ **[24,25]**. Thus, at a point r to which corresponds a density $\rho(\vec{r})$ it will be associated with an exchange and correlation potential comparable to that of a homogeneous gas of electrons of the same density $\rho(\vec{r})$ the exchange and correlation energy $E_{XC}^{LDA}\left[\rho(\vec{r})\right]$ is then expressed as follows:

$$E_{XC}^{LDA}\left[\rho(\vec{r})\right]=\int \rho(\vec{r})\varepsilon_{XC}^{LDA}\left[\rho(\vec{r})\right]d^{3}\vec{r} \qquad \textbf{(I.36)}$$

Where $E_{XC}^{LDA}\left[\rho(\vec{r})\right]$ represents the exchange-correlation energy for a homogeneous gas of electrons of density ρ.

the corresponding exchange-correlation potential is:

$$V_{XC}^{LDA}(\vec{r})=\frac{\delta(\rho(\vec{r})\varepsilon_{XC}^{LDA}\left[\rho(\vec{r})\right])}{\delta\rho(\vec{r})} \qquad \textbf{(I.37)}$$

Finally, the term $E_{XC}^{LDA}\left[\rho(\vec{r})\right]$ of the relation **(I.36)** can be approximated by a sum of two contributions, so:

$$E_{XC}^{LDA}\rho(\vec{r})=\varepsilon_{X}^{LDA}\left[\rho(\vec{r})\right]+\varepsilon_{C}^{LDA}\left[\rho(\vec{r})\right] \qquad \textbf{(I.38)}$$

$\varepsilon_{X}^{LDA}\left[\rho(\vec{r})\right]$: functional exchange.

$\varepsilon_{C}^{LDA}\left[\rho(\vec{r})\right]$: correlation functional.

Or the exchange term, the so-called "Dirac exchange term" is given by:

$$\varepsilon_{XC}^{LDA}\left[\rho(\vec{r})\right]=-\frac{3}{4}\left(\frac{3}{\pi}\rho(\vec{r})\right)^{\frac{1}{3}} \qquad \textbf{(I.39)}$$

I.7.2- Generalized Gradient Approximations GGA

The Generalized Gradient Approximation (GGA) is a form of exchange-correlation functional designed to enhance the accuracy of electronic-structure calculations beyond what's achieved by the Local Density Approximation (LDA). By incorporating the non-uniform nature of the electron gas, GGA modifies the exchange-correlation energy function to depend not just on electron density but also on its gradient **[26]**.

Then we can write the exchange-correlation energy as:

$$E_{XC}^{GGA}\left[\rho(\vec{r})\right]=\int \rho(\vec{r})\varepsilon_{XC}\left[\rho(\vec{r}).\nabla\rho(\vec{r})\right]d^{3}\vec{r} \quad \textbf{(I.40)}$$

$\varepsilon_{XC}\left[\rho(\vec{r}).\nabla\rho(\vec{r})\right]$: represents the exchange-correlation energy by an electron in a system of electrons mutual interaction of non-uniform density.

I.7.3- Modified Becke-Johnson (mBJ) approximation

A new version of exchange potential first proposed by Becke and Johnson (2006) **[27]**, was recently published by Tran and Blaha. This is the mBJ (modified Becke Johnson) functional (also known as the TB potential: Tran-Blaha) which has been implemented in the latest version of the Wien2k ab-initio code.

The latter quickly proved its efficiency compared with the most commonly used calculation modes, such as LDA **[6]** and GGA **[27]**. In their article published on 3 June 2009 in the journal Physical Review Letters, Tran and Blaha propose a modified version of Becke and Johnson's function **[28]**.

$$V_{X\sigma}^{mBJ}(r)=cV_{X\sigma}^{BR}(r)+(3c-2)\frac{1}{\pi}\sqrt{\frac{5}{12}}\sqrt{\frac{2t_{\sigma}(r)}{\rho_{\sigma}}} \quad \textbf{(I.41)}$$

With:

$\rho_{\sigma}(r)=\sum_{i=1}^{n_{\sigma}}\left(\nabla\Psi_{i\sigma}^{*}(r)\right)^{2}$: Electron density.

$t_{\sigma}(r)=\frac{1}{2}\sum_{i=1}^{n_{\sigma}}\nabla\Psi_{i\sigma}^{*}(r)\nabla\Psi_{i\sigma}(r)$: The density of kinetic energy.

$V_{X\sigma}^{BR}(r)=\frac{1}{b_{\sigma}(r)}\left[1-e^{-x_{\sigma}(r)}-\frac{1}{2}x_{\sigma}(r)e^{-x_{\sigma}(r)}\right]$: is the Becke-Roussel (BR) potential [Becke (1989)] which was proposed to minimize the coulomb potential. The index σ is the spin notation spin notation.

The term x_{σ} was determined from $\rho_{\sigma}(r), \nabla\rho_{\sigma}(r), \nabla^{2}\rho_{\sigma}(r)$ and $t_{\sigma}(r)$ While the term $b_{\sigma}(r)$ was calculated using the following relation:

$$b_{\sigma}(r)=\left(\frac{X_{\sigma}^{3}(r)e^{-x_{\sigma}(r)}}{8\pi\rho_{\sigma}(r)}\right)^{\frac{1}{3}} \quad \textbf{(I.42)}$$

The Becke-Roussel potential proposed here is approximately equivalent to the potential used in Beck and Johnson **[28]**. The main change is in the appearance of the appearance of

parameter c in the functional formula. Note that if we take c=1 we fall back on the Becke and Johnson functional **[28]**. This parameter was chosen to depend linearly on the square root of the mean $\frac{|\nabla\rho_\sigma(r)|}{\rho_\sigma(r)}$

The proposed form for c is as follows:

$$c = \alpha + \beta\left(\frac{1}{V_{cell}}\int\frac{|\nabla\rho_\sigma(r')|}{\rho_\sigma(r')}d^3r'\right)^{\frac{1}{2}} \quad \textbf{(I.43)}$$

α and $\beta$are two free parameters.

V_{cell} : The volume of the system's unit cell.

$\alpha = -0.012$ Dimensionless.

$\beta = 1.023\ bohr^{1/2}$

I.7.4- The EV-GGA approximation

It is well known that LDA and GGA underestimate energy gaps. This is mainly due to the fact that they have simple forms that are not flexible enough to obtain the exact shape of the exchange-correlation potential. Engel and Vosko, considering this deficit, constructed a new form of the GGA functional designed to provide a better exchange-correlation potential. This approach, called EV-GGA aims to address this issue **[29]**, It provides a better gap and some other properties that depend mainly on the accuracy of the exchange-correlation potential. However, in this method, quantities that depend on an exact description of the exchange energy E_{xc}, such as the equilibrium volume and the bulk modulus, disagree with experiment. In general, the exchange-correlation energy is defined in the GGA approximation as:

$$E_{XC}^{GGA}[\rho, \nabla_{\beta\rho}] = \int \varepsilon_{XC}[\rho(\vec{r}), \nabla_{\rho(\vec{r})}]\,\rho(\vec{r})d^3r \quad \textbf{(I.44)}$$

I.8. The Augmented Plane Wave (APW) Method

In 1937, Slater **[30]** proposed using augmented plane waves (APW) as a basis to solve the Schrödinger equation for a single electron, which corresponds to the Kohn-Sham equation based on DFT. The APW method is based on the "Muffin-tin" approximation to describe the crystalline potential. According to this approximation, the unit cell is divided into two regions:

- Inside the sphere of radius R_{MT} **,** we have a base constituted by a linear combination of the radial of radial functions multiplied by spherical harmonics.
- An interstitial region delineating the residual space not occupied by the spheres **(fig. I.1)**, in which two appropriate categories of basis are used:

1. Radial functions multiplied by spherical harmonics inside the atomic "Muffin-tin" spheres (region I).

2. Plane waves for the interstitial region (region II), namely:

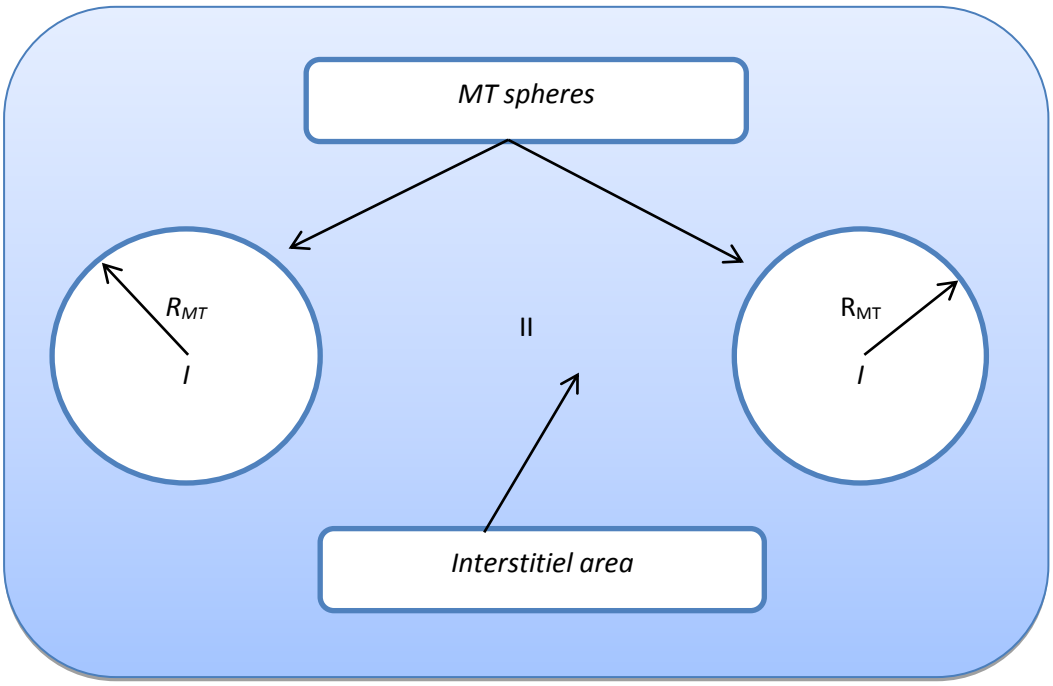

Figure (I.2): Representation of the partition of space according to the Muffin-Tin approximation.

The wave function $\phi(r)$ is then of the form:

$$\phi(r)\begin{cases}\frac{1}{\Omega^{1/2}}\sum_G C_G e^{i(G+K)r} & r > R_{MT}\\ \sum_{lm} A_{lm}U_l(r)Y_{lm}(r) & r < R_{MT}\end{cases} \qquad \textbf{(I.45)}$$

Where:

R_{MT} : The radius of the sphere.

Ω : The volume of the unit cell.

A_{lm}, C_G : The development coefficients.

Y_{lm} : The spherical harmonics.

$U_l(r)$: is the regular solution of the Schrödinger equation for the radial part given by:

$$\left\{-\frac{d^2}{dr^2}+\frac{l(l+1)}{r^2}+V(r)-E_l\right\}rU(r)=0 \qquad \textbf{(I.46)}$$

Hence:

$V(r)$: represents the Muffin-Tin potential, it is the spherical component of the potential in the sphere.

E_l : is the linearization energy.

In the muffin-tin approximation, the radial functions defined by **(I.45)** are orthogonal to any eigenstate of the core. However, this orthogonality disappears in the sphere boundary **[31]**, as shown by the following Schrödinger equation:

$$(E_2-E_1)rU_1U_2 = U_2\frac{d^2rU_1}{dr^2}-U_1\frac{d^2rU_2}{dr^2} \qquad \textbf{(I.47)}$$

Where U_1 and U_2 are the radial solutions for the energies E_1 and E_2.

In this method, Slater made a particular choice for the wave functions, he shows that plane waves are the solutions of the Schrödinger equation in a constant potential. Whereas, the radial functions are the solution in the case of the spherical potential. Therefore, it proves that E_l is equal to the eigenvalue E. This approximation is very good for materials with face-centred cubic structure, and less satisfactory with the decrease of symmetry of the material.

To ensure the continuity of the function Φ(r) on the surface of the MT sphere, the coefficients A_{lm} have to be developed in terms of the coefficients C_G of the existing plane waves in the interstitial regions. Thus, after some algebraic calculations, we find that:

$$A_{lm} = \frac{4\pi_i^l}{\Omega^{1/2} U_l(R_\alpha)} \sum_G C_G J_l(|k+g|R_\alpha) Y_{lm}^*(K+G) \quad \textbf{(I.48)}$$

In the APW method, the origin is taken to be the center of the sphere, and the coefficients A_{lm} are determined from those of the C_G plane waves. The energy parameters E_l are referred to as the variational coefficients of the APW method. The individual functions labeled by G are made compatible with the radial functions in the spheres, resulting in augmented plane waves (APW). The APW functions are solutions of the Schrodinger equation in spheres, but only for the energy E_l. Therefore, the energy E_l must be equal to that of the index band G. This means that the energy bands (for a point k) cannot be obtained by a simple diagonalization, and it is necessary to treat the secular determinant as a function of the energy**.** The (APW) method, as constructed, presents some difficulties related to the function $U_l(R_\alpha)$ appearing in the denominator of equation **(I.47)**. Indeed, depending on the value of the parameter E_l, $U_l(R_\alpha)$ can become zero at the surface of the MT sphere, resulting in a separation of radial functions from plane wave functions. To overcome this issue, several modifications to the (APW) method have been proposed, notably those suggested by Koelling **[32]** and Andersen **[33]**.

I.9. Principle of LAPW Method

The LAPW method is among the most accurate methods for performing electronic structure calculations for crystals. As previously mentioned, the LAPW method is an improvement of the APW method developed by Andersen, Koelling, and Arbman based on Marcus' idea. The APW method uses the muffin-tin potential description, and the augmenting function corresponds to the exact muffin-tin potential eigenstate of eigenenergy. The LAPW method is a modification of the APW method that linearizes the basic functions inside the muffin-tin, leading to a better description of the eigenstate and a smaller basis set size to reach the same accuracy **[34,35]**.

In the LAPW method, the fundamental functions within the Muffin-Tin (MT) are constructed as linear combinations of radial functions $U_l(r)Y_{lm}$ and their derivatives $U_l'(r)Y_{lm}$ with respect to energy. These functions adhere to the definition outlined in equation **(I.46)** of the APW method. Additionally, the $U_l(r)Y_{lm}$ function must satisfy the condition of having both zero value and zero slope at the MT boundary, while also being normalized:

$$\left\{-\frac{d^2}{dr^2} + \frac{l(l+1)}{r^2} + V(r) - E_l\right\} rU'_l(r) = 0 \quad \textbf{(I.49)}$$

The radial functions $U'_l(r)$ and $U_l(r)$ ensure continuity with plane waves at the surface of the Muffin-Tin (MT) sphere. The basic functions of the LAPW method have an explicit form:

$$\phi(r)=\begin{cases}\frac{1}{\Omega^{1/2}}\sum_G C_G e^{i(G+K)r} & r > R_{MT}\\ \sum_{lm}\left[A_{lm}U_l(r,E_0)+B_{lm}U'_l(r,E_0)\right]Y_{lm}(r) & r < R_{MT}\end{cases} \quad \textbf{(I.50)}$$

The coefficients B_{lm} correspond to the function $U'_l(r)$ and share the same characteristics as the coefficients A_{lm}. Within the LAPW method, the linearization energy E_l is utilized, and the coefficients A_{lm} are determined to ensure the continuity of the potential at the surface of the "Muffin-Tin" (MT) sphere. Unlike the APW method, the LAPW method offers greater flexibility because the radial function can be obtained through a Taylor expansion for any linearization energy that deviates only slightly from the actual eigenenergy **[36]**.

where the function $U_l(r)$ be developed as a function of derivative $U'_l(r)$ and energy E_l :

$$U_l(r,E)=U_l(r,E_l)+(E+E_0)U'_l(r,E_0)+0((E-E_0)^2) \quad \textbf{(I.51)}$$

Where:

$$U'_l(r,E_0)=\frac{dU_l}{dE}$$

And $0((E-E_0)^2)$: Represents the energy squared error.

The LAPW method ensures continuity of the wave function at the surface of the Muffin-Tin (MT) sphere, albeit with a reduction in accuracy compared to the APW method. This method introduces errors in the wave functions on the order of $(E-E_0)^2$ and in the band energies on the order of $(E-E_0)^4$. Despite these errors, LAPW functions serve as a reliable basis for capturing all valence bands across a wide energy range using a single value of E_l. However, if U_l is zero at the sphere's surface, its derivative U'_l will be non-zero.

I.10. The roles of linearization energies

To obtain accurate results, it is essential to choose the energy parameter E_l at the center of the energy spectrum band. As previously mentioned, errors in both the wave function and band energies are on the order of $(E-E_0)^2$ and $(E-E_0)^4$ respectively. When the energy parameter E_l equals the eigenvalue E_l the LAPW method reduces to the APW method. Optimizing the

selection of this parameter E_l involves computing the total energy of the system for several E_l values and selecting the parameter that yields the lowest energy **[37]**.

The condition of orthogonality of augmented functions $U_l(r)Y_{lm}(r)\ and\ U'_l(r)Y_{lm}(r)$ to the states of the core is only fulfilled if these core states have the same energy parameter E_l. Thus, the LAPW method depends on the choice of E_l. The overlap between the core states and the LAPW bases leads to the appearance of spurious core states, known as ghost bands **[38]**.

I.11. Development in local orbitals

The goal of the LAPW method is to obtain accurate band energies in the vicinity of the linearization energies E **[39]**. In most materials, it is sufficient to choose these energies in the vicinity of the band center. However, this is not always possible, and there are materials for which choosing a single value of E_l is not sufficient to compute all energy bands. This is the case for materials with 4f orbitals **[40,38]** and transition metals **[40,41]**.

To achieve accurate band energies near the linearization energies, employing multiple energy windows or utilizing a local orbitals expansion can be effective, as illustrated in Figure **(I.3)**. The utilization of multiple energy windows becomes necessary when a single value of E_l is inadequate for computing all band energies, particularly in materials containing 4f orbitals and transition metals **[42]**.

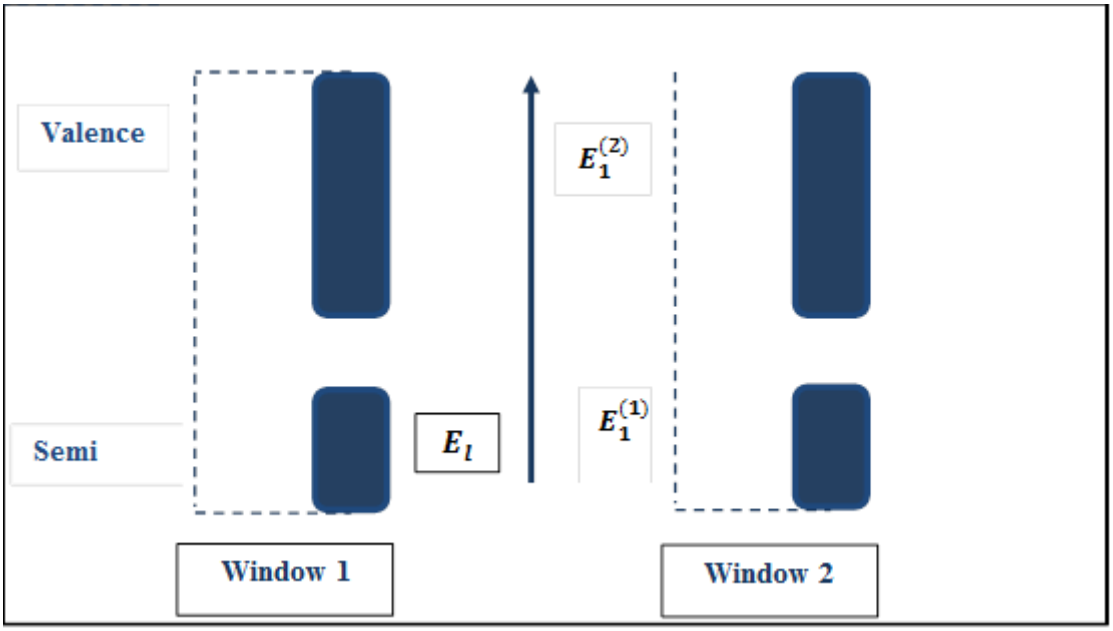

Figure (I.3): Multiple energy windows.

I.11.1- LAPW+lo method

The development of the LAPW method in local orbital basis involves modifying the base orbitals to avoid the use of multiple energy windows, by employing a third category of basis functions. The principle is to handle all bands from a single energy window. Singh **[43]** provided these orbitals, denoted as "LO," in the form of a linear combination of two radial functions corresponding to two different energies, along with the derivative with respect to energy of one of these functions.

$$\phi(r)=\begin{cases} 0 & r > R_{MT} \\ \left[A_{lm}U_l(r,E_l)+B_{lm}U'(r,E_l)C_{lm}U_l(r,E_l)\right]Y_{lm}(r) & r < R_{MT} \end{cases} \quad \textbf{(I.52)}$$

Where the C_{lm} coefficients are of the same nature as the A_{lm} and B_{lm} coefficients defined above.

Where the C_{lm} coefficients are of the same nature as the previously defined A_{lm} and B_{lm} coefficients. A local orbital is defined for a given *l* and m, as well as for a given atom (in the unit cell, all atoms are considered, not just the inequivalent ones). These local orbitals can also be used beyond the treatment of core states to improve the basis with respect to the conduction bands. This enhancement of the LAPW method is behind the success of the linearization method based on the LAPW method, as it extends this original method to a much broader category of compounds.

I.11.2- APW+lo method

An "APW+lo" base is defined by the combination of the following two types of wave functions:

- APW plane waves with a set of fixed E_l energies:

$$\phi(r)=\begin{cases}\frac{1}{\Omega^{1/2}}\sum_G C_G e^{i(G+K)r} & r > R_{MT}\\ \sum_{lm} A_{lm}U_l(r)Y_{lm}(r) & r < R_{MT}\end{cases} \quad \textbf{(I.53)}$$

- Local orbitals different from those of the LAPW+LO method defined by:

$$\phi(r)=\begin{cases}0 & r > R_{MT}\\ \left[A_{lm}U_l(r,E_l)+B_{lm}U'_l(r,E_l)\right]Y_{lm}(r) & r > R_{MT}\end{cases} \quad \textbf{(I.54)}$$

In computations, a combined LAPW and APW+lo approach can be applied to various atoms, and even for differing quantum numbers. The APW+lo approach is commonly employed to characterize orbitals that converge less rapidly with the plane wave number, such as the 3d states of transition metals or atoms with small sphere sizes. Meanwhile, LAPW is utilized for the remaining atoms. Both LAPW and APW+lo techniques can be utilized concurrently within the full potential augmented plane wave method **[44]**.

I.12. FP-LAPW method

I.12.1- Principle of the FP-LAPW method

In the Full Potential Linearized Augmented Plane Waves method (Full Potential Linearized Augmented Plane Waves : FP-LAPW) **[38]** No approximation is made for the shape of the potential or charge density. Instead, they are expanded into lattice harmonics within each atomic sphere and Fourier series in interstitial regions. This is the origin of the name « Full-Potential » This method ensures the continuity of the potential at the surface of the sphere (MT) and develops it in the following form:

$$V(r)=\begin{cases}\sum_{lm} v_{lm}(r)Y_{lm}(r) & \textit{inside the sphere}\\ \sum_k v_k e^{ikr} & \textit{outside the sphere}\end{cases} \quad \textbf{(I.55)}$$

I.12.2- Some advantages of the FP-LAPW method over the APW method

The Full Potential Linearized Augmented Plane Wave (FP-LAPW) method offers several advantages over the Augmented Plane Wave (APW) method. It allows for precise calculations of electronic and magnetic properties of materials, incorporating spin-orbit coupling effects and treating d bands, which the APW method cannot handle. Moreover, the FP-LAPW method exhibits greater accuracy, particularly for systems with extensive core states. Another notable advantage is that it eliminates the need for pseudopotentials, thereby avoiding potential errors in the calculation process **[45]**.

I.13. WIEN2k calculation code

WIEN2k is a Fortran-based computer program designed for conducting quantum mechanical computations on periodic solids. It employs the Full-Potential Linearized Augmented Plane Wave and Local-Orbitals method [FP-LAPW+lo] to solve the Kohn-Sham equations within density functional theory **[44]**. The Wien2 code was developed at the Institute of Materials Chemistry at the Technical University of Vienna (Austria) by Blaha and his colleagues **[46]**. It was first distributed in versions of the original WIEN code that have been developed (WIEN93, WIEN95, WIEN97, and WIEN2k). After its initial release, WIEN2k has undergone several updates, including WIEN93, WIEN97, and WIEN2K. The most recent version, WIEN2k_21.1, was launched on April 14, 2021. WIEN2k is extensively utilized for solid-state computations and has been licensed by over 3400 user groups, accruing approximately 16000 citations on Google Scholar **[47]**.

The different programs in WIEN2k and their flow are illustrated in Figure **(I.4).** The first step in the calculation process is initialization, which involves running a series of small auxiliary programs that produce inputs for the main programs.

NN: calculates the nearest neighbors up to a specified distance and thus helps to determine the atomic sphere radius.

LSTART: generates atomic densities (see section 6.4) and determines how the orbitals are treated in the band structure calculations (i.e., as core or band states, with or without local orbitals).

SYMMETRY: generates from a raw **case. Struct** file the space group symmetry operations, determines the point group of the individual atomic sites.

KGEN: generates a k-mesh in the Brillouin zone (BZ).

DSTART: generates a starting density for the SCF cycle by superposition of atomic densities generated in **lstart**.

LAPW0: (POTENTIAL) generates potential from density

LAPW1: (BANDS) calculates valence bands (eigenvalues and eigenvectors).

LAPW2: (RHO) computes valence densities from eigenvectors.

LCORE: computes core states and densities.

MIXER: mixes input and output densities.

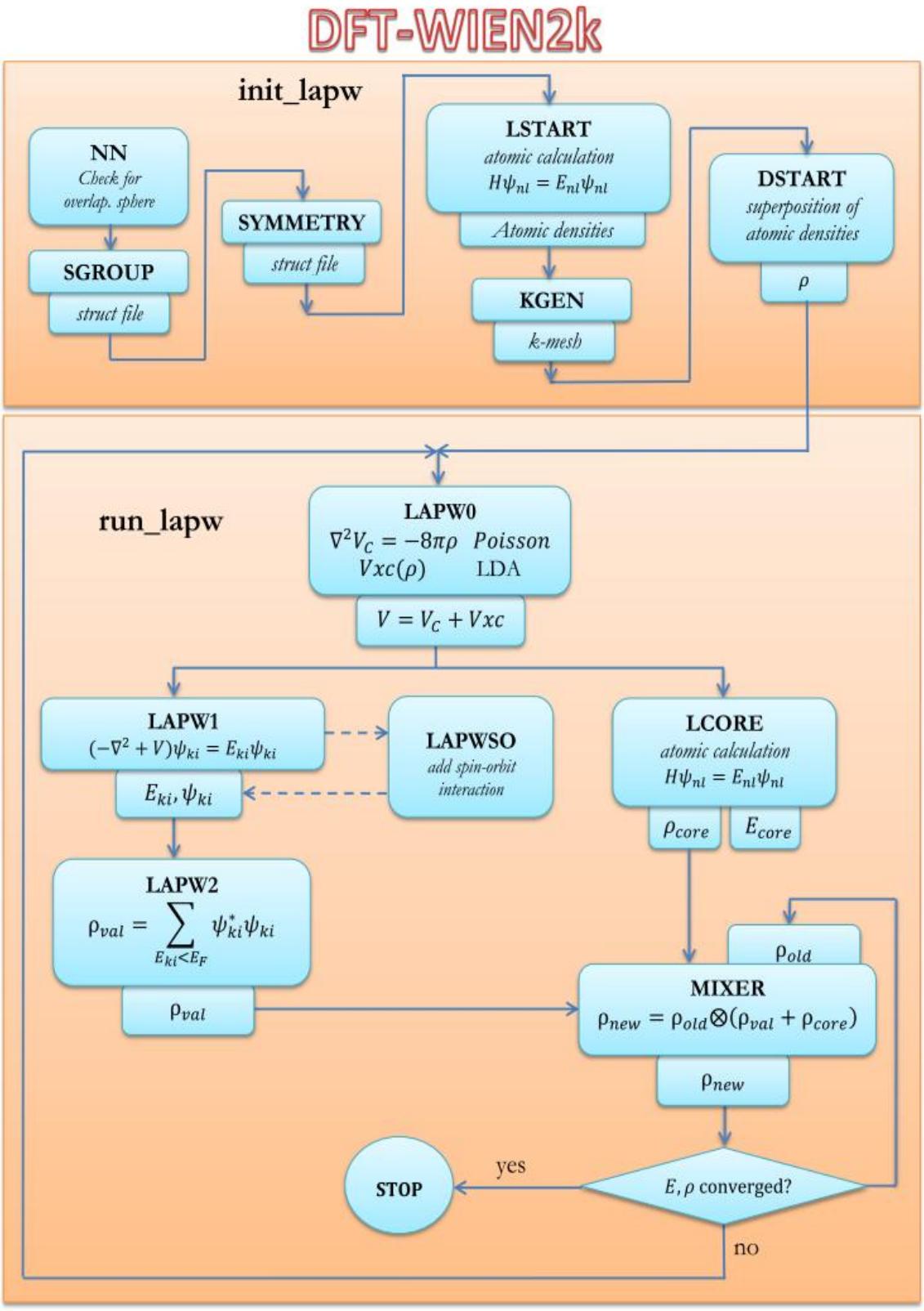

Figure (I.4): The Wien2k code program flowchart.

References:

[1] I. H .Calderon, **Optical properties and electronic structure of wide band gap II-VI semiconductors**, in II-VI semiconductors materials and their Applications , Taylor and Francis New York , (2002) **113**-170.

[2] C. kittel, Introduction à la physique de l'état solide. 5e édition Dunod (1972).

[3] L. Chen, C. Lan, B. Xe, K. Bi, Progress on material characterization methods under big data environment, Adv. Compos. Hybrid Mater. 4 (2021) 235-247. https://dio.org/10.1007/s42114-021-00229-w.

[4] Kryachko, E. S., & Ludena, E. V. Density functional theory: Foundations reviewed. Physics Reports, 544(2), (2014) 123-239.

[5] P. Hohenberg et W. Kohn, Phys. Rev. B 864, (1964) 136.

[6] W. Kohn et L.J. Sham, Phys. Rev. A1133. 140.

[7] K. Capelle, A bird's-eye view of density-functional theory, Brazilian J. Phys. 36 (2006) 1318–1341. https://doi.org/10.1590/s0103-97332006000700035. (1965).

[8] C. Kittel. 5e édition Dunod. (1996).

[9] E. Schrödinger, Ann. Phys. 79 (1926) 489.

[11] M. Born, J. R. Oppenheimer, Ann. Phys. 87 (1927) 457.

[12] O. Kahn, Molecular Magnetism; Wiley - VCH, (1993).

[13] J.E. Enderby, A. C. Barnes, Rep. Prog. Phys. 53 (1990) 85.

[14] B. E. Mellander, Phys. Rev. B 26, (1982) 5886.

[15] S. Hull and D. A. Keen: Phys. Rev. B 59, (1999) 7501.

[16] N. W. Ashcroft, N. D. Mermin, "Solid State physics", Saunders College (1976).

[17] L.H. Thomas, Proc. Cam. Phil. Soc. 26 (1930) 376.

[18] E. Fermi, Z. Phys. 48 (1928) 73.

[19] S. Ali, Colour Centres in 2-D hexagonal Boron Nitride. (2019).

[20] Wijesooriya.K, Naval postgraduate, Security. (2017) 1–55. https://apps.dtic.mil/sti/pdfs/AD1046101.pdf.

[21] S. Cottenier, S. Cottenier, Density Functional Theory and the Family of (L)APW-methods: a step-by-step introduction. 2004.

[22] N. Shan, M. Zhou, M.K. Hanchett, J. Chen, B. Liu, Practical principles of density functional theory for catalytic reaction simulations on metal surfaces–from theory to applications, Mol. Simul. 43 (2017) 861–885.

[23] R. M. Dreizler and J. da Provincia, Density Functional Methods in Physics, (Plenum, NewYork), (1985).

[24] A. D. Becke, Phys. Rev. A 38, (1988) 3098.

[25] J. P. Perdew, J. A. Chevary, S. H. Vosko, K. A. Jackson, M. R. Peederson, D. J. Singh et C. Fiolhais, Phys. Rev. B 46, (1992) 6671.

[26] J.P. Perdew, A. Zunger, Self-interaction correction to density-functional approximations for many-electron systems, Phys. Rev. B 23, (1981) 5048–5079. https://doi.org/10.1103/PhysRevB.23.5048.

[27] V. Fock, Z. Phys. 61, (1930) 126; 62 (1930) 795.

[28] A. D. Becke and E. R. Johnson, J. chem. Phys.124 (2006) 221101.

[29] E. Engel, S. H. Vosko, Phys. Rev. B 47, (1993) 20.

[30] O. K. Andersen, Phys. Rev. B12 (1975) 3060-3083.

[31] V.O. Lume, October 1975, Weatherwise. 28 (1975) 276–283. https://doi.org/10.1080/00431672.1975.9931783.

[32] D.D. Koelling and G.O. Arbman, J. Phys. F 5, (1975) 2041.

[33] O.K. Andersen, Phys. Rev. B 12, (1975) 3060.

[34] Phys. Rev. B 12, 3060_2.pdf, (n.d.).

[35] L.M. Wienk, D.J. Singh, The Linearized Augmented Planewave Scintillators for Radiation Detection, (2014).

[36] C.A.B. Set, Chapter 3 The (L) APW + lo Method, (n.d.).

[37] D.J. Singh, Phys.Rev. B44, (1991) 7451.

[38] S. Goedecker, K. Marschke, Phys. Rev. B42, (1990) 8858.

[39] C. Herring, Phys. Rev. 57 (1940) 1169.

[40] D. Singh, Phys. Rev. B 43, (1991) 6388.

[41] D. J. Singh, K Schwarz and P. Blaha, Phys. Rev. B 46, (1992) 5849.

[42] L.M. Wienk, D.J. Singh, The Linearized Augmented Planewave Scintillators for

Radiation Detection, (2014).

[43] D. Singh, Phys. Rev. B 43, (1991) 6388.

[44] P. Blaha, K. Schwarz, G. Madsen, D. Kvasnicka, J. Luitz, WIEN2k, 2011. http://www.wien2k.at/reg_user/textbooks/%5Cnpapers2://publication/uuid/ADD13F18-BF1F-44CC-8F3F-86E0D0673373.

[45] P. Blaha, The FP-LAPW and APW + lo methods Overview of DFT concepts, (n.d.).

[46] P. Blaha, K. Schwarz, and J. Luitz, WIEN97. Technical University, Vienna, (1997).

[47] K. Schwarz, P. Blaha, Solid state calculations using WIEN2k, Comput. Mater. Sci. 28 (2003) 259–273. https://doi.org/10.1016/S0927-0256(03)00112-5.

[48] T. Van Mourik, M. Bühl, M.P. Gaigeot, Density functional theory across chemistry, physics and biology, Philos. Trans. R. Soc. A Math. Phys. Eng. Sci. (2014) 372. https://doi.org/10.1098/rsta.2012.0488.

CHAPTER II

Nanomaterials and its Applications

II.1. Introduction

Nanomaterials science is a branch of science and technology that studies the properties and applications of nanomaterials. It has been one of the fastest-growing fields in applied science and technology in the last decade. Nanomaterials science investigates the mechanical, chemical, and physical properties of nanoscale materials and, subsequently, methods to prepare and fabricate them on a very fine scale to optimize cost and increase the speed of information transfer and storage. Nanomaterials are used in the development of precision medicines and medical treatments, in improving the efficiency of solar cells and atomic storage technologies, and even in the manufacture of lightweight and strong materials for airplanes and spacecraft. Given the rapid development of the field, nanomaterials science is a vital and interesting field for researchers and engineers alike, opening new doors for innovation and technology development in a wide range of applications.

II.2. Definitions

Nanomaterials are substances that are, or have been, reduced in size to the range from 1 nm to ~ 100 nm (i.e. 1 to ~ 100 nanometers, or 1 to ~ 100 × 10-9 meters) **[1]**. The length scale shown in Figure **(II.1)** provides a frame of reference for the reader.

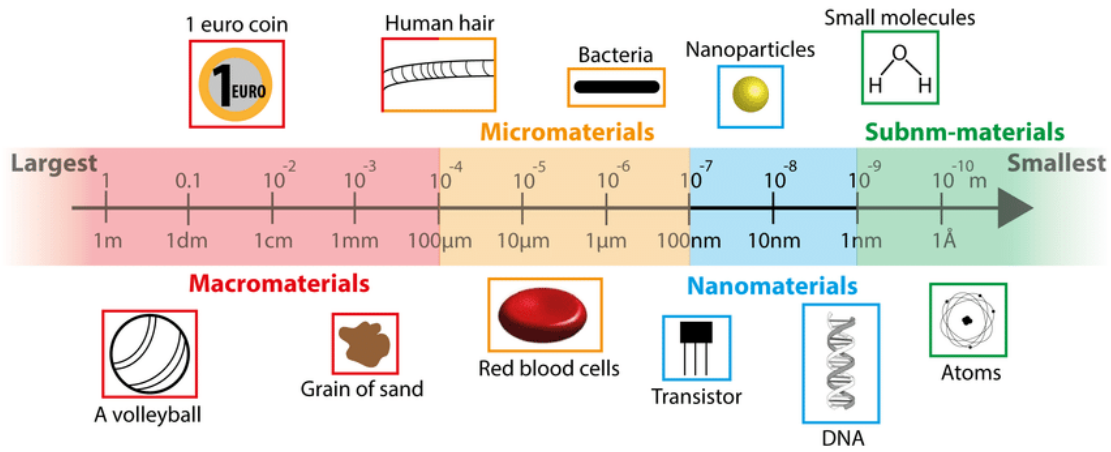

Figure (II.1): Nanomaterials size range **[2]**.

This size range is said to be intermediate between molecules and bulk matter in all aspects. More concretely, compared to bulk materials, nanomaterials exhibit different and useful physicochemical properties attributed fully to their small sizes. Due to confinement effects and increased surface-to-volume

ratios in nanostructures, for example, their melting point, chemical reactivity, catalytic activities, optical properties, fluorescence, magnetic susceptibility and conductivity all change with size **[3-4]**.

II.3. Types and classification of nanomaterials

Nanomaterials can be classified based on their four material-based categories or by their dimension levels **[5]**, as illustrated in Figure **(II.2)**.

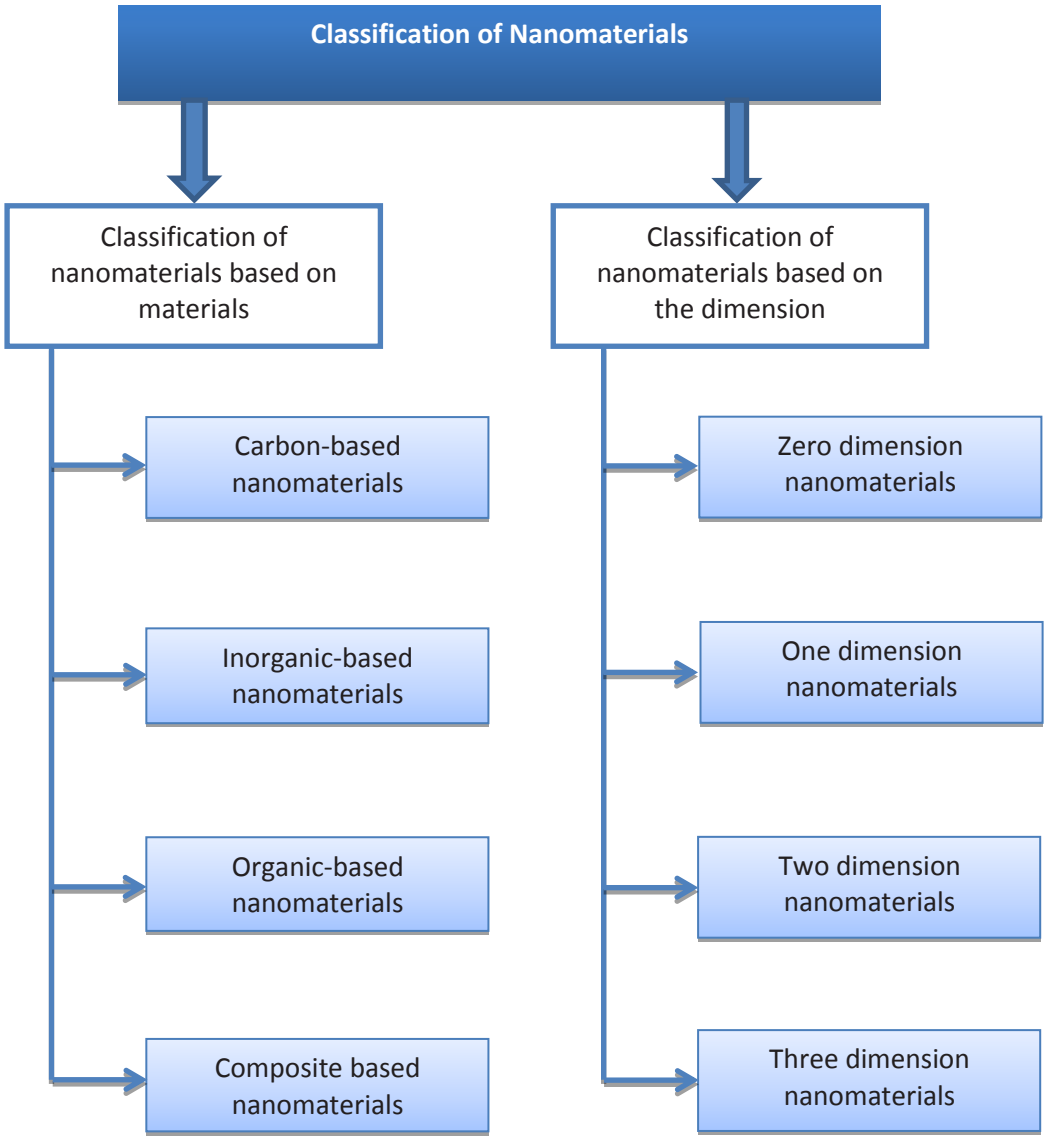

Figure (II.2): Schematic diagram showed the basic classification of nanomaterials.

II.3.1- Classification of nanomaterials based on their materials

Nanomaterials can be classified based on their materials into different categories. The most common classification includes: Carbon-based nanomaterials, Inorganic-based materials, Organic-based materials, and Composite-based nanomaterials **[6]**.

II.3.1-1-Carbon-based Nanomaterials

Carbon-based nanomaterials such as fullerenes (C_{60}), carbon nanotubes (CNTs), carbon nanofibers, carbon black, and graphene (Gr) are found in various morphologies, such as hollow tubes, ellipsoids, or spheres **[7].** These materials are produced through methods such as laser ablation, arc discharge, and chemical vapor deposition. Carbon nanomaterials exhibit distinct physical and chemical properties compared to bulk materials, offering diverse applications in various fields **[8]**.

II.3.1-1- a. Fullerenes

Fullerenes are a type of carbon allotropes with molecules consisting of carbon atoms connected by single and double bonds to form a closed or partially closed cage-like structure. They are made up of 12 pentagonal and varying numbers of hexagonal faces, often forming a roughly spherical shape known as a "buckyball" **[9]**. Fullerenes exhibit diverse shapes and sizes, showing stability while retaining a degree of reactivity. Their unconventional reactivity makes them a unique participant in organic reactions, which have diverse applications due to their distinctive properties. **[10]**. Figure **(II.3)**.

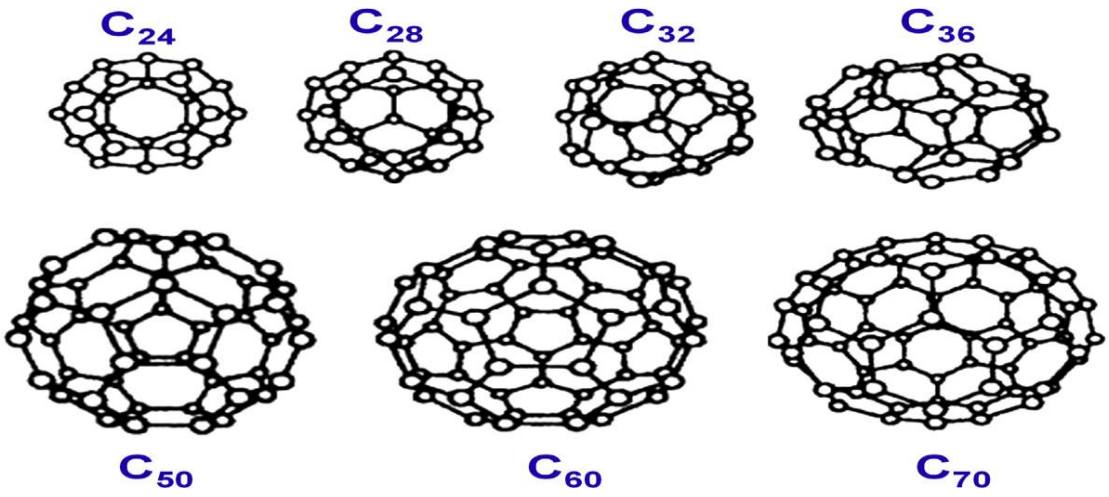

Figure (II.3): Types of Fullerenes **[10].**

II.3.1-1-b. Carbon nanotubes (CNTs)

Carbon nanotubes (CNT) are the fundamental building blocks of nanotechnology. Nanotechnology heavily relies on carbon, which has an atomic number of six. While researching the graphite electrode surface used in electric arc discharge, Iijima unintentionally discovered them. This unintentional discovery laid the groundwork for the exciting field of nanotechnology and launched a new direction in carbon research. A carbon nanotube (CNT) is a hexagonal array of carbon atoms rolled up into a long, thin, hollow cylinder known for its size, shape, and extraordinary physical properties. They can be chemically and physically manipulated in material science, electronics, energy management, biomedical applications, and many other fields **[11]**. They can be single-walled (SWCNT) with a diameter of less than 1 nanometer (nm) or multi-walled (MWCNT) with diameters greater than 100 nm. Their length can range from a few micrometers to several millimeters **[11]**. Wherein:

1. Single-walled nanotubes (SWNTs) in which we can observe three possible classes, named: Zigzag, Chiral, and Armchair **[12]**, and
2. Multi-walled carbon nanotubes (MWNTs).

To describe these nanotubes, the chiral vector (Ch) defines the unit cell, which is defined as the circumference of the surface of the tube. The chiral vector is given by **[13]**:

$$\vec{C}_h = n\vec{a}_1 + m\vec{a}_2 \qquad \textbf{(II.1)}$$

Where:

a_1 and a_2 : are unit vectors in the two-dimensional hexagonal lattice.

n and m : are integers.

The chiral index or chirality is determined by the pair of integers (n, m). The chiral angle (θ) can be obtained from the relation **[13]**:

$$\tan\theta = \frac{\sqrt{3}m}{2n+m} \qquad \textbf{(II.2)}$$

Therefore, the three types of CNTs can be determined by the chiral angle and chirality indices, which their values are **[13]**:

- Zigzag if (m =0 or n=0, θ = 30°).
- Armchair if (n =m, θ = 0°).
- Chiral if (0 < |m| < n, 0 < θ < 30◦).

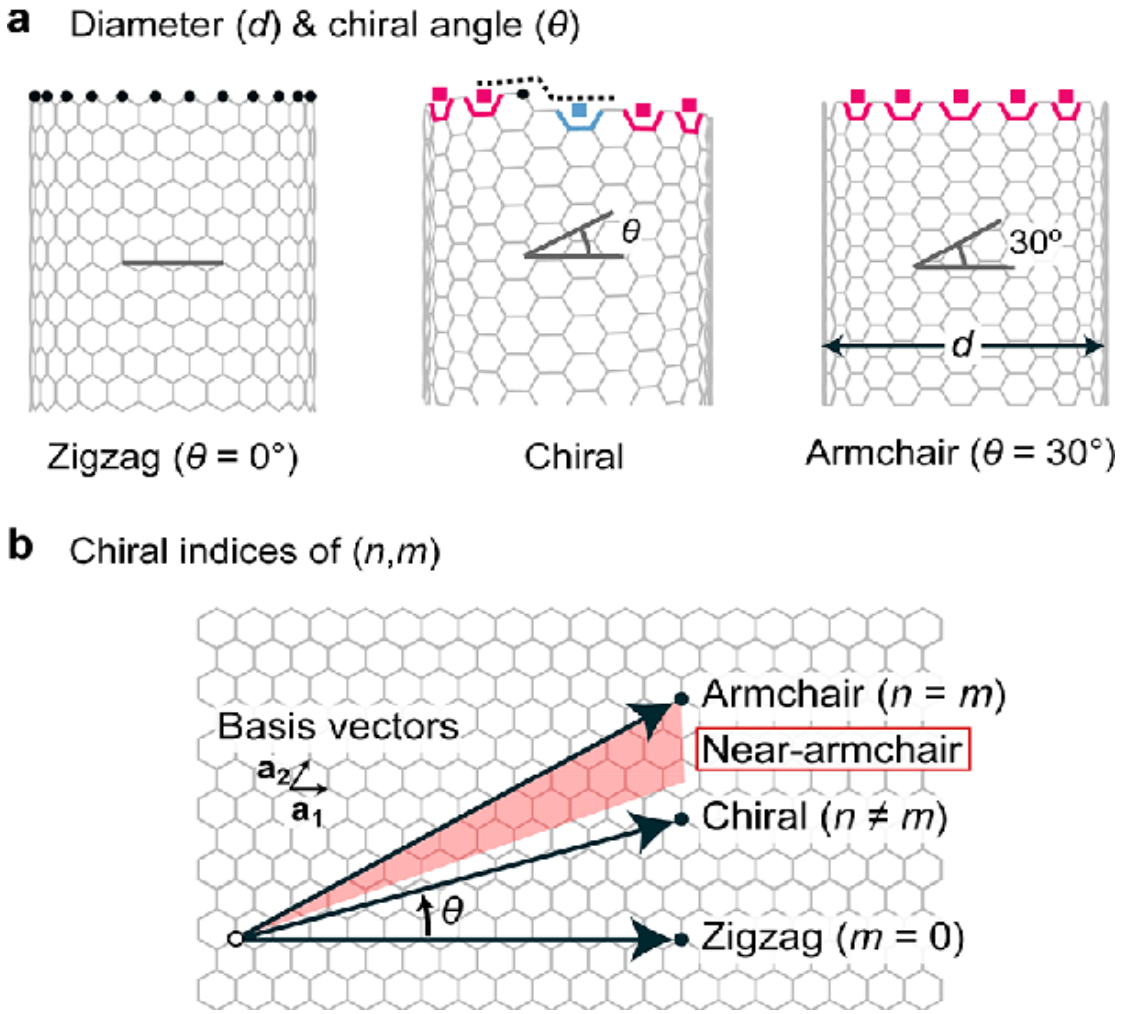

Figure (II.4): Structural classification of single-walled carbon nanotubes **[14]**.

II.3.1-1-c. Carbon nanofibers

Graphene nanofoils utilized in carbon nanofiber manufacturing possess a distinct structure from carbon nanotubes (CNTs), despite being composed of the same graphene material. In contrast to the cylindrical tubes of CNTs, the graphene molecules in nanofoils are arranged in a conical or cup-like configuration. They are typically produced through the chemical vapor decomposition of hydrocarbon feedstock on a metallic catalyst, with diameters ranging from 50-200 nm and lengths up to around 100 µm **[15,16]**.

II.3.1-1-d. Carbon black

Carbon black is a form of amorphous nanomaterial consisting of carbon atoms arranged in spherical shapes, typically ranging from 20 to 70 nm in diameter. The strong particle-particle interaction of carbon black leads to their aggregation, forming clusters with sizes around 500 nm **[17]**.

II.3.1-1-e. Graphene

Graphene is a two-dimensional material composed of a single layer of carbon atoms arranged in hexagons resembling a honeycomb structure. It is considered the first and simplest example of a two-dimensional crystal, exhibiting unique properties due to its two-dimensional nature. has significant potential for various applications in electronics, touch screens, thermal management, and biological studies. Graphene science and technology have advanced fast since its discovery in 2004, with ongoing research focusing on industrial-scale production methods to unlock its full potential **[18]**. Graphene can be wrapped up into zero-dimensional (0D) fullerenes, rolled into one-dimensional (1D) nanotubes, or stacked into three-dimensional (3D) graphite **[19]**, as depicted in Figure **(II.5)**:

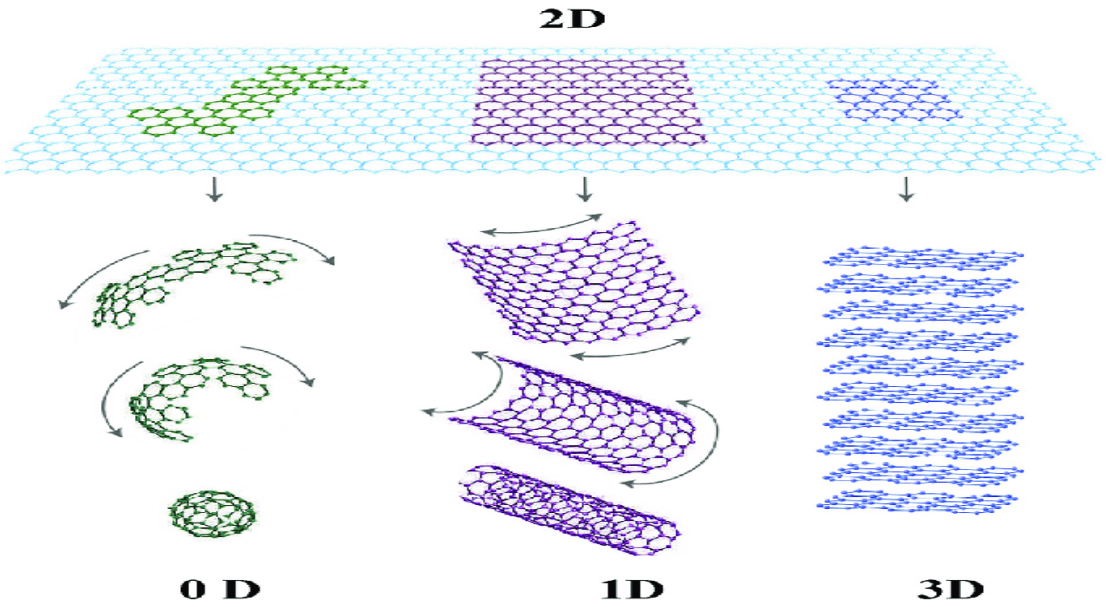

.

Figure (II.5): Graphene similar structures **[19]**.

II.3.1-2-Inorganic-based Nanomaterials

Metals like Ag, Au, and Fe, along with metal oxides such as TiO_2, ZnO, and MnO_2, can indeed be synthesized into nanomaterials. Furthermore, semiconductor nanomaterials can be synthesized from silicon and ceramic materials. These processes involve advanced techniques to create nanoparticles with unique properties suitable for various applications in fields like medicine, energy, and biotechnology **[20]**.

II.3.1-3-Organic-based Nanomaterials

Organic-based nanomaterials are synthesized through self-assembly or transformation from organic matter into the desired structure. These nanomaterials, composed of organic matter other than carbon and inorganic material, rely on noncovalent weak interactions for their formation **[21]**.

II.3.1-4-Composite-based Nanomaterials

Composite nanomaterials are composed of one or more layers of nanoparticles integrated with other types of nanoparticles, bulk materials, or intricate substances such as metal frameworks. These composites encompass a diverse range of materials including metals, ceramics, organics, inorganics, carbon-based compounds, and bulk polymers. The structures and configurations of these materials vary depending on the synthesis method employed and the specific properties needed for their intended applications **[22,23]**.

II.3.2- Classification of nanomaterials based on their dimensions

Siegel categorized nanomaterials into four groups: zero-dimensional, one-dimensional, two-dimensional, and three-dimensional nanostructures. This classification is determined by the number of dimensions that are not restricted to the nanoscale range **[24]**.

II.3.2-1- Zero-Dimensional materials

Zero-dimensional nanoparticles are nanomaterials characterized by all dimensions falling within the nanoscale range, meaning none of their dimensions exceed 100 nm. These nanoparticles are essentially point-like particles, incredibly small in size. They represent the most prevalent type of nanomaterials. Examples of zero-dimensional nanoparticles include quantum dots, hollow spheres, and nano lenses. The classification of nanomaterials according to their dimensionality divides them into nanoparticles, nanotubes, and nanofilms **[25]**.

II.3.2-2- One-Dimensional materials

One-dimensional nanoparticles are a class of nanomaterials defined by having at least one dimension larger than the nanoscale, while the remaining dimensions fall within the nanoscale range. Common examples of one-dimensional nanoparticles include nanofibers, nanotubes, and nanorods. Nanotubes, nanorods, and nanowires exemplify one-dimensional structured materials that are within the nanoscale in two dimensions **[26,27]**.

II.3.2-3- Two-Dimension materials

Two-dimensional nanomaterials are defined by having two dimensions larger than the nanoscale (100 nm), while the remaining dimension falls within the nanoscale range. Common examples of this category include nanofilms, nanolayers, and nanocoating. These nanomaterials typically exhibit plate-like structures, such as graphene. Nanosheets or nanolayers are considered nano-objects, as they are nanoscale in only one dimension **[28]**.

II.3.2-4- Three-Dimensional materials

Three-dimensional nanomaterials are characterized by all three dimensions being larger than 100 nm, while their components remain below 100 nm in size. These materials are formed when nanoparticles within the nano range aggregate to create three-dimensional structures. Typically nonporous, these materials find numerous applications. Common examples include nanocomposites, bundles of nanofibers, and multi-layered nanolayer structures **[29]**.

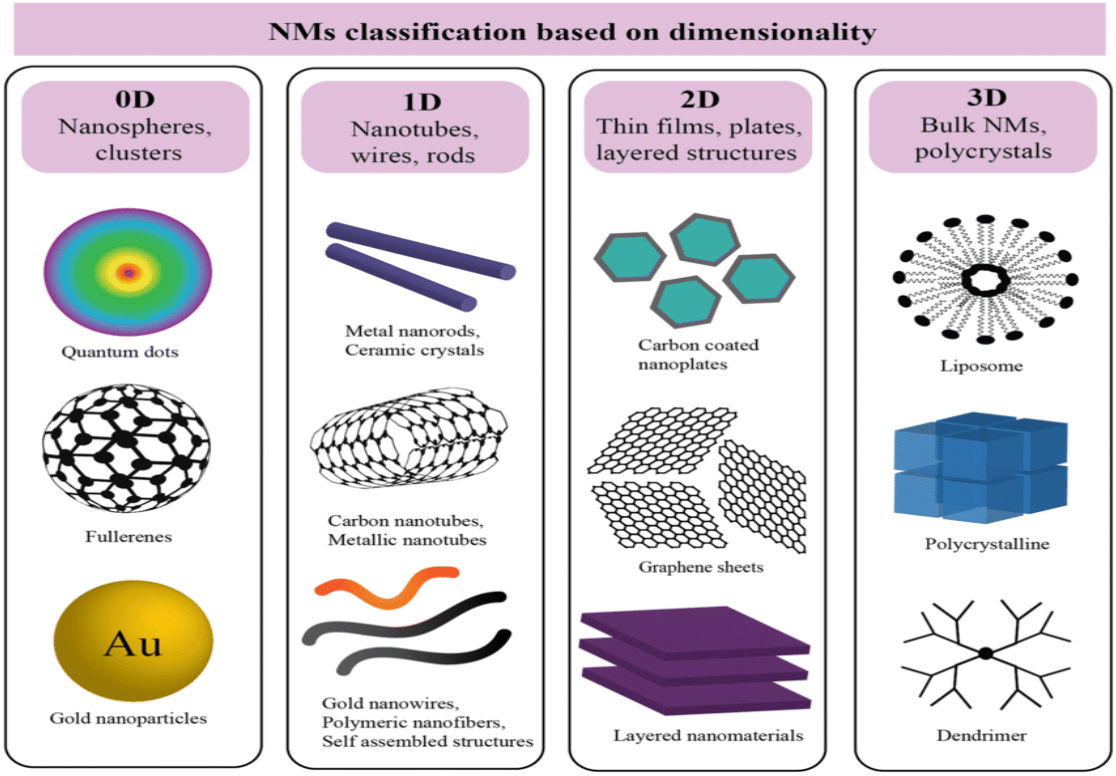

Figure (II.6): Nanomaterials classification based on dimensions **[30]**.

II.4. Nanomaterial's properties

Nanomaterials exhibit unique properties attributed to their increased surface area and reduced size compared to bulk materials. These properties are characterized in terms of both physical and chemical attributes **[31]**.

II.4.1-Physical properties

Nanomaterials exhibit a variety of physical properties, including optical, mechanical, hydrophilic, hydrophobic, suspended, stabilized, thermal, magnetic, and electrical properties **[32]**. The following points provide brief explanations of these properties.

II.4.1-1-Optical properties

Nanomaterials showcase distinctive and captivating optical properties **[33]**, which comprise characteristics such as color, transparency, absorption, transmission, reflection, and light emission **[34]**.

II.4.1-2-Magnetic and electrical properties

The magnetic and electrical properties of nanomaterials hold paramount importance across a spectrum of applications spanning electronics, energy, and various other domains. Electrical characteristics of nanomaterials encompass conductivity, resistivity, and dielectric permittivity, heavily influenced by nanoparticle size and morphology. Notably, the electrical conductivity of nanomaterials may elevate in correlation with their aspect ratio and alignment. Conversely, the magnetic properties, including coercivity, magnetization, and magnetic susceptibility, are contingent upon nanoparticle size, shape, and composition **[35,36]**.

II.4.1-3-Mechanical Properties

Nanoparticles boast a range of mechanical properties, including elasticity, tensile strength, hardness, and flexibility, which are instrumental in their application across diverse fields **[17]**. The mechanical robustness and modulus of nanomaterials are intricately linked to their structure, size, and composition **[37,38]**.

II.4.1-4-Other Properties

Nanomaterials encompass significant attributes like hydrophilicity, hydrophobicity, suspension, diffusion, and thermal conductivity. These characteristics, along with their potential impact on various properties, have spurred numerous innovative applications in fields such as medicine and beyond **[32]**.

II.4-2. Chemical properties

Chemical properties, including stability, sensitivity, corrosion and corrosion resistance, oxidation, reduction, antifungal properties, toxicity, antibacterial effects, and disinfection capabilities, are extremely important in nanoparticles, especially in fields such as chemical

and biomedical engineering **[17]**. The high number of atoms on the surface of nanomaterials increases the average energy compared to larger structures, thereby enhancing their catalytic activity compared to bulk materials **[39]**.

II.5. Application of Nanomaterials in Physics

Nanomaterials have numerous applications in various fields, including physics. Some of the key applications of nanomaterials in physics include:

- Energy Applications: Nanotechnology is crucial in the development of new energy storage devices, such as batteries and supercapacitors, and in the creation of more efficient solar cells and fuel cells **[40]**.
- Optical Applications: Nanomaterials can be used to create advanced optical devices, such as nanostructured surfaces for improved light absorption and emission, and nanoscale optical fibers for enhanced data transmission **[41]**.
- Electromagnetic Applications: Nanomaterials can be designed to exhibit unique electromagnetic properties, such as high dielectric constants, high magnetic permeability, and high thermal conductivity, making them useful for applications like electromagnetic shielding, antennas, and thermal management **[42]**.
- Quantum Computing and Information Processing: Nanomaterials can be used to create quantum dots and other nanostructures that are essential for quantum computing and information processing **[43]**.

II.6. Gallium sulfide (GaS)

II.6.1-definition of Gallium Sulfide (GaS)

The compound corresponds to gallium sulfide, a chemical compound made of gallium and sulfur. Gallium sulfide can exist in different forms **[44]**, including gallium (II) sulfide (GaS) and gallium (III) sulfide (Ga2S3). In addition, Gallium sulfide is a semiconductor material **[45].**

Based on the search results provided, the compound GaS (gallium sulfide) which can exist in several different crystalline forms:

- ✓ Hexagonal β-GaS (space group P63mc)
- ✓ Monoclinic α'-GaS (space group Cc)
- ✓ Cubic γ-GaS (space group F-43m)
- ✓ Rhombohedral GaS (space group $R\bar{3}m$)

The gallium sulfide compound (GaS), which can exist in different crystalline forms. One of these forms is hexagonal β-GaS, which has a specific crystal structure characterized by the space group P63mc. This hexagonal β-GaS is the energetically favorable crystal arrangement among the four GaS polytypes. The layers in this structure are stacked together via van der Waals interactions, making it possible to exfoliate the structure into thin 2D layers.

II.6.2- Properties of Gallium Sulfide (GaS)

Gallium sulfide has several distinct properties that make it useful in various applications:

- Optical Properties: Gallium sulfide exhibits nonlinear optical activities, including second-harmonic generation and two-photon excited fluorescence.
- Optical Applications: Gallium sulfide exhibits nonlinear optical properties, such as second-harmonic generation and two-photon excited fluorescence, making it useful for optical and photonic devices.
- Thermal Properties: Gallium sulfide has a melting point of 965 °C (1,769 °F).
- Density: The density of gallium sulfide is 3.86 $g.cm^{-3}$
- Molar Mass: The molar mass of gallium sulfide is 101.788 $g.mol^{-1}$

II.6.3- Applications of Gallium Sulfide (GaS)

Gallium sulfide can be used to produce thin-film transistors, solar cells, and light-emitting diodes (LEDs). Also can be used in the synthesis of various compounds and materials in the chemical industry **[46]**. Gallium sulfide has been investigated for its potential use in electrochemical hydrogen production applications. The current increased attention towards gallium sulfide can be attributed to its use in photocatalysis applications **[47]**.

II.7. Gallium selenide (GaSe)

II.7.1-definition of Gallium Selenide (GaSe)

Gallium selenide (GaSe) is one of the layered group-III metal monochalcogenides, which has an indirect bandgap in monolayer and a direct bandgap in bulk unlike other conventional transition metal dichalcogenides **[48]**, in addition, Gallium selenide (GaSe) is a layered semiconductor material.

The crystalline forms of Gallium selenide (GaSe) include:

- ✓ Hexagonal crystal structure: GaSe has a hexagonal crystal structure, similar to the hexagonal β-GaS polymorph.
- ✓ Monoclinic crystal structure: GaSe can also exist in a monoclinic crystal structure.

- ✓ Cubic crystal structure: GaSe may have a cubic crystal structure as well.

II.7.2- Properties of Gallium Selenide (GaSe)

The properties of Gallium selenide (GaSe) include:

- Bandgap: GaSe has an indirect bandgap of approximately 2.1 eV, making it a semiconductor material **[49]**.
- Optical Properties: Gallium selenide crystals possess wide optical transparency, ranging from the wavelength of 0.65 to 18 mm. This property makes GaSe suitable for applications in integrated optics, optical information communications, and biology **[49]**.
- Crystal Structure: GaSe has a hexagonal crystal structure, similar to the structure of gallium sulfide (GaS), with individual layers consisting of covalently-bonded stacks of Se ions on the top and bottom and Ga ions in the middle. The adjacent layers are bound by weak van der Waals forces, allowing for mechanical or liquid exfoliation into ultra-thin few or single-layer 2D gallium selenide nanosheets or nanoparticles **[49]**.
- Synthesis: GaSe nanoparticles can be synthesized through a reaction of GaMe3 with trioctylphosphine selenium (TOPSe) in a high-temperature solution of trioctylphosphine (TOP) and trioctylphosphine oxide (TOPO) **[50]**.
- GaSe appears to be a possible candidate material for optical frequency conversion in the near to far infrared (1–18 μm) wavelength **[51]**.

II.7.3- Applications of Gallium sulfide (GaSe)

Gallium sulfide is utilized in the semiconductor industry for manufacturing electronic components and optoelectronic devices like transistors and photodetectors. It is studied for its potential in next-generation solar cells, enabling the conversion of solar energy into electrical energy. Due to its optical properties, Gallium sulfide is used in producing optical materials such as lenses, windows, and infrared optical components. Gallium sulfide is applied in the chemical industry for synthesizing various compounds and materials, acting as a precursor for other gallium-based compounds with specific properties **[52]**.

II.8. Gallium telluride (GaTe)

II.8.1-Definition of Gallium telluride (GaTe)

Gallium telluride (GaTe) is a chemical compound of gallium and tellurium. It is a direct band gap semiconductor with an energy of 1.65eV at room temperature **[53,54]**.

Based on the search results provided, the main crystalline forms of Gallium telluride (GaTe) are:

- ✓ Monoclinic crystal structure
- ✓ Hexagonal (superlattice) form

II.8.2- Properties of Gallium telluride (GaTe)

The properties of Gallium telluride (GaTe) include:

- It belongs to the group-13 post-transition metal monochalcogenides and has a monoclinic crystal structure **[55]**.
- The layers of GaTe are stacked together via van der Waals interactions and can be exfoliated into thin 2D layers **[55]**.
- GaTe crystals are typically hexagonal and have a metallic appearance **[55]**.
- The material exhibits good p-type transport properties and a direct bandgap in the bulk, which is unique among layered materials **[56]**.
- The material's properties can also be influenced by the presence of air, where mechanically exfoliated GaTe develops a deep-level defect band, reducing the bandgap in a direct-to-indirect transition to about 0.8 eV **[56]**.

II.8.3- Applications of Gallium telluride (GaTe)

GaTe is widely used as an evaporation material for depositing thin films on semiconductor and optical surfaces. Its high evaporation rates and low melting point make it an ideal choice for many coating and deposition processes. GaTe is used in the fabrication of high-frequency electronic devices due to its high electronic mobility. GaTe has applications in nonlinear optical devices and systems due to its unique optical propertie7R54s. GaTe has been considered a candidate material for radiation detection applications given its semiconductor properties.

References

[1] Wilfred L.F. Armarego. Chapter 5 – Nanomaterials. Purification of Laboratory Chemicals (Ninth Edition). 2 September 2022 P 586-630. https://doi.org/10.1016/B978-0-323-90968-6.50005-9.

[2] W. Brullot, Development, synthesis and characterization of multifunctional nanomaterials, Ku Leuven. (2014).

[3] B. F. Johnson, Nanoparticles in catalysis. Topics in Catalysis **24**, 147–159 (2003).

[4] G. A. Ozin, A. Arsenault, Nanochemistry: A Chemical Approach to Nanomaterials. The Royal Society of Chemistry, Cambridge, UK, 2nd edition (2009).

[5] İ.M. Alkaç, B. Çerçi, C. Timuralp, F. Şen, 2 - Nanomaterials and their classification, in: F.B.T.-N. for D.A.F.C. Şen (Ed.), Micro Nano Technol., Elsevier, 2021: pp. 17–33. https://doi.org/https://doi.org/10.1016/B978-0-12-821713-9.00011-1.

[6] J. Jeevanandam, A. Barhoum, Y.S. Chan, A. Dufresne, M.K. Danquah, Review on nanoparticles and nanostructured materials: History, sources, toxicity and regulations, Beilstein J. Nanotechnol. 9 (2018) 1050–1074. https://doi.org/10.3762/bjnano.9.98.

[7] N. Rao, R. Singh, L. Bashambu, Carbon-based nanomaterials: Synthesis and prospective applications, Mater. Today Proc. 44 (2021) 608–614. https://doi.org/https://doi.org/10.1016/j.matpr.2020.10.593.

[8] A.D. Goswami, D.H. Trivedi, N.L. Jadhav, D. V Pinjari, Sustainable and green synthesis of carbon nanomaterials: A review, J. Environ. Chem. Eng. 9 (2021) 106118. https://doi.org/https://doi.org/10.1016/j.jece.2021.106118.

[9] Kroto, Harold W. and Walton, David R.M.. "fullerene". Encyclopedia Britannica, 22 Dec. 2023, https://www.britannica.com/science/fullerene. Accessed 29 April 2024.

[10] B.D. Malhotra, M.A. Ali, Functionalized Carbon Nanomaterials for Biosensors, Nanomater. Biosens. (2018) 75–103. https://doi.org/10.1016/b978-0-323-44923-6.00002-9.

[11] Jyoti Bashyal, Carbon Nanotube- Definition, Properties, and Applications. Science Info. December 12, 2022. https://scienceinfo.com/carbon-nanotube.

[12] H. An, A. Kumamoto, R. Xiang, T. Inoue, K. Otsuka, S. Chiashi, C. Bichara, A. Loiseau, Y. Li, Y. Ikuhara, S. Maruyama, Atomic-scale structural identification and evolution of Co-W-C ternary SWCNT catalytic nanoparticles: High-resolution STEM

imaging on SiO2, Sci. Adv. 5 (2023) eaat9459. https://doi.org/10.1126/sciadv.aat9459.

[13] A. Aqel, K.M.M.A. El-Nour, R.A.A. Ammar, A. Al-Warthan, Carbon nanotubes, science and technology part (I) structure, synthesis and characterisation, Arab. J. Chem. 5 (2012) 1–23. https://doi.org/https://doi.org/10.1016/j.arabjc.2010.08.022.

[14] T. Nishihara, A. Takakura, K. Matsui, K. Itami, Y. Miyauchi, Statistical Verification of Anomaly in Chiral Angle Distribution of Air-Suspended Carbon Nanotubes, Nano Lett. 22 (2022). https://doi.org/10.1021/acs.nanolett.2c01473.

[15] I. Ijaz, E. Gilani, A. Nazir, A. Bukhari, Detail review on chemical, physical and green synthesis, classification, characterizations and applications of nanoparticles, Green Chem. Lett. Rev. 13 (2020) 223–245. https://doi.org/10.1080/17518253.2020.1802517.

[16] D. Torres, S. Pérez-Rodríguez, D. Sebastián, J.L. Pinilla, M.J. Lázaro, I. Suelves, Graphene oxide nanofibers: A nanocarbon material with tuneable electrochemical properties, Appl. Surf. Sci. 509 (2020) 144774. https://doi.org/https://doi.org/10.1016/j.apsusc.2019.144774.

[17] V. Singh, P. Yadav, V. Mishra, Recent Advances on Classification, Properties, Synthesis, and Characterization of Nanomaterials, Green Synth. Nanomater. Bioenergy Appl. (2020) 83–97. https://doi.org/10.1002/9781119576785.ch3.

[18] Mikhail I. Katsnelson. Graphene as a two-dimensional material. Britannica. https://www.britannica.com/science/graphene/Graphene-as-a-two-dimensional-material.

[19] Abdullah Anwar, Bashar Mohammed, Mubarak bin Abdul Wahab, Enhanced Properties of Cementitious Composite Tailored with Graphene Oxide Nanomaterial - A Review. ResearchGate, October 2019. https://www.researchgate.net/figure/Graphene-can-be-wrapped-up-into-various-other-carbon-allotropes-ie-0-D-fullerenes_fig3_337003782. 10.1016/j.dibe.2019.100002.

[20] Yaqoob AA, Ahmad H, Parveen T, Ahmad A, Oves M, Ismail IMI, Qari HA, Umar K, Mohamad Ibrahim MN. Recent Advances in Metal Decorated Nanomaterials and Their Various Biological Applications: A Review. Front Chem. 2020 May 19;8:341. doi: 10.3389/fchem.2020.00341. PMID: 32509720; PMCID: PMC7248377.

[21] Lombardo D, Calandra P, Pasqua L, Magazù S. Self-Assembly of Organic Nanomaterials and Biomaterials: The Bottom-Up Approach for Functional Nanostructures Formation and Advanced Applications. Materials. 2020; 13(5):1048. https://doi.org/10.3390/ma13051048.

[22] D. Sannino, Types and Classification of Nanomaterials BT - Nanotechnology: Trends

and Future Applications, in: M.B. Tahir, M. Rafique, M. Sagir (Eds.), Springer Singapore, Singapore, 2021: pp. 15–38. https://doi.org/10.1007/978-981-15-9437-3_2.

[23] M. Rizwan, A. Shoukat, A. Ayub, B. Razzaq, M.B. Tahir, Chapter 3 - Types and classification of nanomaterials, in: M.B. Tahir, M. Sagir, A.M.B.T.-N.S. Asiri Characterization, Hazards and Safety (Eds.), Micro Nano Technol., Elsevier, 2021: pp. 31–54. https://doi.org/https://doi.org/10.1016/B978-0-12-823823-3.00001-X.

[24] J. Jeevanandam, A. Barhoum, Y.S. Chan, A. Dufresne, M.K. Danquah, Review on nanoparticles and nanostructured materials: history, sources, toxicity and regulations., Beilstein J. Nanotechnol. 9 (2018) 1050–1074. https://doi.org/10.3762/bjnano.9.98.

[25] I. Khan, K. Saeed, I. Khan, Nanoparticles: Properties, applications and toxicities, Arab. J. Chem. 12 (2019) 908–931. https://doi.org/10.1016/j.arabjc.2017.05.011.

[26] S. Bashir, J.L. Liu, Nanomaterials and Their Application, Adv. Nanomater. Their Appl. Renew. Energy. (2015) 1–50. https://doi.org/10.1016/B978-0-12-801528-5.00001-4.

[27] J. Abraham, A. Rehghunadhan, K.C. Nimitha, S. George, S. Thomas, One-dimensional (1D) nanomaterials: Nanorods and nanowires; nanoscale processing, in: 2021: pp. 71–101. https://doi.org/10.1016/B978-0-12-820569-3.00003-7.

[29] A. Mandal, E. Ray Banerjee, Introduction to Nanoscience, Nanotechnology and Nanoparticles BT - Nanomaterials and Biomedicine: Therapeutic and Diagnostic Approach, in: E. Ray Banerjee (Ed.), Springer Singapore, Singapore, 2020: pp. 1–39. https://doi.org/10.1007/978-981-15-5274-8_1.

[30] İ.M. Alkaç, B. Çerçi, C. Timuralp, F. Şen, 2 - Nanomaterials and their classification, in: F.B.T.-N. for D.A.F.C. Şen (Ed.), Micro Nano Technol., Elsevier, 2021: pp. 17–33. https://doi.org/https://doi.org/10.1016/B978-0-12-821713-9.00011-1.

[31] W.L.F. Armarego, Nanomaterials, Purif. Lab. Chem. (2022) 586–630. https://doi.org/10.1016/B978-0-323-90968-6.50005-9.

[32] N. Čitaković, Physical properties of nanomaterials, Vojnoteh. Glas. 67 (2019) 159–171. https://doi.org/10.5937/vojtehg67-18251.

[33] V.M. Rodriguez, H.A. Abhyankar, Optical Properties of Nanomaterials, Nanocomposite Mater. (2016) 81–103. https://doi.org/10.1201/9781315372310-5.

[34] B. Wiley, Introduction: Chemical, physical and mechanical properties of nanomaterials,

Encycl. Nanomater. (2023) 382. https://doi.org/10.1016/B978-0-12-822425-0.00115-9.

[35] G.Y. Yurkov, A.S. Fionov, Y.A. Koksharov, V. V. Koleso, S.P. Gubin, Electrical and magnetic properties of nanomaterials containing iron or cobalt nanoparticles, Inorg. Mater. 43 (2007) 834–844. https://doi.org/10.1134/S0020168507080055.

[36] A. Barhoum, M. Luisa García-Betancourt, Chapter 10 - Physicochemical characterization of nanomaterials: size, morphology, optical, magnetic, and electrical properties, in: A. Barhoum, A.S.H.B.T.-E.A. of N. and A.N. Makhlouf (Eds.), Micro Nano Technol., Elsevier, 2018: pp. 279–304. https://doi.org/https://doi.org/10.1016/B978-0-323-51254-1.00010-5.

[37] N. Joudeh, D. Linke, Nanoparticle classification, physicochemical properties, characterization, and applications: a comprehensive review for biologists., J. Nanobiotechnology. 20 (2022) 262. https://doi.org/10.1186/s12951-022-01477-8.

[38] Y. Hui, X. Yi, F. Hou, D. Wibowo, F. Zhang, D. Zhao, H. Gao, C.-X. Zhao, Role of Nanoparticle Mechanical Properties in Cancer Drug Delivery, ACS Nano. 13 (2019) 7410–7424. https://doi.org/10.1021/acsnano.9b03924.

[39] A.M. Ealias, M.P. Saravanakumar, A review on the classification, characterisation, synthesis of nanoparticles and their application, IOP Conf. Ser. Mater. Sci. Eng. 263 (2017). https://doi.org/10.1088/1757-899X/263/3/032019.

[40] Ahmed Kadhim Hussein, Renewable and Sustainable Energy Reviews. ScienceDirect. 42, February 2015, Pages 460-476. https://www.sciencedirect.com/science/article/abs/pii/S1364032114008442.

[41] Muhammad Aamir Iqbal a, Maria Malik b, Nadia Anwar c, Sunila Bakhsh d, Saher Javeed e, Siti Sarah Maidin f, Kareem Morsy g, Rey Y. Capangpangan h, Arnold C. Alguno i, Jeong Ryeol Choi j. Basic concepts, advances and emerging applications of nanophotonics. Arabian Journal of Chemistry. 16, Issue 9, September 2023, 105040. https://doi.org/10.1016/j.arabjc.2023.105040

[42] Nan, Z., Wei, W., Lin, Z. et al. Flexible Nanocomposite Conductors for Electromagnetic Interference Shielding. Nano-Micro Lett. **15**, 172 (2023). https://doi.org/10.1007/s40820-023-01122-5

[43] Maximilian Russ. Quantum information processing in semiconductor quantum dots using single and multi-spin qubits. researchgate. January 2019.

https://www.researchgate.net/publication/334696065_Quantum_information_processing_in_semiconductor_quantum_dots_using_single_and_multi-spin_qubits

[44] Greenwood, Norman N.; Earnshaw, Alan (1997). Chemistry of the Elements (2nd ed.). Butterworth-Heinemann. ISBN 978-0-08-037941-8.

[45] V. Zolyomi, N. D. Drummond and V. I. Fal'ko (2013). "Band structure and optical transitions in atomic layers of hexagonal gallium chalcogenides". Phys. Rev.B. **87** (19):195403. arXiv:1302.6067. Bibcode:2013PhRvB..87s5403Z. doi:10.1103/PhysRevB.87.195403

[46] Group of expert Nanotechologists. Gallium sulfide Powder. Nano Research Elements. https://www.nanorh.com/about-us/

[47] Yang Lu, Jun Chen, Tongxin Chen, Jamie H. Warner. Controlling Defects in Continuous 2D GaS Films for High-Performance Wavelength-Tunable UV-Discriminating Photodetectors. ResearchChate. Jan 2020. https://www.researchgate.net/figure/Synthesis-and-SEM-images-of-galliumII-sulfide-a-b-Schematic-of-synthesis-of-defective_fig1_338338030

[48] Soo Yeon Lim, Jae-Ung Lee, Jung Hwa Kim, Liangbo Liang, Kong Xiangru, Thanh Huong T. Nguyen, Zonghoon Lee, Sunglae Cho, Hyeonsik Cheong. Polytypism in Few-Layer Gallium Selenide. ResearchChate. March 2020. https://www.researchgate.net/publication/339812968_Polytypism_in_Few-Layer_Gallium_Selenide. 10.1039/D0NR00165A.

[49] Low price, high purity gallium selenide powder and crystals. Gallium Selenide (GaSe) Powder and Crystals. 12024-1. https://www.ossila.com/products/gallium-selenide. M2138C1-500mg**.**

[50] Chikan, V.; Kelley, D. (2002). "Synthesis of Highly Luminescent Nanoparticles". Nano Letters. 2 (2): 141. Bibcode:2002NanoL...2..141C. doi:10.1021/nl015641m

[51] N.C. Fernelius. Properties of gallium selenide single crystal. Sciencedirect. 28, Issue 4, 1994, P 275-353. https://doi.org/10.1016/0960-8974(94)90010-8

[52] Group of expert Nanotechologists. Gallium sulfide Powder. Nano Research https://www.nanorh.com/product/gallium-sulfide-powder/

[53] Chemical Vapor Deposition of Hexagonal Gallium Selenide and Telluride Films from Cubane Precursors: Understanding the Envelope of Molecular Control, E. G. Gillan and

A. R. Barron Chem. Mater., 9 (12), 3037-3048, 1997.

[54] Anharmonicity in GaTe layered crystals, A. Aydinli, N. M. Gasanly, A. Uka, H. Efeoglu, Cryst. Res. Technol. 37 (2002) 12, pp. 1303–1309

[55] G.Meirstraat 1, 9728TB Groningen, The Netherlands. GaTe (Gallium Telluride). hqgraphene. https://www.hqgraphene.com/GaTe.php

[56] Fonseca Vega, Jose JavierAdvisor(s): Dubon, Oscar D Dubon, Oscar D Fonseca Vega, Jose Javier. Bandgap Engineering of Gallium Telluride. Berkeley. 2017. https://escholarship.org/uc/item/9dp4z0f3

CHAPTER III

Results and discussions

III.1. Introduction

Nanomaterials have emerged as an amazing class of materials that can be produced with outstanding magnetic, electrical, optical, mechanical, and catalytic properties that are substantially different from their bulk counterparts. The aim objective of this chapter is to investigate the electronic properties, such as the band structure and density of states, such as the lattice parameter a and c and the modulus of compressibility B and its first derivative B' for materials GaX (X=S, Se, Te) in both bulk 2D and 3D forms. To conduct this study, the WIEN2K code was performed based on the linearized augmented plane wave (LAPW) method that employs the density functional theory (DFT). The exchange and correlation potential were determined using several approximations such as the GGA approximation, LDA approximation, the EV-GGA (Engel-Vosko) approximation, and the mBJ (modified Becke-Johnson) approximation.

III.2. Details of Calculation

In this thesis, the calculations were performed using the Wien2k code which is an implementation of the (FP-LAPW) method in the (DFT) framework. Semi-relativistic calculations were performed (the spin-orbit effect is neglected). The exchange and correlation potentials are treated in the following approximations:

- ✓ The Local Density Approximation (LDA) parameterized by Perdew and Wang **[1]**.
- ✓ The Generalized Gradient Approximation (GGA) parameterized by Perdew, Burke and Ernzerhof **[2]**.

To improve energy gaps:

- ✓ The Engel-Vosko approximation (EV-GGA) **[3]**.
- ✓ The mBJ (modified Becke - Johnson) approximation **[4]**.

The calculation is for specifying the values of the input parameters. The charge density and potential have been developed on spherical harmonics multiplied by the radial functions around the atomic sites, i.e., in the Muffin-Tin spheres Muffin-Tin spheres and in plane waves in the interstitial region G_{max}.

For each calculation, we specify the following important parameters:

- ✓ The radii of the Muffin-Tin spheres (R_{MT}), given in atomic units (Bohr radius) or in Angstrom (A°).

- ✓ The cut-off parameter $RK_{max} = \boldsymbol{R_{MTmin}} \times K_{max}$, where $\boldsymbol{R_{MTmin}}$ is the mean radius of the Muffin-Tin spheres and K_{max} the norm of the largest wave vector used for the plane-wave expansion of the eigenfunctions. In order to obtain convergence of the energy eigenvalues, the wave functions in the interstitial region were increased in plane waves with a cut-off of $RK_{max} = \boldsymbol{R_{MTmin}} \times K_{max}=8$ in (3D) and $RK_{max} = \boldsymbol{RMTmin} \times K_{max}=8$ in (2D).
- ✓ The number of points k considered in the Brillouin zone: We have chosen k points =1000 in (3D) and k points =500 in (2D).

Knowing that the convergence of the total energy per crystal mesh depends on the number of K points used in the calculation, the Brillouin zone was carefully sampled using the special point technique of Monkhorst and Pack **[5,6]**.

The table below shows the convergence parameters obtained and used to calculate the physical properties of the compounds GaX (X=S, Se, Te) in (3D) and (2D):

Table (III.1): Values of RK_{max}, K-points, and R_{MT} for the compounds GaX (X=S, Se, Te) in (3D) and (2D).

Compound	Approximation	$R_{MT_{min}} \times K_{max}$	K Points	R_{MT} (Ga)	R_{MT} (S)	R_{MT} (Se)	R_{MT} (Te)
GaS (3D)	GGA	8	1000	2.17	1.93	-	-
	LDA	8	1000	2.18	1.93	-	-
GaSe (3D)	GGA	8	1000	2.17	-	2.21	-
	LDA	8	1000	2.18	-	2.2	-
GaTe (3D)	GGA	8	1000	2.18	-	-	2.45
	LDA	8	1000	2.14	-	-	2.41
GaS (2D)	GGA	8	500	2.2	2	-	-
	LDA	8	500	2.2	2	-	-
GaSe (2D)	GGA	8	500	2.25	-	2.28	-
	LDA	8	500	2.2	-	2.24	-
GaTe (2D)	GGA	8	500	2.26	-	-	2.45

III.3. Crystal structure and electronic configuration of GaX (X=S, Se, Te) in (3D) and (2D) materials

III.3.1. The electronic configuration

The electronic configuration refers to the arrangement of electrons around the nucleus of an atom or molecule. It describes how electrons are distributed in atomic orbitals, including shells, sub-shells, and orbitals within the atom. Hence, the electronic structure of the materials GaX (X=S, Se, Te) is as follows:

Table (III.2): the electronic configuration of GaX (X=S, Se, Te).

Element	Number of electrons Z	Electronic Configuration
Ga	**31**	$[Ar]\ 3d^{10}4s^{2}4p^{1}$
S	**16**	$[Ne]\ 3s^{2}3p^{4}$
Se	**34**	$[Ar]\ 3d^{10}4s^{2}4p^{4}$
Te	**52**	$[Kr]\ 4d^{10}5s^{2}5p^{4}$

III.3.2. Crystal structure of GaX (X=S, Se, Te) in (3D) and (2D)

GaX (X=S, Se, Te) materials crystallize in a hexagonal crystal system and belong to the space group with the following:

- GaX (X=S, Se, Te) in 3D: P63/mmc, (n=194).
- GaX (X=S, Se, Te) in 2D: P63/mmc, (n=194).

The Figures below shows the crystal structure of GaX (X=S, Se, Te) in (3D) and (2D):

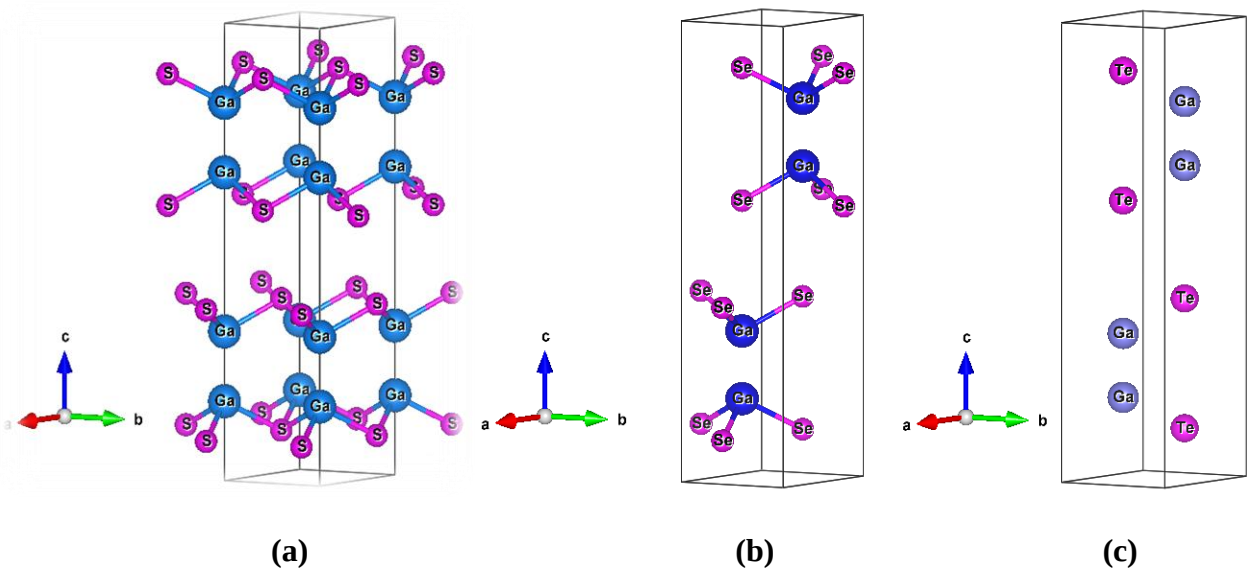

(a) **(b)** **(c)**

Figure (III.1): The crystal structure of GaS (a), GaSe (b) and GaTe (c) in (3D).

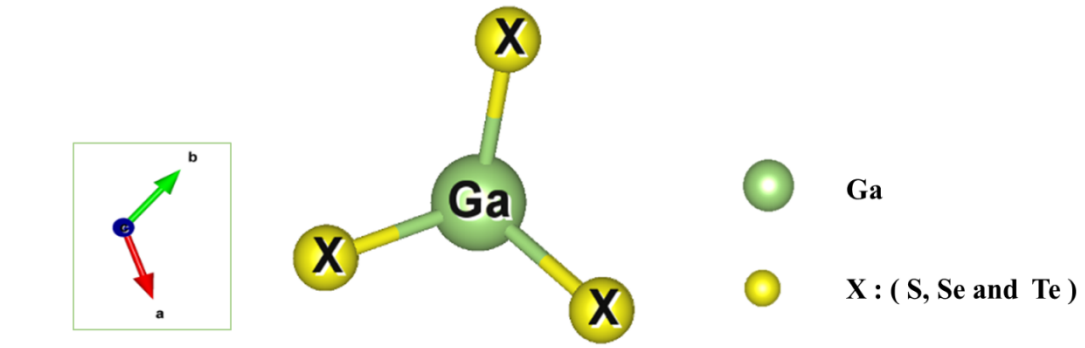

(a)

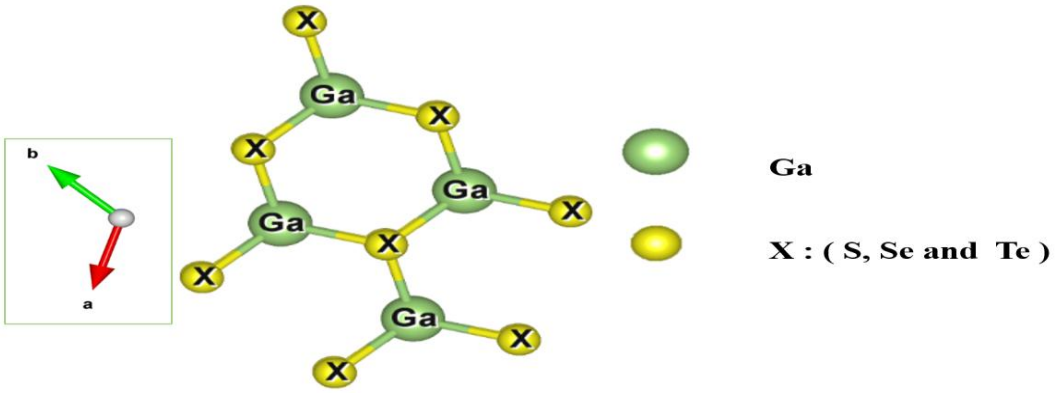

(b)

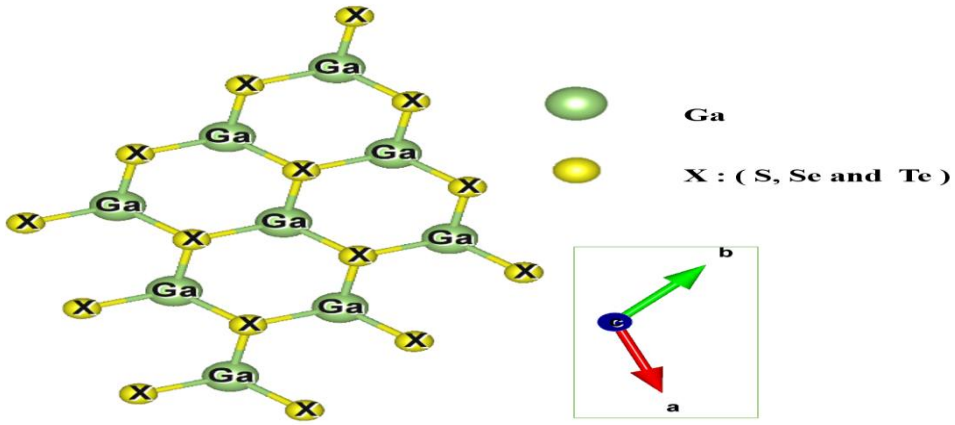

(c)

Figure (III.2): The crystal structure of GaS, GaSe and GaTe in (2D), **(a):**is super-cell (1x1x1). **(b):** is super-cell (2x2x1). **(c):** is super-cell (3x3x1).

.

III.4. Structural properties

The arrangement of atoms and molecules at the microscopic level determines a material's physical and chemical properties, known as its structural properties. The relationship between the structure and properties of materials is important in rationally designing new materials **[7]**.

To evaluate the structural properties of the two-dimensional (2D) and three-dimensional (3D) as theoretical lattice parameters, the compressibility modulus B and its derivative concerning pressure B' from the fundamental equilibrium state, the total energy obtained is extrapolated, and the energy values thus obtained are then interpolated by Murnaghan (1944) **[8,9]**.

$$E(V) = E_0 + \frac{B}{B'(B'+1)}\left[V\left(\frac{V_0}{V} - V_0\right)\right] + \frac{B}{B'}(V - V_0) \quad \textbf{(III.1)}$$

Where:

E_0 : is the total energy.

V_0 : is the volume at equilibrium.

B : the compressibility modulus.

The compressibility modulus is determined at the minimum of the E(V) curve by the relation:

$$B = V\frac{\partial^2 E}{\partial V^2} \quad \textbf{(III.2)}$$

B' : The derivative of the modulus of compressibility:

$$\beta' = \frac{\partial \beta}{\partial P} \quad \textbf{(III.3)}$$

III.4.1. Optimization Curves

To precisely explain the structural properties of our 2D and 3D materials GaX (X=S, Se, Te). We optimized a computation using two different approximations GGA and LDA as shown in Figure (Ⅲ.3) and Figure (Ⅲ.4). Therefore, it can be inferred that the GGA and LDA approximations are the most suitable for describing the structural properties

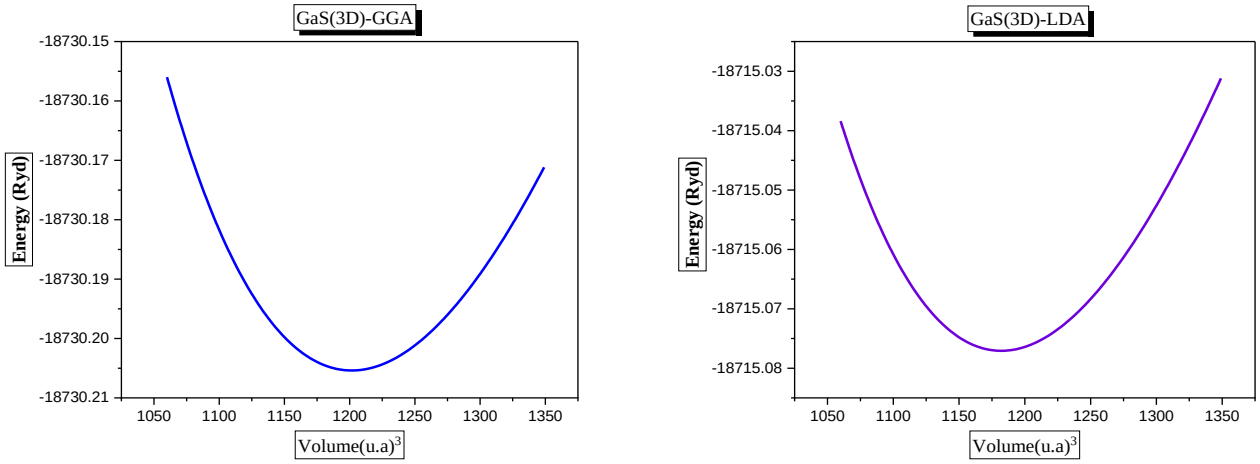

Figure (III.3): (a): The variation of energy as a function of volume for GaS (3D) using GGA and LDA approximations.

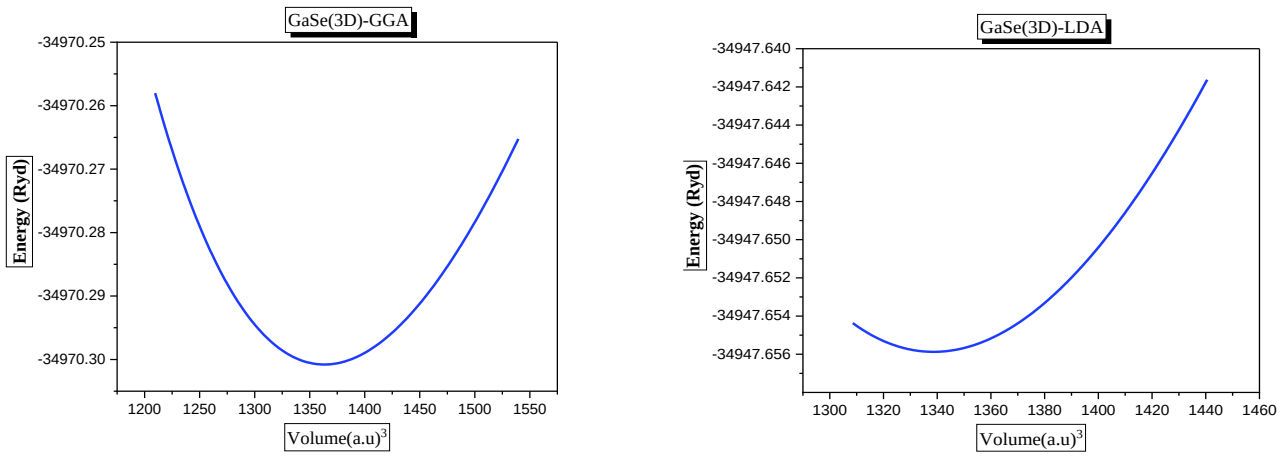

Figure (III.3): (b): The variation of energy as a function of volume for GaSe (3D) using GGA and LDA approximations.

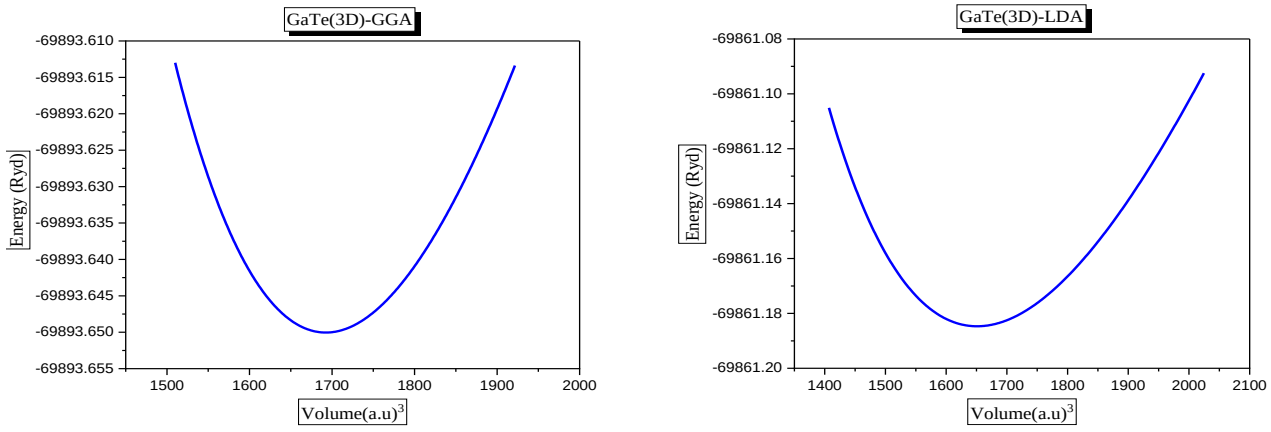

Figure (III.3): (c): The variation of energy as a function of volume for GaTe (3D) using GGA and LDA approximations.

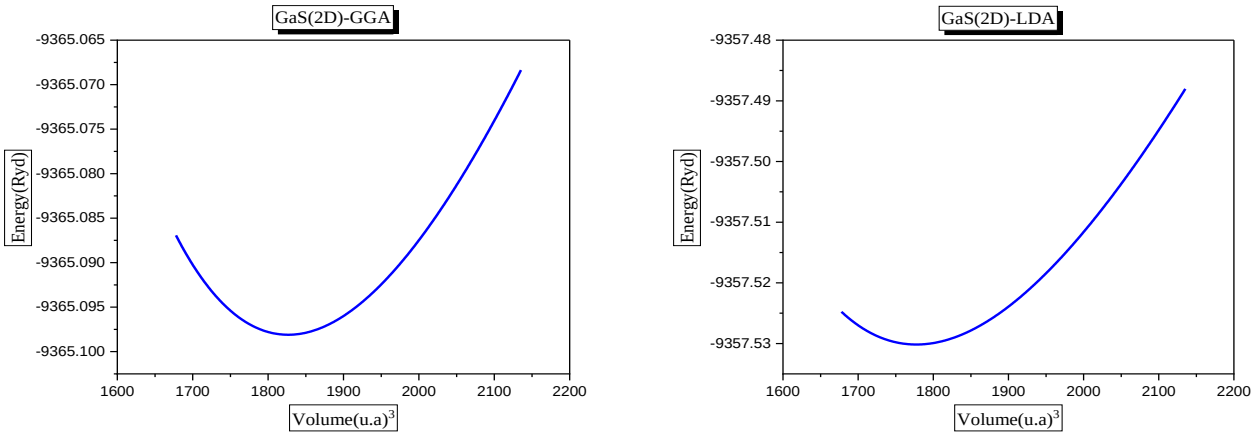

Figure (III.4): (a): The variation of energy as a function of volume for GaS (2D) using GGA and LDA approximations.

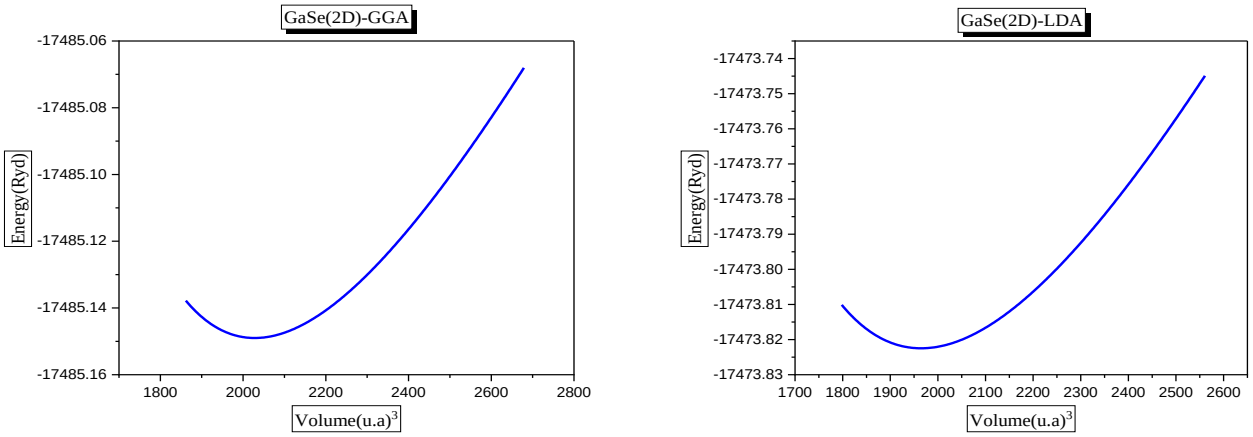

Figure (III.4): (b): The variation of energy as a function of volume for GaSe (2D) using GGA and LDA approximations.

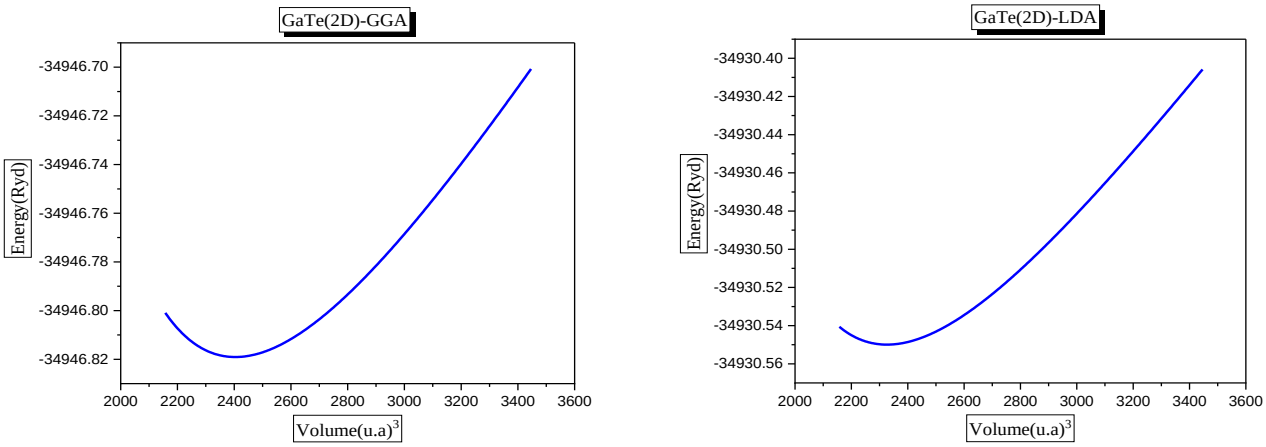

Figure (III.4): (c): The variation of energy as a function of volume for GaTe (2D) using GGA and LDA approximations.

III.4.2. Table of Structural Properties

In the table below we put the structural properties of the materials GaX (X=S, Se, Te) in 3D and 2D:

Table (III.3): Calculated structural parameters of GaX (X=S, Se, Te) in (3D) using GGA and LDA approximations.

Compound	Parameters	GGA	LDA	Theoretical Value	Relative error (%)	
					GGA	LDA
GaS (3D)	a(Å)	3.59	3.58	3.59	0	-0.003
	c(Å)	16.09	16.11	15.58	0.033	0.034
	c /a	4.48	4.49	4.34	0.031	0.034
	B(Gpa)	68.931	73.3863	-	-	-
	B´	4 .5737	4.6013	-	-	-
	E_{min}	-18730.20545	-18715.077091	-	-	-
	V_0	1201.5928	1182.1674	-	-	-
GaSe (3D)	a(Å)	3.76	3.74	3.77	-0.003	-0.008
	c(Å)	16.61	16.62	16.53	0.0048	0.0054
	c /a	4.41	4.44	4.38	0.0068	0.0137
	B(Gpa)	57.7491	62.4752	-	-	-
	B´	4.6846	4.9019	-	-	-
	E_{min}	-34970.300808	-34947.655873	-	-	-
	V_0	1363.3314	1338.6425	-	-	-
GaTe (3D)	a(Å)	4.08	4.04	4.09	-0.002	-0.012
	c(Å)	17.51	17.38	17.52	-0.0006	-0.007
	c /a	4.29	4.30	4.28	0.002	0.004
	B(Gpa)	44.3791	47.4923	-	-	-
	B´	4.7244	4.6808	-	-	-
	E_{min}	-69893.650058	-69861.184781	-	-	-
	V_0	1692.6082	1651.5265	-	-	-

In Table **(III.3)** we have brought all the values of structural properties at the equilibrium such as the lattice parameters **a**, **c** and the ratio **c/a**, the modulus of compressibility and its first

derivative, the minimum total energy, and the volume by using the GGA and LDA approximations. Also, we have included the theoretical values in the table to make the comparison easy and clear.

- **For (GaS) (3D) structure**

As shown in the table above we can note that the relative error in GGA (0) is higher than in LDA (-0.003). Still, GGA approximation gives better results than LDA approximation in lattice parameters.

Also, we can note that the value of compressibility modulus B in GGA approximation (68.931 GPa), is less than in LDA approximation (73.3863 GPa).

The value of volume in GGA approximation is higher than the one in LDA.

- **For (GaSe) (3D) structure**

Based on the given table, it is clear that the relative error of GGA (-0.003) is higher compared to LDA (-0.008), but GGA gives better results than LDA approximation in lattice parameters.

We can note also note that the compressibility modulus B in GGA (57.7491 GPa), its value is less than it is in LDA (62.4752 GPa).

The value of volume in GGA is higher than the one in LDA.

- **For (GaTe) (3D) structure**

The table shows that the relative error in GGA(-0.002) is greater than LDA(-0.012), but GGA approximation gives much closer results than LDA.

the compressibility modulus B in GGA (44.3791 GPa), its value is less than it is in LDA (47.4923 GPa).

The value of volume in GGA is higher than the one in LDA.

Table (III.4): Calculated structural parameters of GaX (X=S, Se, Te) in (2D) using GGA and LDA approximations.

Compound	Parameters	GGA	LDA	Theoretical value	Relative error (%)	
					GGA	LDA
GaS (2D)	a(Å)	3.63	3.60	3.68	-0.01	-0.02
	c(Å)	24.09	24.09	24.09	0	0
	c /a	6.64	6.70	6.55	0.01	0.02
	β(Gpa)	22.7349	24.7111	-	-	-
	β'	4.9552	4.8423	-	-	-
	E_{min}	-9365.098101	-9357.530138	-	-	-
	V_0	1827.0324	1777.6970	-	-	-
GaSe (2D)	a(Å)	3.78	3.74	3.92	-0.04	-0.05
	c(Å)	25.28	25.28	25.28	0	0
	c /a	6.70	6.77	6.45	0.03	0.04
	β(Gpa)	19.3798	20.8094	-	-	-
	β'	4.5864	4.5340	-	-	-
	E_{min}	-17485.148922	-17473.822424	-	-	-
	V_0	2029.0288	1965.6417	-	-	-
GaTe (2D)	a(Å)	4.02	3.97	4.28	-0.06	-0.07
	c(Å)	27.12	27.12	27.12	0	0
	c /a	6.75	6.83	6.34	0.06	0.08
	β(Gpa)	15.4217	16.5838	-	-	-
	β'	4.6321	4.5866	-	-	-
	E_{min}	-34946.818896	-34930.549789	-	-	-
	V_0	2405.5799	2321.5777	-	-	-

- **For (GaS) (2D) structure**

It can be seen that the relative error for the GGA (-0.01) is higher than that for the LDA (-0.02). To sum up, GGA is more suitable than LDA for calculating two-dimensional structural properties.

We can also find that the compressive modulus B in GGA (22.7349 GPa) is smaller than that in LDA (24.7111 GPa).

The volume value in GGA is higher than that in LDA.

- **For (GaSe) (2D) structure**

The relative error in GGA (-0.04) is higher than that in LDA (-0.05). This suggests that GGA approximation is more suitable than LDA for accurately calculating structural properties in 2D systems.

We can also find that the compressive modulus B in GGA (19.3798 GPa) is smaller than that in LDA (20.8094 GPa).

The volume value in GGA is higher than that in LDA.

- **For (GaTe) (2D) structure**

We also note that the values given by the LDA (-0.06) approximation are less than the values given by the GGA (-0.07) approximation for accurately calculating structural properties in (2D) systems.

The modulus of compressibility β in GGA (15.4217 GPa), its value is less than it is in LDA (16.5838 GPa).

The value of volume in GGA is higher than the one in LDA.

III.5. Electronic properties

The electronic properties of materials are important because they allow us to analyze and understand the types of bonds formed between different elements of the material. These properties include band structure, charge density, and density of states. The behavior of electrons in materials determines their magnetic, thermal, optical, and electrical properties.

III.5.1- Band Structure

Band structure is a representation of the allowed electron energy levels of a solid material. It describes the range of energy levels that electrons can have within a solid, as well as the range of energies that they may not have (called the band gap or forbidden band). The energies of adjacent energy levels are so close to each other that they can be viewed as a continuum, an energy band. Band structure is often used to determine whether a material is a conductor,

semiconductor, or insulator **[10]**. The energy gap defined by the difference between the maximum of valence band and the minimum of the conduction band.

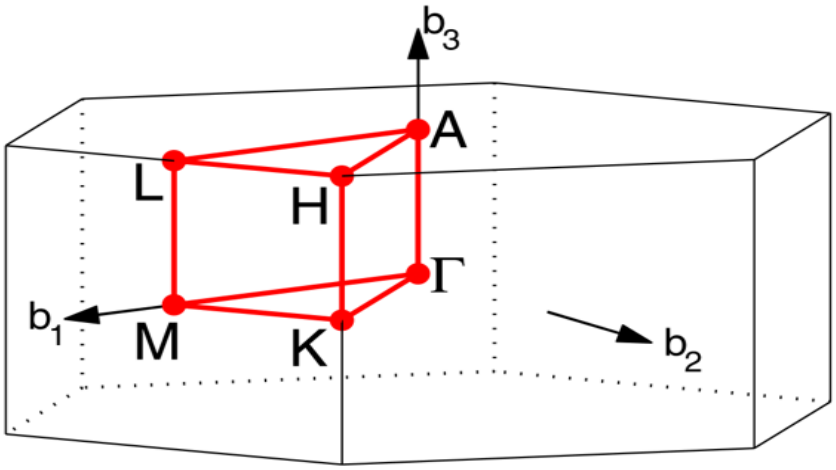

Figure (III.5): Graphic representation of the first Berlin zone (hexagon).

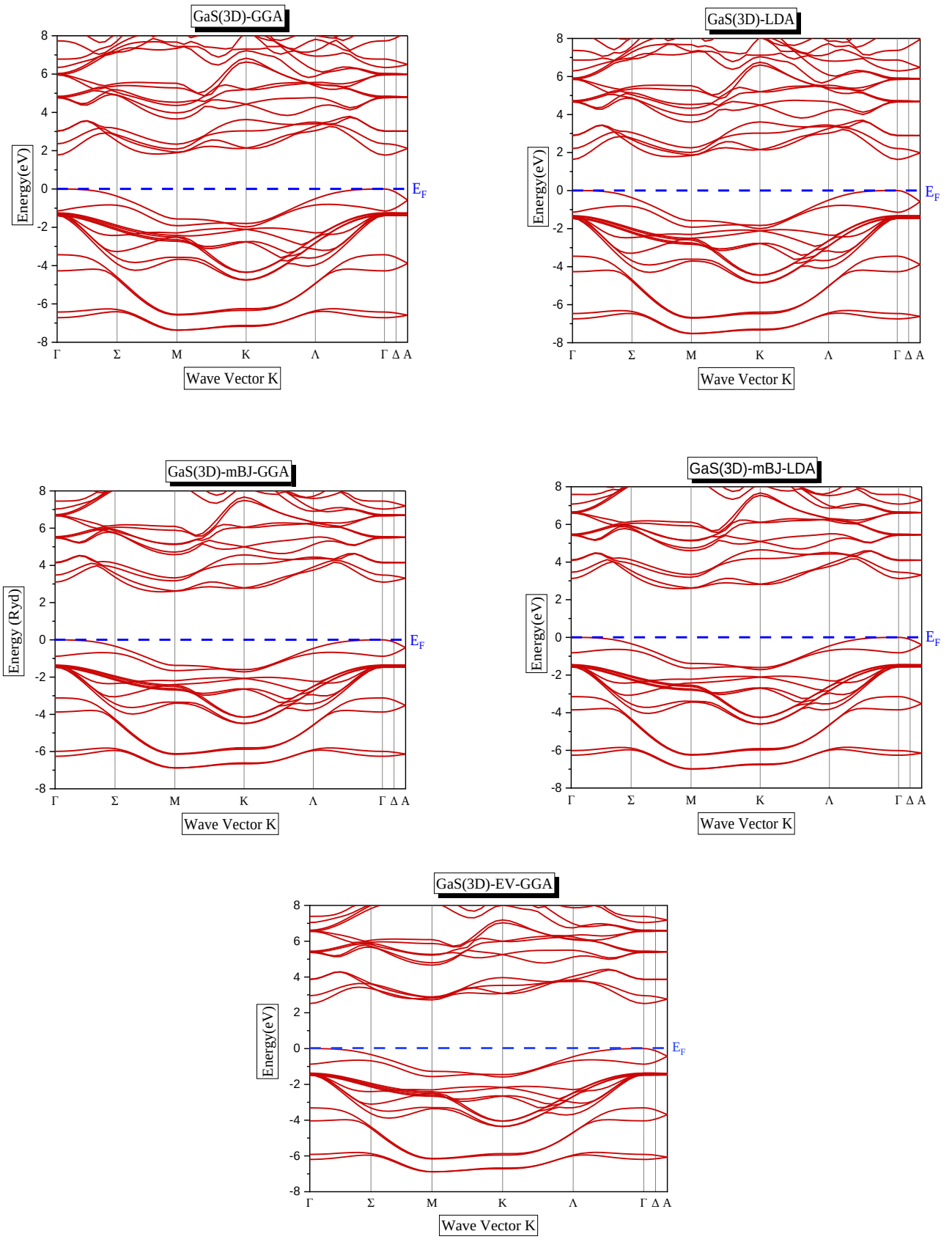

Figure (III.6): The band structure of GaS (3D) using GGA, LDA, mBJ-GGA, mBJ-LDA and EV-GGA approximations.

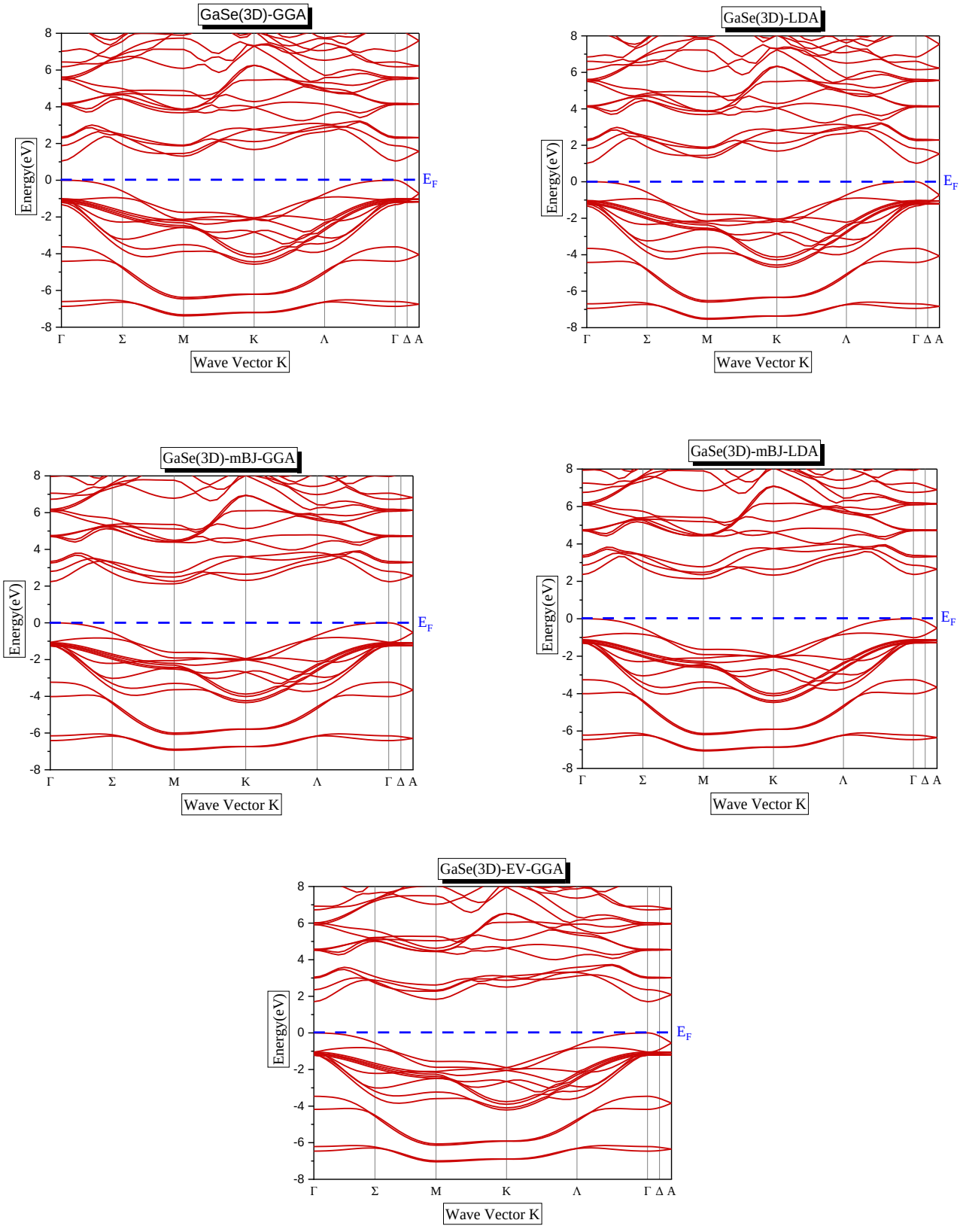

Figure (III.7): The band structure of GaSe (3D) using GGA, LDA, mBJ-GGA, mBJ-LDA and EV-GGA approximations.

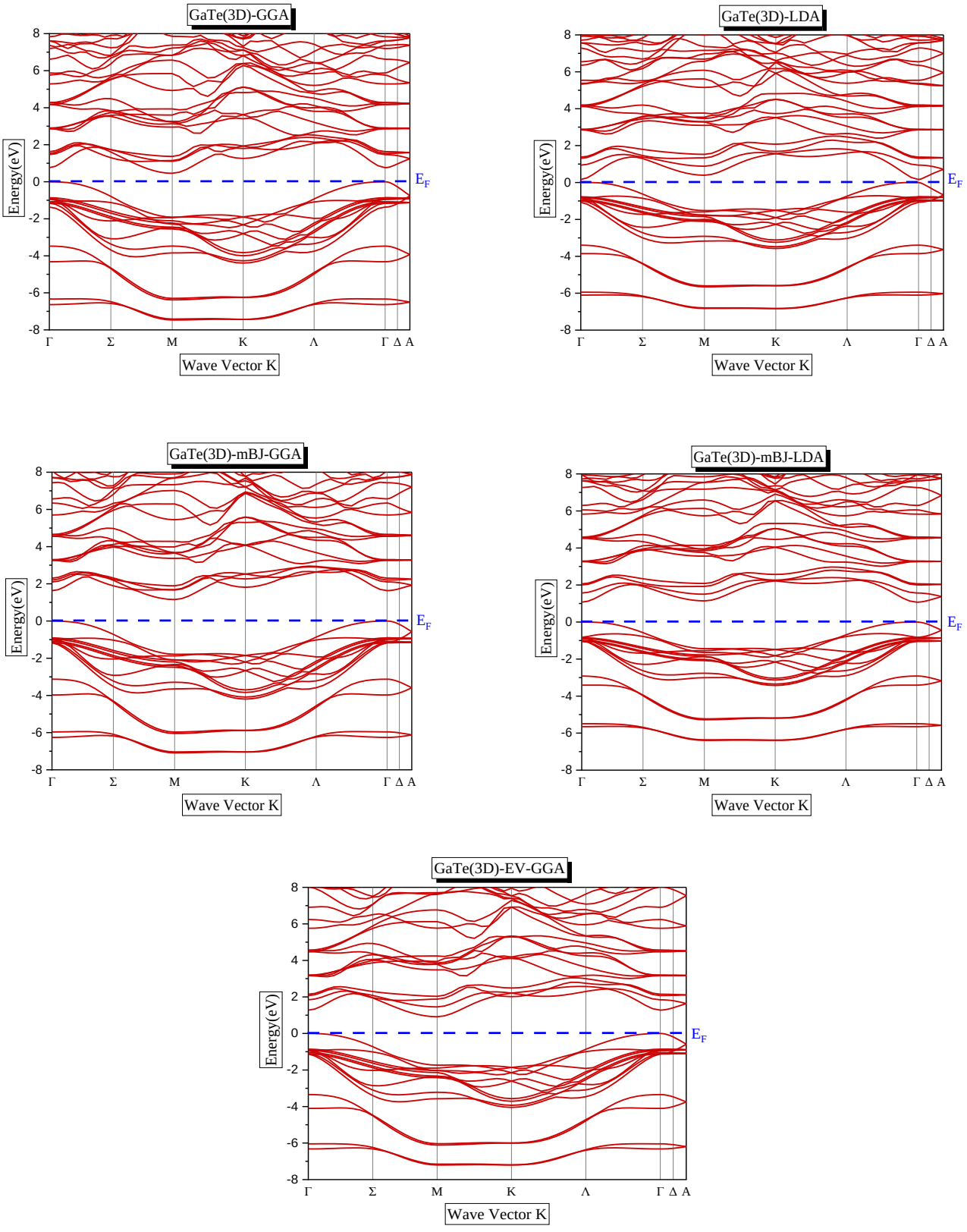

Figure (III.7): The band structure of GaTe (3D) using GGA, LDA, mBJ-GGA, mBJ-LDA and EV-GGA approximations.

Band structures for GaS, GaSe, and GaTe materials were calculated using the FP-LAPW methodFP-LAPW method based on: LDA, GGA, EV-GGA, mBJ-GGA, and mBJ-LDA. Our results are shown in Figures **(III-5, III-6, III-7)**.

- ✓ Figure **(III.5)** represents the electronic band structure of GaS in (3D) bulk according to the directions of the Brillouin zone associated with the ground state. As illustrated in the diagram of Figure **(III.5)**, the compound GaS has a maximum limit in the valence band (VBM) and a minimum limit in the conduction band (CBM) located at the point (Γ→Γ), with a non-zero gap which means that we have a direct gap semiconductor, the LDA, GGA, EV-GGA, mBJ-GGA, mBJ-GGA, and mBJ-LDA approximations.
- ✓ Figure **(III.6)**: shows also the electronic band structure of GaSe in (3D) and we conclude that it has a maximum limit in point Γ and a minimum limit in point *Γ*also (*Γ*→Γ), and a non-zero gap which means that we have a direct gap semiconductor, in LDA, GGA, EV-GGA, mBJ-GGA, and mBJ-LDA.
- ✓ The Figure **(III.7)**: in this figure, the material GaTe in (3D) is visibly clear that it has a maximum value at *Γ* point and a minimum value at *Γ* point (Γ→Γ), and a non-zero gap so we conclude that we have a direct-gap semiconductor in LDA, GGA, EV-GGA, mBJ-GGA, and mBJ-LDA.

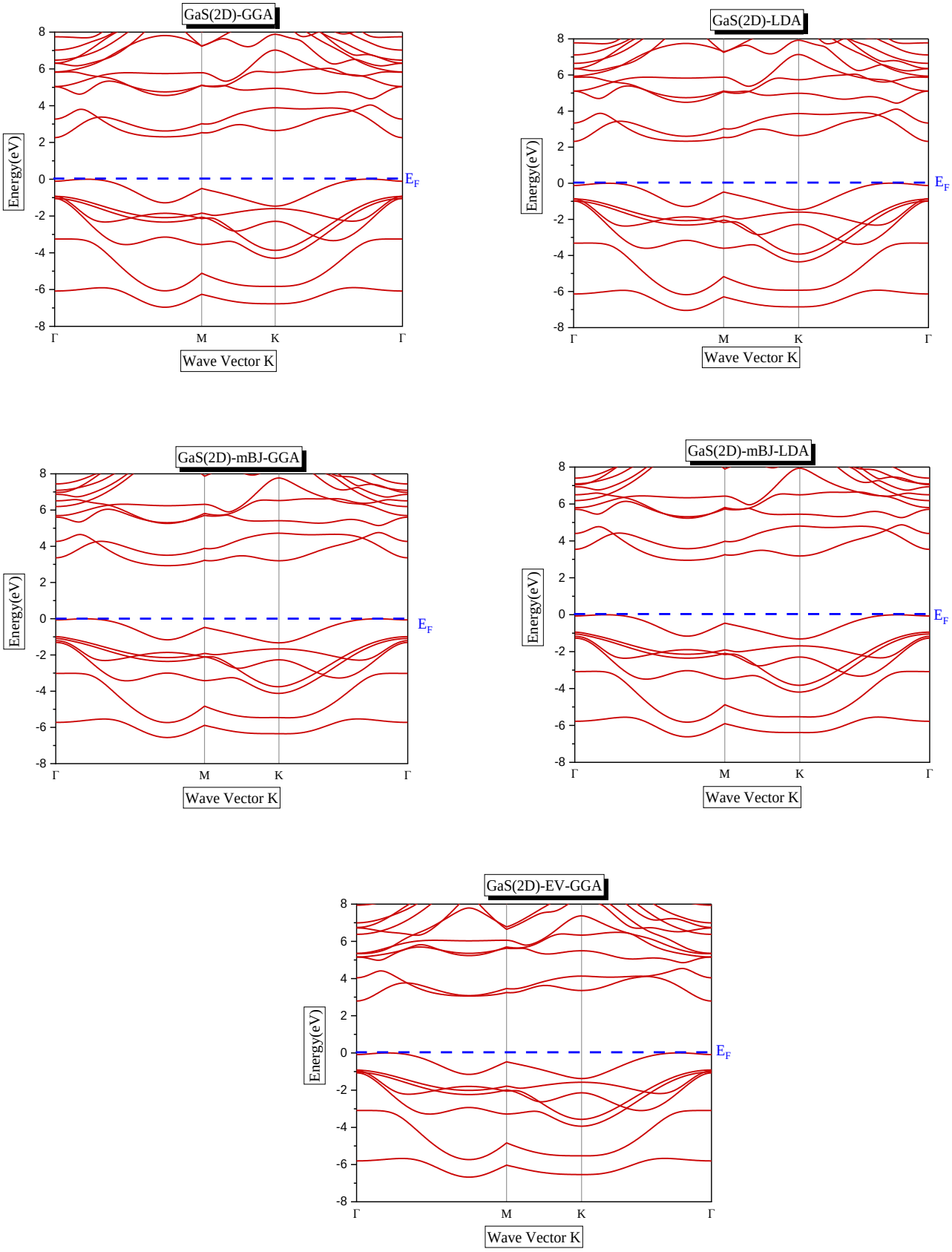

Figure (III.8): The band structure of GaS (2D) using GGA, LDA, mBJ-GGA, mBJ-LDA, and EV-GGA approximations.

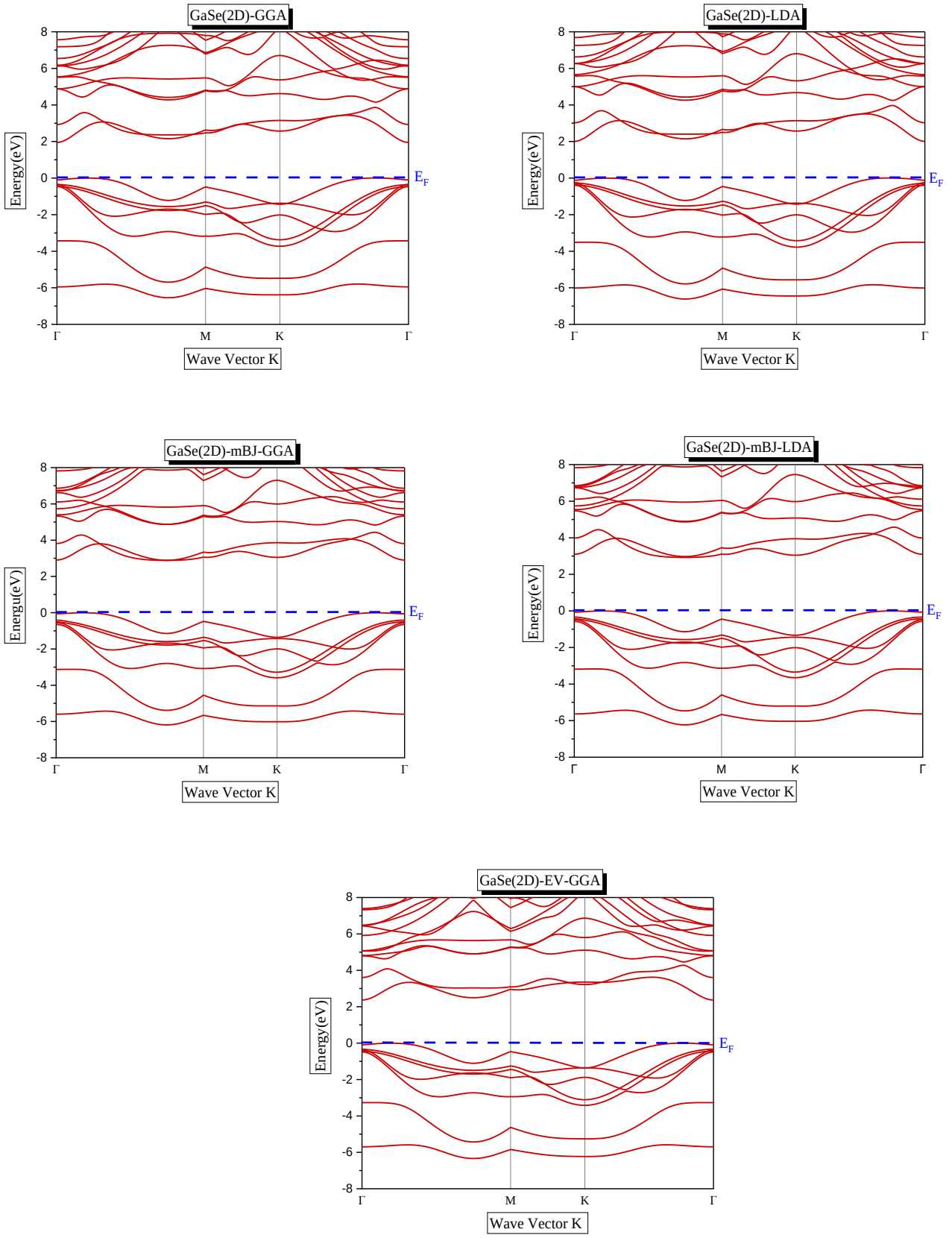

Figure (III.9): The band structure of GaSe (3D) using GGA, LDA, mBJ-GGA, mBJ-LDA, and EV-GGA approximations.

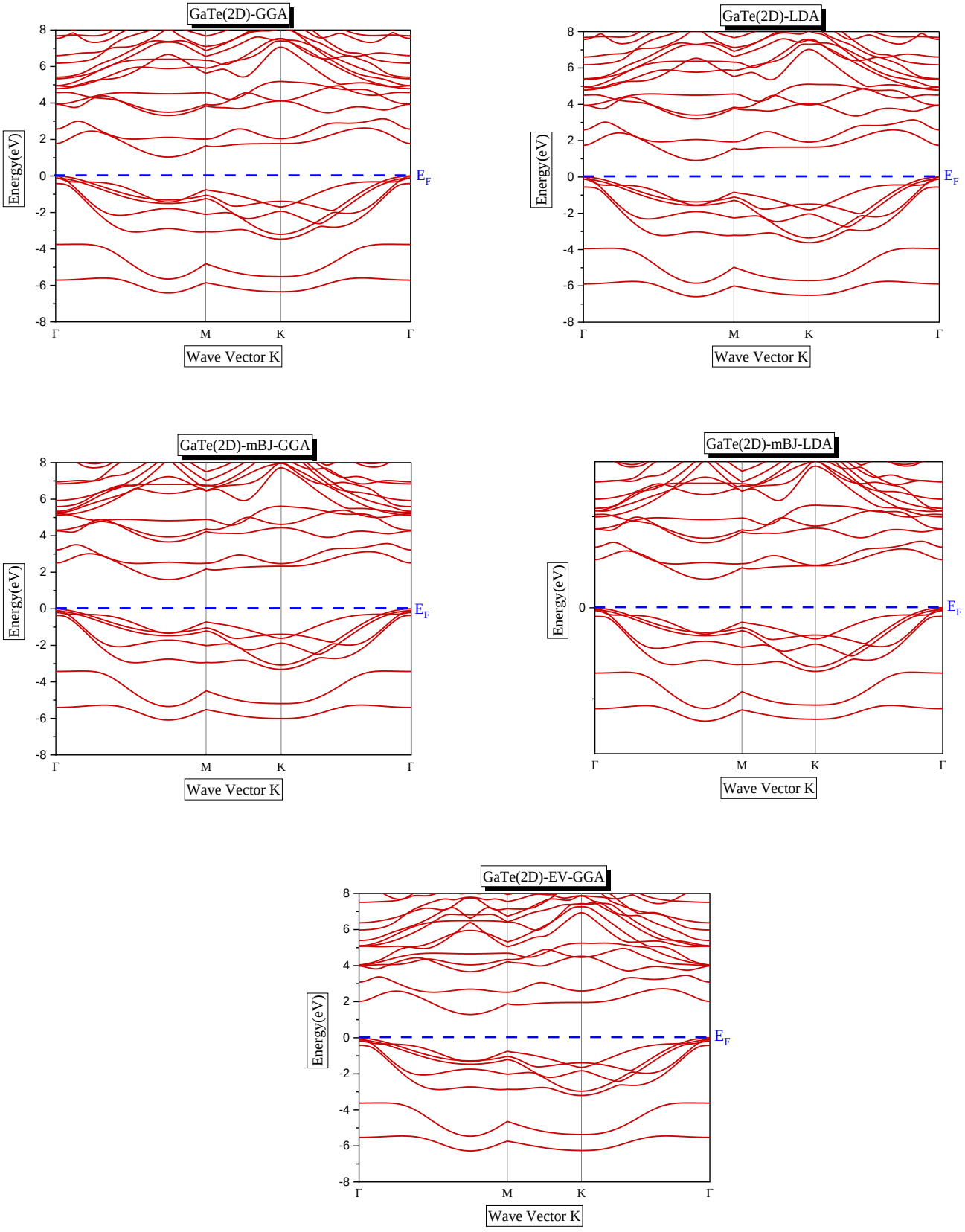

Figure (III.10): The band structure of GaTe (2D) using GGA, LDA, mBJ-GGA, mBJ-LDA, and EV-GGA approximations.

- ✓ The Figure **(III.8)**: in this figure, the material GaS in 2D is visibly clear that it has a maximum value at Γ point and a minimum value at Γ point (Γ→Γ), and a non-zero gap so we conclude that we have a direct gap semiconductor in LDA, GGA, EV-GGA, mBJ-GGA, and mBJ-LDA.
- ✓ From figure **(III.9)** we can see that GaSe in 2D has a maximum limit in point Γ and a minimum limit located at the point Γ, (Γ→Γ), and a non-zero gap is mean that we have a semiconductor with a direct gap in LDA, GGA, EV-GGA, mBJ-GGA, and mBJ-LDA.
- ✓ Figure **(III.10)**: shows the electronic band structure of GaTe in 2D and we conclude that it has a maximum limit in point Γ and a minimum limit in point Γ also (Γ→Γ), and a non-zero gap that is means we have a semiconductor with a direct gap, in LDA, GGA, EV-GGA, mBJ-GGA and mBJ-LDA.

Table (III.5): Energy gap values in 3D and 2D of GaS , GaSe and GaTe calculated with GGA, LDA, EV-GGA, mBJ-GGA, and mBJ-LDA.

Compound		E_g(eV)				
		GGA	LDA	mBJ-GGA	mBJ-LDA	EV-GGA
GaS	**(3D)**	1.771	1.641	2.575	2.583	2.519
	(2D)	2.264	2.320	2.939	2.961	2.794
GaSe	**(3D)**	1.048	1.016	2.125	2.140	1.708
	(2D)	1.953	2.011	2.889	2.929	2.37
GaTe	**(3D)**	0.479	0.162	1.173	1.072	0.935
	(2D)	1.069	0.945	1.626	1.594	1.320

From table **(III.6)** we notice that the values in 3D are less than the ones in 2D. So, we conclude that the energy gap can increase in the 2D structures.

III.5.2- Density State

Density of states (DOS) is an important physical quantity that helps understand the electronic band structure. Most transport properties of conducting solids depend on DOS. DOS provides a partial density of states that describes the structure of chemical bonds between atoms in a crystal or molecule.

As shown below:

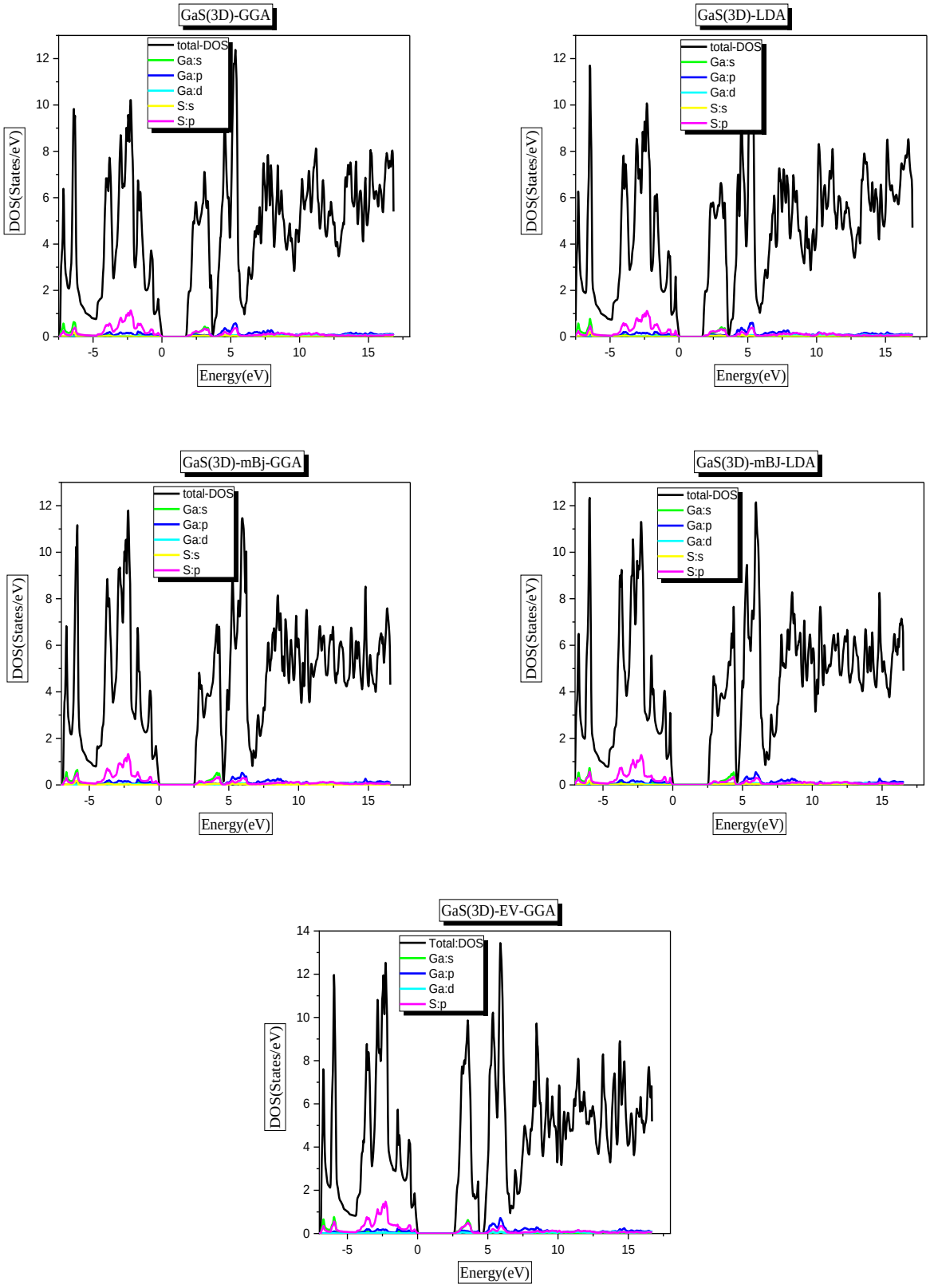

Figure (III.11): The density states of GaS in (3D) for GGA, LDA, EV-GGA, mBJ-GGA and mBJ-LDA.

The Figure **(III.11)** represent density states of GaS in 3D calculated by GGA, LDA, EV-GGA, mBJ-GGA and mBJ-LDA :

Density states calculated by GGA and LDA for GaS:

- The first energetic zone from (-7.5 eV and 0 eV) is mainly dominated by the p orbital of the Sulfur orbital, followed by the s orbitals of the Gallium orbital, and the p orbital of the Gallium orbital with a small contribution.
- Above the Fermi level (1.68 eV – 3.62 eV) density state is made of a mixture of the orbital p of S and s of Ga.
- From (3.62 eV – 16.81 eV) there is a mixture of the p orbitals from Sulfur and Gallium, wddith a low turnout of the s orbitals of Sulfur.

Density states calculated by mBJ-GGA and mBJ-LDA for GaS:

- The first energetic zone from (-7 eV and 0 eV) is mainly dominated by the p orbital of the Sulfur orbital, followed by the s orbitals of the Gallium orbital, and the p orbital of the Gallium orbital with a small contribution.
- Above the Fermi level (2.49 eV – 4.51 eV), the density state consists of a mixture of p orbitals of S and s orbitals of Ga.
- From (4.51 eV – 16.56 eV) there is a mixture of the p orbitals from Sulfur and Gallium, wddith a low turnout of the s orbitals of Sulfur.

Density states calculated by EV-GGA for GaS:

- The energetic zone (-7 eV and 111eV) is mainly dominated by the p orbital of the Sulfur orbital, followed by the s orbitals of the Gallium orbital, and the p orbital of the Gallium orbital with a small contribution.
- Above the Fermi level (2.56 eV – 4.41 eV), the density state consists of a mixture of p orbitals of S and s orbitals of Ga.
- From (4.63 eV – 16.68 eV) there is a mixture of the p orbitals from Sulfur and Gallium, wddith a low turnout of the s orbitals of Sulfur.

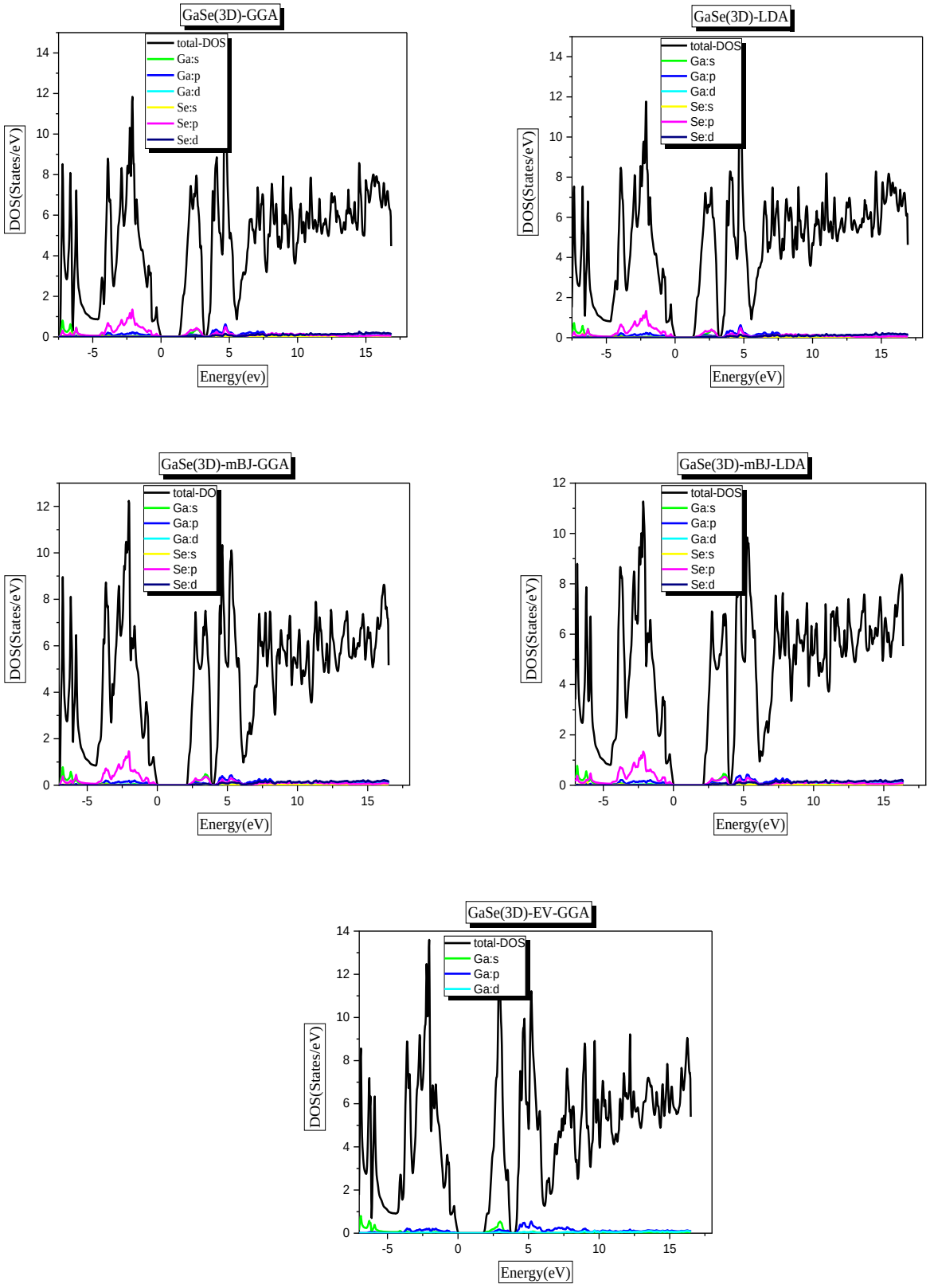

Figure (III.12): The density states of GaSe in (3D) for LDA, GGA, EV-GGA, mBJ-GGA and mBJ-LDA.

The Figure **(III.12)** represent density states of GaSe in 3D calculated by GGA, LDA, EV-GGA, mBJ-GGA and mBJ-LDA :

Density states calculated by GGA and LDA for GaSe:

- The first energetic zone from (-7.5 eV and 0 eV) is mainly dominated by the p orbital of the Sellenium orbital, followed by the s orbitals of the Gallium orbital, and the p orbital of the Gallium orbital with a small contribution.
- Above the Fermi level (1.3 eV – 3.24 eV), the density state consists of a mixture of p orbitals of Se and s orbitals of Ga.
- From (3.45 eV – 16.81 eV) the largest contribution is from orbital p of Se, and a weak contribution of s orbital of Se, and p orbitals of Ga.

Density states calculated by mBJ-GGA and mBJ-LDA for GaSe:

- The first energetic zone from (-7.5 eV and –0 eV) is mainly dominated by the p orbital of the Sellenium orbital, followed by the s orbitals of the Gallium orbital, and the p orbital of the Gallium orbital with a small contribution.
- Above the Fermi level (2.1 eV – 4.03 eV), the density state consists of a mixture of p orbitals of Se and s orbitals of Ga.
- From (4.03 eV – 16.49 eV) the largest contribution is from orbital p of Se, and a weak contribution of s orbital of Se, and p orbitals of Ga.

Density states calculated by EV-GGA for GaSe:

- The first energetic zone from (-7.5 eV and 0 eV) is mainly dominated by the p orbital of the Sellenium orbital, followed by the s orbitals of the Gallium orbital, and the p orbital of the Gallium orbital with a small contribution.
- Above the Fermi level (1.79 eV – 3.75 eV), the density state consists of a mixture of p orbitals of Se and s orbitals of Ga.
- From (4.05 eV – 16.49 eV) the largest contribution is from orbital p of Se, and a weak contribution of s orbital of Se, and p orbitals of Ga.

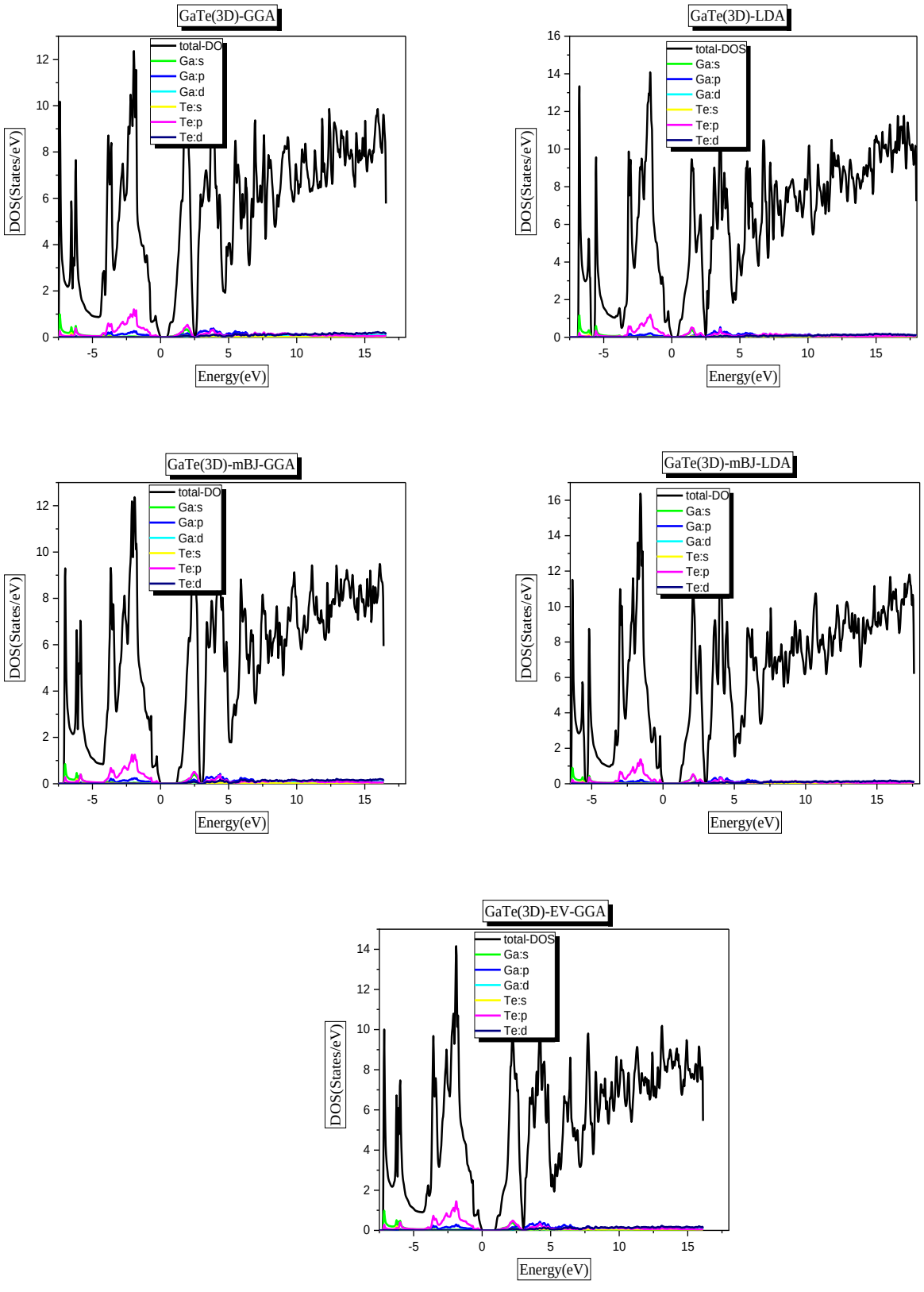

Figure (III.13): The density states of GaTe in (3D) for LDA, GGA, EV-GGA, mBJ-GGA, and mBJ-LDA.

Figure **(III.13)** represents density states of GaTe in 3D calculated by GGA, LDA, EV-GGA, mBJ-GGA, and mBJ-LDA :

Density states calculated by GGA and LDA for GaTe:

- The first energetic zone from (-7.5 eV until -4.61 eV), the largest contribution is from orbital p of Tellurium, hence the orbital s of Gallium and a weak contribution of p orbital of Gallium.
- Above the Fermi level (0.44 eV – 2.53 eV), the density state consists of a mixture of p orbitals of Tellurium and s orbitals of Gallium a weak contribution from the p orbital of Gallium.
- From (2.53 – 16.55 eV) there is a mixture of the p orbitals from Te and Ge, a weak contribution from the d orbital of Te.

Density states calculated by mBJ-GGA and mBJ-LDA for GaTe:

- The first energetic zone from (-7.24 eV until -4.22 eV), the largest contribution is from orbital p of Tellurium, hence the orbital s of Gallium and a weak contribution of p orbital of Gallium.
- Above the Fermi level (1.6 eV – 3.04 eV), the density state consists of a mixture of p orbitals of Tellurium and s orbitals of Gallium a weak contribution from the p orbital of Gallium.
- From (3.04 – 16.37 eV) there is a mixture of the p orbitals from Te and Ge, a weak contribution from the d orbital of Te.

Density states calculated by EV-GGA for GaTe:

- The first energetic zone from (-7.33 eV until -4.29 eV), the largest contribution is from orbital p of Tellurium, hence the orbital s of Gallium and a weak contribution of p orbital of Gallium.
- Above the Fermi level (0.9 eV – 2.97 eV), the density state consists of a mixture of p orbitals of Tellurium and s orbitals of Gallium a weak contribution from the p orbital of Gallium.
- From (2.97 – 16.11 eV) there is a mixture of the p orbitals from Te and Ge, a weak contribution from the d orbital of Te atom.

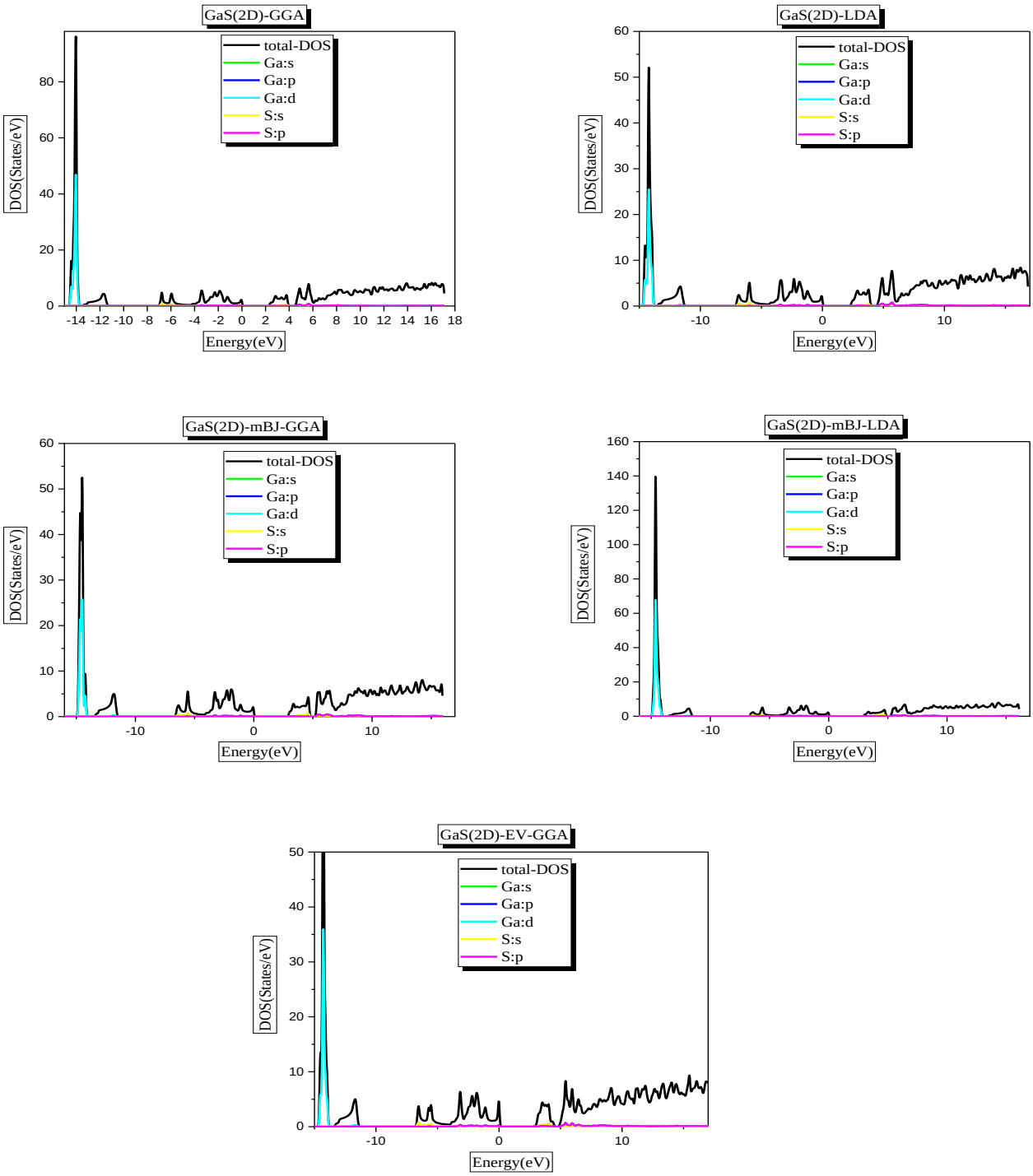

Figure (III.14): The density states of GaS in (2D) for LDA, GGA, EV-GGA, mBJ-GGA, and mBJ-LDA.

The Figure **(III.14)** represent density states of GaTe in 2D calculated by GGA, LDA, EV-GGA, mBJ-GGA and mBJ-LDA :

Density states calculated by GGA and LDA:

- The first energetic zone from (-14.68 eV until -11.34 eV), is completely dominated by the d orbitals of Gallium.
- The second active region from (-7.06 eV – -4.48 eV), we note a small equal contribution between the s orbitals of Gallium and Sulfur.
- The energetic zone (-4.48 eV – 0 eV) we note a small equal contribution between the p orbitals of Gallium and Sulfur.
- Above Fermi level (2.26 eV – 3.95 eV), we note a small equal contribution between the s orbitals of Gallium and Sulfur.
- The energetic zone (4.46 eV – 17.09 eV) we note a small equal contribution between the p orbitals of Ga and S.

Density states calculated by mBJ-GGA and mBJ-LDA:

- The first energetic zone from (-15.12 eV until -11.37 eV), is completely dominated by the d orbitals of Gallium.
- The second active region from (-6.69 eV – -4.16 eV), we note a small equal contribution between the s orbitals of Gallium and Sulfur.
- The energetic zone (-4.16 eV – 0 eV) we note a small equal contribution between the p orbitals of Gallium and Sulfur.
- Above Fermi level (2.91 eV – 4.68 eV), we note a small equal contribution between the s orbitals of Ga and S.
- The energetic zone (5.3 eV – 15.94 eV) we note a small equal contribution between the p orbitals of Gallium and Sulfur.

Density states calculated by EV-GGA:

- The first energetic zone from (-14.85 eV until -11.21 eV), is completely dominated by the d orbitals of Gallium.
- The second active region from (-6.85 eV – -4.08 eV), we note a small equal contribution between the s orbitals of Gallium and Sulfur.

- The energetic zone (-4.08eV – 0 eV) we note a small equal contribution between the p orbitals of Gallium and Sulfur.
- Above Fermi level (2.77 eV – 4.48 eV), we note a small equal contribution between the s orbitals of Gallium and Sulfur.
- The energetic zone (5 eV – 17.87 eV) we note a small equal contribution between the p orbitals of Gallium and Sulfur.

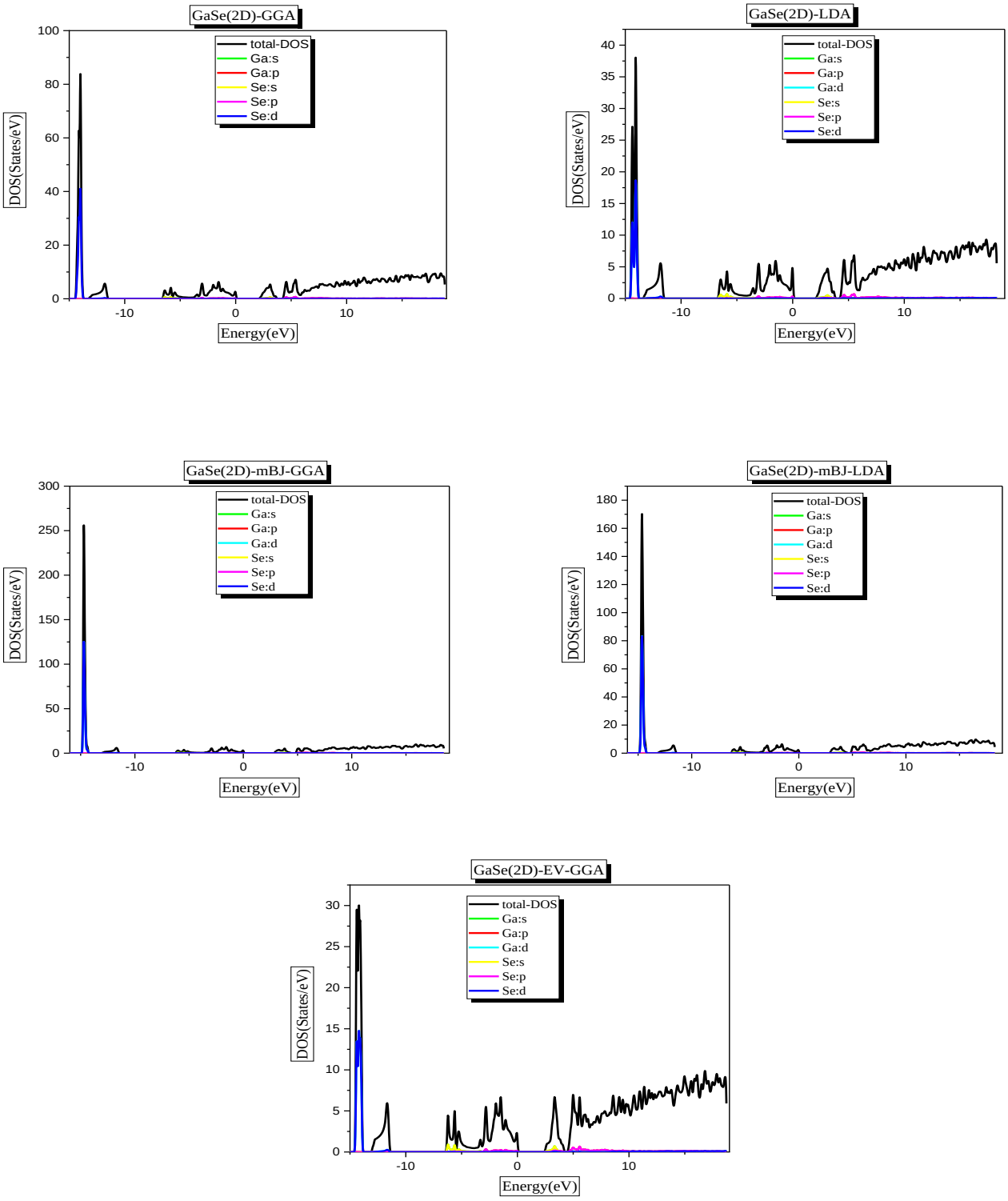

Figure (III.15): The density states of GaSe in (2D) for LDA, GGA, EV-GGA, mBJ-GGA and mBJ-LDA.

Figure **(III.15)** represents the density states of GaSe in 2D calculated by GGA, LDA, EV-GGA, mBJ-GGA, and mBJ-LDA :

Density states calculated by GGA and LDA:

- The first energetic zone from (-14.48 eV until -11.51 eV), is completely dominated by the d orbitals of Gallium and Selenium.
- The second active region from (-6.48 eV – -3.89 eV), we note a small equal contribution between the s orbitals of Gallium and Selenium.
- In The energetic zone (-3.89 eV – 0 eV) we note a small equal contribution between the p orbitals of Gallium and Selenium.
- Above the Fermi level (1.9 eV – 3.82 eV), we note a small equal contribution between the s orbitals of Gallium and Selenium.
- The energetic zone (4.12 eV – 18.84 eV) we note a small equal contribution between the p orbitals of Ga and Se.

Density states calculated by mBJ-GGA and mBJ-LDA:

- The first energetic zone from (-15.03 eV until -11.3 eV), is completely dominated by the d orbitals of Gallium and Selenium.
- The second active region from (-6.29 eV – -3.79 eV), we note a small equal contribution between the s orbitals of Gallium and Sellenium.
- The energetic zone (-3.79 eV – 0 eV) we note a small equal contribution between the p orbitals of Gallium and Selenium.
- Above the Fermi level (2.7 eV – 4.53 eV), we note a small equal contribution between the s orbitals of Ga and Se.
- In The energetic zone (4.72 eV – 18.49 eV) we note a small equal contribution between the p orbitals of Gallium and Selenium.

Density states calculated by EV-GGA:

- The first energetic zone from (-14.74 eV until -11.23 eV), is completely dominated by the d orbitals of Gallium and Selenium.
- The second active region from (-6.46 eV – -3.69 eV), we note a small equal contribution between the s orbitals of Gallium and Sellenium.

- In The energetic zone (-3.69 eV – 0 eV) we note a small equal contribution between the p orbitals of Gallium and Sellenium.
- Above the Fermi level (2.34 eV – 4.36 eV), we note a small equal contribution between the s orbitals of Gallium and Sellenium.
- In The energetic zone (4.36 eV – 18.72 eV) we note a small equal contribution between the p orbitals of Gallium and Sellenium.

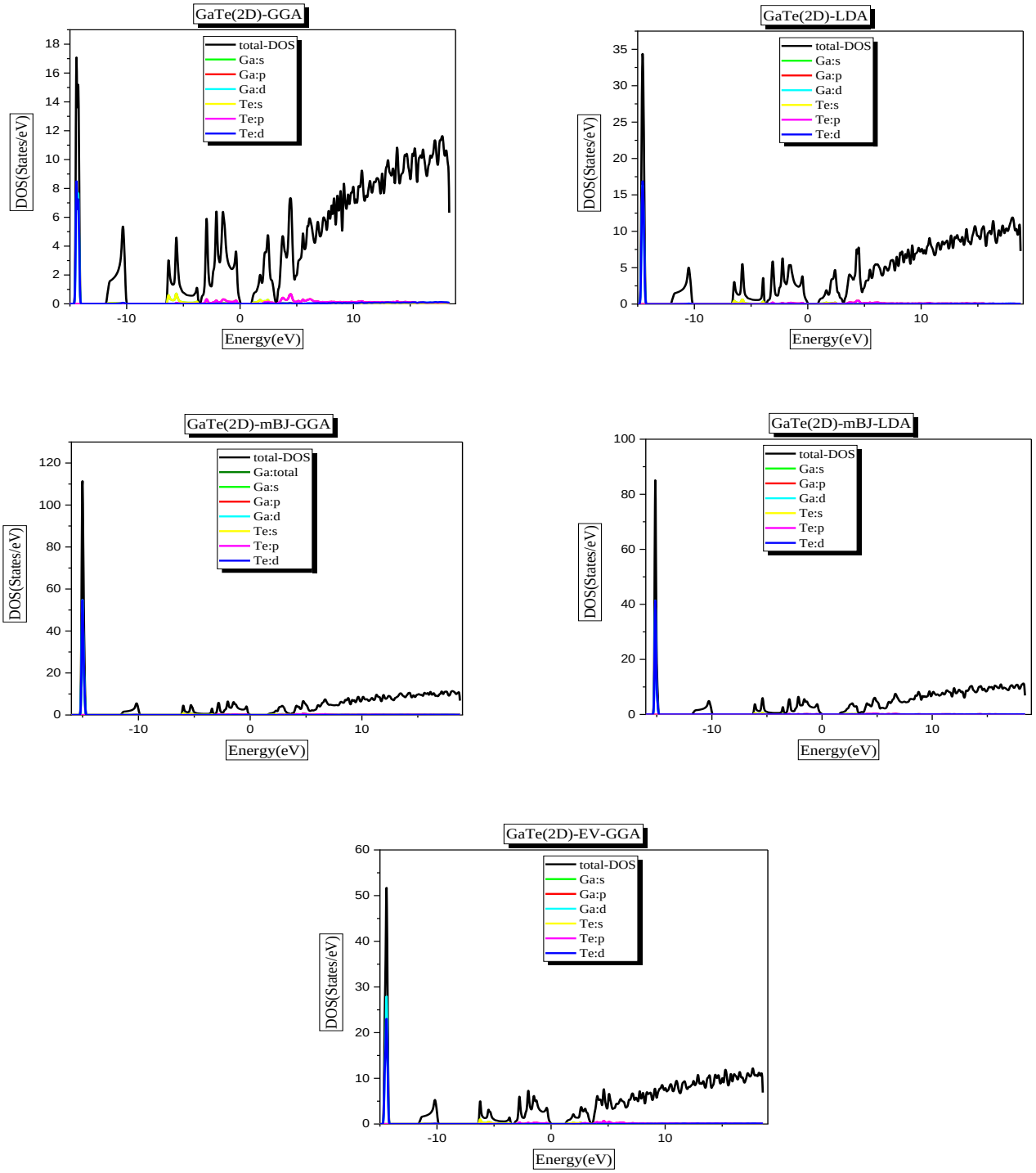

Figure (III.16): The density states of GaTe in (2D) for LDA, GGA, EV-GGA, mBJ-GGA and mBJ-LDA.

Figure **(III.16)** represents density states of GaTe in 2D calculated by GGA, LDA, EV-GGA, mBJ-GGA, and mBJ-LDA :

Density states calculated by GGA and LDA:

- The first energetic zone from (-14.72 eV until -9.93 eV), is completely dominated by the d orbitals of Gallium and Tellurium.
- The second active region from (-6.64 eV – -3.54 eV), we note a small equal contribution between the s orbitals of Gallium and Tellurium.
- The energetic zone (-3.54 eV – 0 eV) we note a small equal contribution between the p orbitals of Gallium and Tellurium.
- Above the Fermi level (1.003 eV – 3.2 eV), we note a small equal contribution between the s orbitals of Gallium and Sellenium.
- The energetic zone (3.2 eV – 18.44 eV) we note a small equal contribution between the p orbitals of Ga and Te.

Density states calculated by mBJ-GGA and mBJ-LDA:

- The first energetic zone from (-15.24 eV until -10 eV), is completely dominated by the d orbitals of Gallium and Tellurium.
- The second active region from (-6.23 eV – -3.05 eV), we note a small equal contribution between the s orbitals of Gallium and Tellurium.
- The energetic zone (-3.05 eV – 0 eV) we note a small equal contribution between the p orbitals of Gallium and Tellurium.
- Above Fermi level (1.51 eV – 3.77 eV), we note a small equal contribution between the s orbitals of Ga and Te.
- The energetic zone (3.77 eV – 18.77 eV) we note a small equal contribution between the p orbitals of Gallium and Tellurium.

Density states calculated by EV-GGA:

- The first energetic zone from (-14.85 eV until -9.76 eV), is completely dominated by the d orbitals of Gallium and Tellurium.
- The second active region from (-6.47 eV – -3.31 eV), we note a small equal contribution between the s orbitals of Gallium and Tellurium.

- The energetic zone (-3.31 eV – 0 eV) we note a small equal contribution between the p orbitals of Gallium and Tellurium.
- Above the Fermi level (1.27 eV – 3.51 eV), we note a small equal contribution between the s orbitals of Gallium and Sellenium.
- The energetic zone (3.51 eV – 18.55 eV) we note a small equal contribution between the p orbitals of Gallium and Tellurium.

III.6. Elastic properties

In 1678, Robert Hooke published a paper containing the results of Hooke's experiments **[11]** on elastic bodies. This is the first published article in which the elastic properties of materials are discussed. elastic properties of materials. Hooke's law is a law of behavior for solids subjected to solids subjected to elastic deformation of small amplitude. Hooke wanted to obtain a theory of springs by subjecting them to successively increasing forces. Two aspects of his law are important:

1. Linearity.

2. Elasticity.

When a crystalline solid is subjected to stress, the deformation it undergoes is proportional to this stress, as long as the deformation remains small ($\varepsilon = \frac{\Delta l}{l} < 10^{-4}$). This is Hooke's law **[11]**:

$$\sigma = C.\varepsilon \qquad \textbf{(III.4)}$$

The constant C is equivalent to the stiffness of a spring and is called the elastic constant. When we consider a three-dimensional solid, generalized Hooke's law can be written as **[12]**:

$$\sigma_{ij} = C_{ijkl}.\varepsilon_{kl} \qquad \textbf{(III.5)}$$

C_{ijkl} is a fourth-order tensor with 81 elements.

III.6.1. Voigt notation:

ε and σ are symmetric matrices, their representation can be reduced to a vector of dimension 6. The change of representation also applies to the matrix of elastic constants constants. The first pair of indices corresponds to the σ and the second pair corresponds to the ε: $C_{ijkl} \rightarrow C_{IJ}$ With ij →I and kl →J. The relationship between stress and strain can be written as **[13]**:

$$\sigma_I = C_{IJ}.\varepsilon_J \qquad \textbf{(III.6)}$$

This can be written in matrix form:

$$\begin{pmatrix}\sigma_1\\ \sigma_2\\ \sigma_3\\ \sigma_4\\ \sigma_5\\ \sigma_6\end{pmatrix} = \begin{pmatrix}C_{11} & C_{12} & C_{13} & C_{14} & C_{15} & C_{16}\\ C_{21} & C_{22} & C_{23} & C_{24} & C_{25} & C_{26}\\ C_{31} & C_{32} & C_{33} & C_{34} & C_{35} & C_{36}\\ C_{41} & C_{42} & C_{43} & C_{44} & C_{45} & C_{46}\\ C_{51} & C_{52} & C_{53} & C_{54} & C_{55} & C_{56}\\ C_{61} & C_{62} & C_{63} & C_{64} & C_{65} & C_{66}\end{pmatrix}\begin{pmatrix}\varepsilon_1\\ \varepsilon_2\\ \varepsilon_3\\ \varepsilon_4\\ \varepsilon_5\\ \varepsilon_6\end{pmatrix} \qquad \textbf{(III.6)}$$

Case of a Hexagonal system:

$$\begin{pmatrix} C_{11} & C_{12} & C_{13} & 0 & 0 & 0\\ C_{12} & C_{11} & C_{13} & 0 & 0 & 0\\ C_{13} & C_{13} & C_{33} & 0 & 0 & 0\\ 0 & 0 & 0 & C_{44} & 0 & 0\\ 0 & 0 & 0 & 0 & C_{44} & 0\\ 0 & 0 & 0 & 0 & 0 & 1/2(C_{11}-C_{12}) \end{pmatrix} \qquad \textbf{(III.7)}$$

III.6. 2. Mechanical stability criteria of the crystal

One of the most common types of instability in crystals is the so-called mechanical instability. when one or more elastic constants (or special combinations) tend towards zero. Consideration of the mechanical stability of the crystal lattice was originally formulated by Born and Huang **[14,15]**. who showed that by developing the internal energy of a crystal into a power series of stresses, it is possible to obtain stability criteria in terms of conditions on the elastic constants, while at the same time positive energy. A necessary condition for mechanical stability is that the matrix of elastic constants is positively defined (Born criterion). A matrix is positively defined if the determinants of the successive order matrices of which it is composed are all positive. The condition of dynamic or mechanical stability of a network implies that the

variation in energy under any small deformation is positive. This condition can be formulated in terms of elastic constants **[15]**.

- ✓ The mechanical stability of systems with hexagonal symmetry requires that the nine independent elastic constants C_{11}, C_{12}, C_{13}, C_{33}, and C_{44} obey the Born criteria given below:

$$\begin{cases} C_{11} > 0,\ C_{33} > 0,\ C_{44} > 0,\ C_{66} > 0,\ C_{11} > |C_{12}| \\ C_{11}C_{33} > C_{13}^2 \\ (C_{11} + C_{12})C_{33} > 2C_{13}^2 \end{cases} \quad \textbf{(III.8)}$$

The results of our calculations are shown in the following table **(III.4) :**

Table (III.6): The elastic constants in (3D) for GaS, GaSe and GaTe computed using GGA and LDA approximation.

Elastic Constants	Compounds					
	GaS		GaSe		GaTe	
	GGA	LDA	GGA	LDA	GGA	LDA
C_{11}	142.0807	142.9341	117.0788	122.3712	84.4033	50.4211
C_{33}	115.3661	111.5318	104.4433	106.3053	81.7731	44.7043
C_{55}	49.1589	49.0511	43.0230	44.5330	2.6415	19.6427
C_{12}	40.8017	40.9471	32.2872	34.1482	32.1824	9.0625
C_{13}	30.7784	30.9702	26.5358	27.5859	20.5283	3.3366
C_{66}	50.6245	50.9935	42.3958	44.1115	52.2209	20.6793
A_1	1.0038	1.0191	1.0216	1.0266	0.05	0.8882
A_2	1	1	1	1	1	1

III.6.3. Study in a polycrystalline state

III.6.3.1. Isotropic elastic modules

To determine isotropic modulus of elasticity such as the Bulk modulus B, Shear modulus G, Young's modulus E, and Poisson's ratio σ for materials GaS, GaSe, and GaTe.

$$B_V = \frac{2C_{11}+2C_{12}+4C_{13}+C_{33}}{9} \quad \textbf{(III.9)}$$

$$B_R = \frac{-2C_{13}^2+C_{33}(C_{11}+C_{12})}{C_{11}+C_{12}-4C_{13}+2C_{33}} \quad \textbf{(III.10)}$$

$$B_H = \frac{B_R+B_V}{2} \quad \textbf{(III.11)}$$

$$G_V = \frac{4C_{11}+2C_{33}-4C_{13}-2C_{12}+12C_{55}+6C_{66}}{30} \quad \textbf{(III.12)}$$

$$G_R = 15\left(\left(\frac{4C_{11}+4C_{12}+8C_{13}+2C_{33}}{-2(C_{13})^2+C_{33}(C_{11}+C_{12})}\right)+\left(\frac{6}{C_{11}-C_{12}}\right)+\left(\frac{6}{C_{55}}\right)+\left(\frac{3}{C_{66}}\right)\right)^{-1} \quad \textbf{(III.13)}$$

$$G_H = \frac{G_R+G_V}{2} \quad \textbf{(III.14)}$$

$$E_V = \frac{9(B_V)(G_V)}{3B_V+G_V} \quad \textbf{(III.15)}$$

$$E_R = \frac{9(B_R)(G_R)}{3B_R+G_R} \quad \textbf{(III.16)}$$

$$E_H = \frac{9(B_H)(G_H)}{3B_H+G_H} \quad \textbf{(III.17)}$$

The results of our calculations are shown in the following table **(III.5) :**

Table (III.7): Modules of elasticity B_V, B_R, B_H, G_V, G_R, G_H, E_V, E_R, E_H, σ_V, σ_R, σ_H, A_B, A_G, A^u for GaS, GaSe and GaTe in (3D).

Elasticity Modules	Compounds					
	GaS		GaSe		GaTe	
	GGA	LDA	GGA	LDA	GGA	LDA
B_V	67.138	67.019	56.590	58.854	44.117	19.668
B_R	66.105	65.675	56.292	58.414	43.888	19.453
B_H	66.621	66.347	56.441	58.634	44.002	19.560
G_V	49.602	49.453	42.570	44.083	18.100	20.646
G_R	49.428	49.200	42.521	44.010	5.785	20.551
G_H	49.515	49.326	42.545	48.046	11.942	20.598
E_V	119.401	119.071	102.106	105.826	47.767	45.883
E_R	118.699	118.106	101.904	105.527	16.624	45.596
E_H	119.050	118.589	102.004	105.676	32.853	45.738
σ_V	0.203	0.203	0.199	0.200	0.319	0.111
σ_R	0.200	0.200	0.198	0.198	0.436	0.109
σ_H	0.202	0.202	0.198	0.199	0.375	0.110
B_H/G_H	1.3454	1.345	1.327	1.220	3.684	0.952
A_B	0.775	1.013	0.266	0.375	0.260	0.549
A_G	0.176	0.256	0.058	0.083	51.559	0.231
A^u	0.0332	0.0462	0.0111	0.0158	10.649	0.0342

III.6.3.2. Elastic anisotropy

Anisotropic behavior is an essential feature that defines the different arrangement of atoms in various orientations. Anisotropic behavior has significant implications for both crystal physics and engineering research. In other words, the degree of anisotropy in the bonding between atoms in various planes is quantified by the shear anisotropic factors. for the shear anisotropy factor for the {100} shear planes between the <011> and <010> directions are **[16]**.

$$A_1 = \frac{4C_{55}}{C_{11}-2C_{13}+C_{33}} \quad \textbf{(III.18)}$$

$$A_2 = \frac{2C_{66}}{C_{11}-C_{12}} \quad \textbf{(III.19)}$$

The percentage anisotropy for the bulk modulus A_B and shear modulus A_G is given by:

$$A_B = \frac{100(-B_R+B_V)}{B_R+B_V} \quad \textbf{(III.20)}$$

$$A_G = \frac{100(-G_R+G_V)}{G_R+G_V} \quad \textbf{(III.21)}$$

The universal anisotropy index A^u is given by:

$$A^u = 5\frac{G_V}{G_R} + \frac{B_V}{B_R} - 6 \quad \textbf{(III.22)}$$

II.6.4. Debye temperature and elastic wave propagation velocities

The Debye temperature θ_D can be determined from the average sound velocity v_m as follows:

$$\theta_D = \frac{h}{k_B}\left(\frac{3n}{4\pi}\left(\frac{N_a\rho}{M}\right)\right)^{\frac{1}{2}} V_m \quad \textbf{(III.23)}$$

h: denotes Planck's constant.

k_B: Boltzmann's constant.

N_a: Avogadro's number.

ρ: molecule density.

M: denotes molecular weight.

n: is the number of atoms in the molecule.

In polycrystalline materials, the average velocity V_m is approximated by:

$$\mathrm{Vm} = \left(\frac{1}{3}\left(\frac{2}{V_t^3} - \frac{1}{V_l^3}\right)\right)^{-\frac{1}{3}} \quad \textbf{(III.24)}$$

V_l and V_t are the propagation velocities of longitudinal and transverse elastic waves respectively. They are obtained using the stiffness modulus B, the shear modulus G and the crystal density g from the Navier equation **[17]**:

$$V_l = \left(\frac{3B+4G}{3\rho}\right)^{\frac{1}{2}} \quad \textbf{(III.25)}$$

$$V_t = \left(\frac{G}{\rho}\right)^{\frac{1}{2}} \quad \textbf{(III.26)}$$

The results of our calculations are shown in the following table **(III.6) :**

Table (III.8): Longitudinal, transversal, and average sound velocity (V_l V_t, V_m in m/s), Debye temperature (θ_D in K) for GaS, GaSe, and GaTe in (3D) using GGA approximation.

Compounds		V_l	V_t	V_m	θ_D
GaS	**GGA**	5932	3624.35	4002.15	422.562
	LDA	5918.2	3616.19	3993.12	421.704
GaSe	**GGA**	4830.26	2961.65	3269.19	330.889
	LDA	4889.97	2995.68	3307.04	336.043
GaTe	**GGA**	3393.27	1514.8	1709.04	161.145
	LDA	3238.87	2143.61	2345.56	210.427

Table (III.9): The elastic constants in (2D) for GaS, GaSe, and GaTe were computed using GGA approximation.

Elastic Constants	Compounds		
	GaS	**GaSe**	**GaTe**
C_{11}	112.0775	93.4598	79.6590
C_{22}	112.0775	93.4598	79.6590
C_{66}	39.8635	33.9824	30.2125
C_{12}	32.3506	25.4950	19.2341
C_{16}	0	0	0
C_{26}	0	0	0

Table (III.10): Modules of elasticity G, E_x , E_y, σ_{xy} and σ_{yx} for GaS, GaSe and GaTe in (2D).

Elasticity Modules	Compounds		
	GaS	GaSe	GaTe
G	39.8635	33.9824	30.2125
E_x	102.739	86.504	75.014
E_y	102.739	86.504	75.014
σ_{xy}	0.288	0.272	0.241
σ_{yx}	0.288	0.272	0.241

From the two tables **(III.6)** and **(III.9)** we notice that materials GaS, GaSe and GaTe increase in stiffness in the (2D) compared to the (3D).

References

[1] J. P. Perdew and Y.Wang, Phys. Rev., B **45**, 13244 (1992).

[2] J. P. Perdew, S. Burke et M. Ernzerhof, Phys. Lett. **77**, 3865 (1996).

[3] E. Engel, S. H. Vosko, Phys. Rev. B **47**, 20 (1993).

[4] A. D. Becke and E. R. Johson , J. chem. Phys.**124**. 221101 (2006).

[5] E. Sjösted, L. Nordström and D. J. Singh, Solid State Commun. 114, 15 (2000).

[6] D. R Hamann, Phys. Rev. Lett. 212, 662 (1979).

[7] J. Korbmacher, G. Schiemer, What Are Structural Properties?†, Philos. Math. 26 (2018) 295–323. https://doi.org/10.1093/philmat/nkx011.

[8] V.G. Tyuterev, N. Vast, Murnaghan's equation of state for the electronic ground state energy, Comput. Mater. Sci. 38 (2006) 350–353. https://doi.org/10.1016/j.commatsci.2005.08.012.

[9] Z. Cancarevic, Prediction of not-yet-synthesized solids at extreme pressures, and the development of algorithms for local optimization on ab-initio level, (2006). http://elib.uni-stuttgart.de/opus/volltexte/2007/2894/.

[10] L.K. Lamontagne, Band structures and the meaning of the wave vector k, Lect. Notes. 1 (2018) 7–8. http://www.sciencemag.org/lookup/doi/10.1126/science.aag0410%0Ahttp://www.nature.com/articles/s41563-018-0217z%0Ahttp://pubs.acs.org/doi/10.1021/acsaem.8b00617%0Ahttp://www.nature.com/articles/s41563-018-0266-3%0Ahttp://www.nature.com/articles/s41563-018.

[11] D. Royer, Ondes élastiques dans les solides. Masson (1996).

[12] N. Labgaa, *Thèse de Doctorat en physique du solide*, Université Ferhat Abbas-Sétif (2011).

[13] J. F. Nye, Physical propertie of cristal, Oxford University Press, Oxford, (1957).

[14] M. Born, Proc. Cambridge Philos. Soc. **36** (1940) 160.

[15] M. Born et K. Huang, Dynamical Theory of Crystal Lattices, Clarendon, Oxford (1956).

[16] P. Ravindran, L. Fast, P.A. Korzhavyl, B. Johansson, J. Wills, O. Eriksson, J. Appl.Phys. 84 (1998) 4891.

[17] Schreiber E , Anderson O L , Soga N , Elastic Constants and their Measurements , McGraw-Hill , New York , (1973).

General Conclusion

General Conclusion

In this work, we have studied the structural properties (lattice parameter, compressibility modulus B and its derivative B'), electronic properties (band structure and density of electronic states), and elastic properties of GaS, GaSe, and GaTe compounds. The calculations were carried out using the linearized augmented plane wave method (FP-LAPW) within the density functional framework (DFT) implemented in the code (Wien2K), using the exchange and correlation potential, such as the approximations: LDA, GGA, mBJ, and EV-GG.

Initially, we focused our attention on the study of structural properties by determining the lattice parameter and the compressibility modulus and its derivative. The results obtained for our compounds agree with those determined theoretically, however, our results with GGA approximation are closer to the theoretical values than those obtained by LDA concerning the lattice parameters.

Second, the electronic properties of three-dimensional (3D) and two-dimensional (2D) GaS, GaSe, and GaTe compounds are calculated using LDA, GGA, EV-GGA, and mBJ approximations, respectively. the band structure results indicate that these compounds have a semiconductor behavior with a direct gap at Γ .Moreover, the energy gap in two-dimensional (2D) increases compared to three-dimensional (3D). On the other hand, the use of the EV-GGA and mBJ approximations significantly improved the energy gap values.

In addition, we have investigated the total and partial densities of states (DOS), of three-dimensional (3D) and two-dimensional (2D) GaS, GaSe, and GaTe compounds using LDA, GGA, EV-GGA, and mBJ approximations, and we can distinguish the type of atom and orbital formed between the different elements in each compound.

The independent elastic constants of three-dimensional (3D) and two-dimensional (2D) GaS, GaSe, and GaTe compounds, including the compressibility modulus B and shear modulus G, were determined at zero pressure. Furthermore, the Voigt-Reuss-Hill approximation was employed to estimate the elastic parameters (Young's modulus E, Poisson's ratio). The GaS compound is a ductile material compared to other compounds.

Abstract

In this work, we have studied the structural and electronic properties of GaS, GaSe, and GaTe compounds in both three-dimensional (3D) and two-dimensional (2D) configurations using the first-principles linearized augmented plane wave (FP-LAPW) method within the framework of density functional theory (DFT). We employed the generalized gradient approximation (GGA) and local density approximation (LDA) using the WIEN2k program to calculate the structural properties. For electronic properties, we utilized the modified Becke-Johnson (mBJ) and EV-GGA approximations, in addition to the previous approximations, to enhance the results. We also investigated the elastic properties.

Keywords

Nanomaterials, 2D materials, 3D materials, bandgap, semiconductor, Wien2k.

ملخص

في هذا العمل قمنا بدراسة نظرية للخصائص البنيوية و الالكترونية لمركبات GaS و GaSe و GaSe و GaTe ثلاثية الأبعاد (D3) وثنائية الأبعاد (D2) باستعمال طريقة الأمواج المستوية المتزايدة خطيا (FP-LAPW) في إطار نظرية كثافة الدالي(DFT) وهذا باستعمال تقريب التدرج المعمم (GGA) وتقريب كثافة الموضع (LDA) بواسطة برنامج WIEN2K لحساب الخصائص البنيوية، اما بالنسبة للخصائص الالكترونية فقد استعملنا التقريب المعدل (mBJ) و (EV-GGA) اضافة الى التقريبات السابقة من اجل تحسين النتائج كما تطرقنا ايضا الى دراسة الخصائص المرونية.

كلمات مفتاحية

المواد النانوية، المواد ثنائية الأبعاد ، المواد ثلاثية الأبعاد ، ، فجوة الحزمة ، أشباه الموصلات ، Wien2k.

Résumé

À travers ce travail, nous avons étudié les propriétés structurales et électroniques des composés GaS, GaSe et GaTe en configurations à la fois tridimensionnelles (3D) et bidimensionnelles (2D) en utilisant la méthode des plans d'onde augmentés linéarisés (FP-LAPW) de premiers principes dans le cadre de la théorie de la fonctionnelle de la densité (DFT). Nous avons utilisé l'approximation du gradient généralisé (GGA) et l'approximation de la densité locale (LDA) en utilisant le programme WIEN2k pour calculer les propriétés structurales. Pour les propriétés électroniques, nous avons utilisé les approximations de Becke-Johnson modifiées (mBJ) et (EV-GGA), en plus des approximations précédentes, pour améliorer les résultats. Nous avons également étudié les propriétés élastiques.

Mots clés

Nanomatériaux, matériaux (2D), matériaux (3D), bande interdite, semi-conducteur, Wien2k.